



Vestnik of Don State Technical University

Theoretical and scientific-partical journal

Vol. **19**

no. **3**
2019

ISSN 1992-5980 
eISSN 1992-6006

1

Mechanics

2

Machine Building and Machine Science

3

Information Technology, Computer Science, and Management

DOI 10.23947/1992-5980

vestnik.donstu.ru



**Theoretical
and scientific-practical journal**

Published since 1999

4 issues a year
July-September 2019

ISSN 1992-5980
eISSN 1992-6006
DOI: 10.23947/1992-5980

Founder and publisher — Don State Technical University

Included in the list of peer-reviewed scientific editions where the basic research results of doctoral, candidate's theses should be published (State Commission for Academic Degrees and Titles List) in the following research areas:

01.02.01 – Analytical Mechanics (Engineering Sciences)
01.02.04 – Deformable Solid Mechanics (Engineering Sciences)
01.02.04 – Deformable Solid Mechanics (Physicomathematical Sciences)
01.02.06 – Dynamics, Strength of Machines, Gear, and Equipment (Engineering Sciences)
05.02.02 – Engineering Science, Drive Systems and Machine Parts (Engineering Sciences)
05.02.04 – Machine Friction and Wear (Engineering Sciences)
05.02.07 – Technology and Equipment of Mechanical and Physicotechnical Processing (Engineering Sciences)
05.02.08 – Engineering Technology (Engineering Sciences)
05.02.10 – Welding, Allied Processes and Technologies (Engineering Sciences)
05.02.11 – Testing Methods and Diagnosis in Machine Building (Engineering Sciences)
05.13.11 – Software and Mathematical Support of Machines, Complexes and Computer Networks (Engineering Sciences)
05.13.17 – Foundations of Information Science (Engineering Sciences)
05.13.18 – Mathematical Simulation, Numerical Methods and Program Systems (Engineering Sciences)

***The journal is indexed and archived in the Russian Science Citation Index (RSCI),
and in EBSCO International Database***

The journal is a member of Directory of Open Access Journals (DOAJ), Association of Science Editors and Publishers (ASEP) and Cross Ref

Certificate of mass media registration III № ФС 77-66004 of 06.06.2016 is issued by the Federal Service for Supervision of Communications, Information Technology, and Mass Media

The subscription index in Rospechat catalogue is 35578

The issue is prepared by:

Inna V. Boyko, Marina P. Smirnova (English version)

Passed for printing 26.09.2019,
imprint date 26.09.2019.

Format 60×84/8. Font «Times New Roman».

C.p.sh. 22.6. Circulation 1000 cop. Order no. 26/09 Free price.

Founder's, Publisher's and Printery Address:

Gagarin Sq. 1, Rostov-on-Don, 344000, Russia. Phone: +7 (863) 2-738-372

E-mail: vestnik@donstu.ru <http://vestnik.donstu.ru>



The content is available under Creative Commons Attribution 4.0 License

© Don State Technical University, 2019

Editorial Board

Editor-in-Chief — **Besarion Ch. Meskhi**, Dr.Sci. (Eng.), professor, Don State Technical University (Rostov-on-Don);

deputy chief editor — **Valery P. Dimitrov**, Dr.Sci. (Eng.), professor, Don State Technical University (Rostov-on-Don);

executive editor — **Manana G. Komakhidze**, Cand.Sci. (Chemistry), Don State Technical University (Rostov-on-Don);

executive secretary — **Elena V. Petrova**, Don State Technical University (Rostov-on-Don);

Evgeny V. Ageev, Dr.Sci. (Eng.), professor, South-Western State University (Kursk);

Sergey M. Aizikovich, Dr.Sci. (Phys.-Math.), professor, Don State Technical University (Rostov-on-Don);

Kamil S. Akhverdiev, Dr.Sci. (Eng.), professor, Rostov State Transport University (Rostov-on-Don);

Vladimir I. Andreev, member of RAACS, Dr.Sci. (Eng.), professor, National Research Moscow State University of Civil Engineering (Moscow);

Imad R. Antipas, Cand.Sci. (Eng.), Don State Technical University (Rostov-on-Don);

Torsten Bertram, Dr.Sci. (Eng.), professor, TU Dortmund University (Germany);

Dmitry A. Bezuglov, Dr.Sci. (Eng.), professor, Rostov branch of Russian Customs Academy (Rostov-on-Don);

Larisa V. Cherkasova, Dr.Sci. (Phys.-Math.), professor, Don State Technical University (Rostov-on-Don);

Alexandr N. Chukarin, Dr.Sci. (Eng.), professor, Rostov State Transport University (Rostov-on-Don);

Oleg V. Dvornikov, Dr.Sci. (Eng.), professor, Belarusian State University (Belarus);

Nikita G. Dyurgerov, Dr.Sci. (Eng.), professor, Rostov State Transport University (Rostov-on-Don);

Karen O. Egiazaryan, Dr.Sci. (Eng.), professor, Tampere University of Technology (Tampere, Finland);

Sergey V. Eliseev, corresponding member of Russian Academy of Natural History, Dr.Sci. (Eng.), professor, Irkutsk State Railway Transport Engineering University (Irkutsk);

Victor A. Eremeev, Dr.Sci. (Phys.-Math.), professor, Southern Scientific Center of RAS (Rostov-on-Don);

Mikhail B. Flek, Dr.Sci. (Eng.), professor, "Rostvertol" JSC (Rostov-on-Don);

Nikolay E. Galushkin, Dr.Sci. (Eng.), professor, Institute of Service and Business (DSTU branch) (Shakhty);

LaRoux K. Gillespie, Dr.Sci. (Eng.), professor, President-elect of the Society of Manufacturing Engineers (USA);

Victor M. Kureychik, Dr.Sci. (Eng.), professor, Southern Federal University (Rostov-on-Don);

Geny V. Kuznetsov, Dr.Sci. (Phys.-Math.), professor, Tomsk Polytechnic University (Tomsk);

Vladimir I. Marchuk, Dr.Sci. (Eng.), professor, Institute of Service and Business (DSTU branch) (Shakhty);

Igor P. Miroshnichenko, Cand.Sci. (Eng.), professor, Don State Technical University (Rostov-on-Don);

Vladimir G. Mokrozub, Dr.Sci. (Eng.), associate professor, Rostov State Transport University (Rostov-on-Don);

Murman A. Mukutadze, Cand.Sci. (Eng.), professor, Tambov State Technical University (Tambov);

Rudolf A. Neydorf, Dr.Sci. (Eng.), professor, Don State Technical University (Rostov-on-Don);

Nguyen Dong Ahn, Dr.Sci. (Phys.-Math.), professor, Institute of Mechanics, Academy of Sciences and Technologies of Vietnam (Vietnam);

Petr M. Ogar, Dr.Sci. (Eng.), professor, Bratsk State University (Bratsk);

Gennady A. Ougolnitsky, Dr.Sci. (Phys.-Math.), professor, Southern Federal University (Rostov-on-Don);

Valentin L. Popov, Dr.Sci. (Phys.-Math.), professor, Institute of Mechanics, Berlin University of Technology (Germany);

Nikolay N. Prokopenko, Dr.Sci. (Eng.), professor, Don State Technical University (Rostov-on-Don);

Anatoly A. Ryzhkin, Dr.Sci. (Eng.), professor, Don State Technical University (Rostov-on-Don);

Igor B. Sevostianov, Cand.Sci. (Phys.-Math.), professor, New Mexico State University (USA);

Vladimir N. Sidorov, Dr.Sci. (Eng.), Russian University of Transport (Moscow);

Arkady N. Solovyev, Dr.Sci. (Phys.-Math.), professor, Don State Technical University (Rostov-on-Don);

Alexandr I. Sukhinov, Dr.Sci. (Phys.-Math.), professor, Don State Technical University (Rostov-on-Don);

Mikhail A. Tamarkin, Dr.Sci. (Eng.), professor, Don State Technical University (Rostov-on-Don);

Valery N. Varavka, Dr.Sci. (Eng.), professor, Don State Technical University (Rostov-on-Don);

Igor M. Verner, Cand.Sci. (Eng.), Docent, Technion (Israel);

Batyr M. Yazyev, Dr.Sci. (Phys.-Math.), professor, Don State Technical University (Rostov-on-Don);

Vilor L. Zakovorotny, Dr.Sci. (Eng.), professor, Don State Technical University (Rostov-on-Don);

CONTENT

MECHANICS

- Galaburdin A. V.** The problem of infinite plate loaded with normal force following a complex trajectory.. 208

MACHINE BUILDING AND MACHINE SCIENCE

- Soloviev A. N., Tamarkin M. A., Nguyen Van Tho** Finite element modeling method of centrifugal rotary processing..... 214
- Ghias Kharmanda, Antypas Imad R.** Efficient optimum safety factor approach for system reliability-based design optimization with application to composite yarns..... 221
- Martynova E. G., Velichko S. A., Martynov A. V.** Micrometric research results of vacuum dough divider components..... 231
- Rybak A. T., Tsybriy I. K., Nosachev S. V., Zenin A. R.** Theoretical background of hydraulic drive control system analysis for testing piston hydraulic cylinders 242
- Lebed A. D., Glushko S. P.** Selection rationale for leakage monitoring in gas pipeline 250
- Dyachenko A. G., Savostina T. P., Imad S. B.** Comparison of graphic expression of dependences of transporter cut profile of threshing-separating unit on the second volume and spike fraction humidity 256
- Kolybenko E. N.** Distinction between the concepts of mathematical and logical modeling 262

INFORMATION TECHNOLOGY, COMPUTER SCIENCE, AND MANAGEMENT

- Chubyr N. O., Kovalenko A. V., Urtenov M. Kh., Sukhinov A. I., Gudza V. A.** Modeling and numerical analysis of the effect of dissociation/recombination of water molecules on the transport of salt ions in diffusion layer..... 268
- Duong V. L.** The problem of mathematical finite element modeling of inhomogeneous deformable solids using scanning 281
- Mazurenko A. V., Boldyrikhin N. V.** Accelerated preprocessing in task of searching substrings in a string 290

МЕCHANICS МЕХАНИКА



UDC 539.3

<https://doi.org/10.23947/1992-5980-2019-19-3-208-213>

The problem of infinite plate loaded with normal force following a complex trajectory*

A. V. Galaburdin^{1**}

¹ Don State Technical University, Rostov-on-Don, Russian Federation

Задача о бесконечной пластине, нагруженной нормальной силой, движущейся по сложной траектории***

А. В. Галабурдин^{1**}

¹ Донской государственный технический университет, г. Ростов-на-Дону, Российская Федерация

Introduction. A method for solving the problem of an infinite plate on an elastic foundation is proposed. The plate is affected by a periodic load in the form of a force following an arbitrary closed path. The work objective is to develop a numerical method for solving problems of the elasticity theory for bodies under a moving load.

Materials and Methods. Given the periodicity of the load under consideration, it is decomposed in a Fourier series in a time interval whose length is equal to the load period. The solution to the original problem is constructed by superposition of the solutions to the problems corresponding to the load specified by the terms of the Fourier series described above. The final solution to the problem is presented as a segment of a series. In this case, each term corresponds to the solution of the problem of the impact on an infinite plate of a load distributed along a closed curve (the trajectory of the force motion). To find these solutions, the fundamental solution to the equation of vibration of an infinite plate lying on an elastic base is used.

Research Results. A new method is proposed for solving problems on the elasticity theory for bodies with a load following a closed path of arbitrary shape. The problem of an infinite plane along which a concentrated force moves at a constant speed is solved. It is determined that the trajectory of motion is a smooth closed curve consisting of circular arcs. The behavior of displacements and stresses near a moving force is considered. The energy propagation of the elastic waves is studied. For this purpose, the coordinates of the Umov – Poynting vector are calculated. The effect of the force motion speed on the length of the Umov – Poynting vector is investigated.

Discussion and Conclusions. The method is applicable when considering more complex objects (plates of complex shape, layered plates, viscoelastic plates). Its advantage is profitability since the known problem solutions are used to build the solution.

Введение. Предлагается метод решения задачи о бесконечной пластине, лежащей на упругом основании. На пластину действует периодическая нагрузка в виде силы, перемещающейся по произвольной замкнутой траектории. Цель исследования — разработка численного метода решения задач теории упругости для тел, находящихся под действием подвижной нагрузки.

Материалы и методы. Учитывая периодичность рассматриваемой нагрузки, она раскладывается в ряд Фурье на временном отрезке, длина которого равна периоду нагрузки. Решение исходной задачи строится посредством суперпозиции решений задач, соответствующих нагрузке, задаваемой слагаемыми описанного выше ряда Фурье. Окончательное решение задачи представляется в виде отрезка ряда. Каждое слагаемое при этом соответствует решению задачи о воздействии на бесконечную пластину нагрузки, распределенной по замкнутой кривой (траектории движения силы). Для нахождения этих решений используется фундаментальное решение уравнения колебания бесконечной пластины, лежащей на упругом основании.

Результаты исследования. Предложен новый метод решения задач теории упругости для тел с нагрузкой, движущейся по замкнутой траектории произвольной формы. Решена задача о бесконечной плоскости, по которой с постоянной скоростью движется сосредоточенная сила. Определено, что траектория движения представляет собой гладкую замкнутую кривую, состоящую из дуг окружностей. Рассмотрен характер изменения перемещений и напряжений вблизи движущейся силы. Изучено распространение энергии упругих волн. С этой целью выполнено вычисление координат вектора Умова — Пойтинга. Исследовано влияние скорости движения силы на длину вектора Умова — Пойтинга.

Обсуждение и заключения. Метод применим и при рассмотрении более сложных объектов (плиты сложной формы, слоистые плиты, вязкоупругие плиты). Его преимущество — экономичность, так как для построения решения используются уже известные решения задач. Окончательное решение выра-



* The research is done within the frame of the independent R&D.

** E-mail: Galaburdin@mail.ru

*** Работа выполнена в рамках инициативной НИР.

The final decision is expressed in a convenient form – as the sum of curvilinear integrals. The results obtained can be used in the road design process. Studying the energy propagation of elastic waves from moving vehicles will enable to evaluate the impact of these waves on buildings near the road. The wear of the pavement is estimated considering data on the behavior of displacements and stresses.

жается в удобном виде — как сумма криволинейных интегралов. Полученные результаты могут быть использованы в процессе проектирования дорог. Изучение распространения энергии упругих волн от движущихся транспортных средств позволит оценить воздействие указанных волн на строения, расположенные вблизи дороги. С учетом данных о характере изменения перемещений и напряжений оценивается износ дорожного покрытия.

Keywords: infinite plate, moving force, arbitrary closed path, energy of elastic waves

Ключевые слова: бесконечная пластина, движущаяся нагрузка, произвольная замкнутая траектория, энергия упругих волн.

For citation: A.V. Galaburdin. The problem of infinite plate loaded with normal force following a complex trajectory. Vestnik of DSTU, 2019, vol. 19, no. 3, pp. 208–213. <https://doi.org/10.23947/1992-5980-2019-19-3-208-213>

Образец для цитирования: Галабурдин, А. В. Задача о бесконечной пластине, нагруженной нормальной силой, движущейся по сложной траектории / А. В. Галабурдин // Вестник Дон. гос. техн. ун-та. — 2019. — Т. 19, № 3. — С. 208–213. <https://doi.org/10.23947/1992-5980-2019-19-3-208-213>

Introduction. The study on dynamic phenomena caused by the action of a moving load is an urgent task that has application significance (for example, when solving transport development issues). In the papers devoted to this problem, various tasks with a moving load were considered. In particular, it is shown how a load moving in an infinite straight line at a constant speed acts on a half-plane or half-space (elastic isotropic, transversal isotropic, viscoelastic). In this case, when solving the problem, a moving coordinate system associated with a moving force is introduced; this enables to exclude time from the number of independent variables [1–5]. Some papers consider the action on an infinite plate or strip (elastic or viscoelastic) moving uniformly along a rectilinear load path. In this case, the same method of eliminating a temporary variable is used, or a quasistatic formulation of the problem is considered [6–12]. The tasks in which the length of the load path is finite and the path itself is a curved line are of main interest. In this case, finite element modeling of a moving load is frequently used [11–13]. In a number of papers, when solving such problems, variational methods are used (in particular, the Rayleigh – Ritz method) [14–16] or a variation of the Galerkin method, which makes it possible to reduce the problem to ordinary differential equations. In this case, various objects of the application of a moving load are considered (plates, layered plates, viscoelastic plates, half-spaces – both isotropic and anisotropic) [17–19]. This paper presents a method that develops the ideas described in [20–23].

Materials and Methods. Consider an infinite plate lying on an elastic Winkler base, which is under the action of a normally applied force moving along a closed path.

The problem is reduced to the integration of the equation of motion of a plate lying on an elastic Winkler base [14]:

$$\Delta^2 W + c^{-2} \partial_t^2 W + kW = \frac{P}{D}, \quad (1)$$

where W is the plate deflection; $D = \frac{Eh^3}{12(1-\nu^2)}$; E is Young's modulus; ν is Poisson's ratio; h is the plate thickness;

$c^{-2} = \frac{\rho h}{D}$; ρ is the density of the material; $k = \frac{K}{D}$; K is the compliance coefficient of the elastic base; P is the concentrated force moving along a closed curve γ with the constant speed a .

Let us introduce the coordinate s counted from some fixed point of the curve γ . Then the force P moving along the curve γ with the velocity a will be described by the relation $P = P(s - at)$. The function $P(s - at)$ is periodic in t , with period $T = \frac{L}{a}$, where L is the length of the curve.

Solution. Consider the steady state. We expand the function $P(s - at)$ in the Fourier series in the variable t on the segment $\left[-\frac{L}{2a}; \frac{L}{2a}\right]$. In this case, the expansion coefficients appear as:

$$c_k = \int_{-L/2a}^{L/2a} P(s - at) e^{2iak\pi t/L} dt.$$

After changing the integration variable in the integral $s - at = z$, we obtain:

$$c_k = \int_{-L/2}^{L/2} P(z) e^{-2ik\pi z/L} dz \frac{e^{2ik\pi y/L}}{a} = d_{-k} \frac{e^{2ik\pi y/L}}{a},$$

where d_k are Fourier series expansion coefficients on a function segment $\left[-\frac{L}{2}; \frac{L}{2}\right]$ of the function $P(z)$.

Then the moving load can be presented as a Fourier series:

$$P(s-at) = \frac{1}{a} \sum_{k=-\infty}^{\infty} d_{-k} e^{2ik\pi(s-at)/L}.$$

Given the linearity of the problem, its solution can be presented as:

$$W = \sum_{k=-\infty}^{\infty} d_{-k} \hat{W}_k, \quad (2)$$

where \hat{W}_k are plate deflections caused by the action of a vertical load whose distribution along the curve γ is described by the function $e^{2ik\pi y/L}$ that varies in time according to the law $e^{-2ik\pi t/L}$.

To determine \hat{W}_k , we use the fundamental solution to the equation (1), which corresponds to $P = \delta(x-x_0)\delta(y-y_0)e^{-i\omega_k t}$, где $\omega_k = \frac{2ika\pi}{L}$.

Using the limiting absorption principle and traditional methods for constructing solutions to differential equations, we can obtain a fundamental solution to the equation (1), which at $k > \frac{\omega_k^2}{c^2}$, has the form:

$$w_k(x, y, x_0, y_0) = \frac{i}{4\pi\epsilon^2 D} [K_0(\alpha_1 R) - K_0(\alpha_2 R)],$$

where $R = [(x-x_0)^2 + (y-y_0)^2]^{1/2}$, $\epsilon = \sqrt{k - \omega_k^2/c^2}$, $\alpha_1 = \epsilon e^{i\pi/4}$, $\alpha_2 = \epsilon e^{-i\pi/4}$, $K_0(z)$ is the Macdonald function.

At $k < \frac{\omega_k^2}{c^2}$, the solution is given by:

$$w_k(x, y, x_0, y_0) = \frac{i}{4\pi\gamma^2 D} \left[\frac{\pi i}{2} H_0^{(1)}(\gamma R) - K_0(\gamma R) \right],$$

where $\gamma = \sqrt{\frac{\omega_k^2}{c^2} - k}$, $H_0^{(1)}(\gamma R)$ is the Hankel function.

Then $\hat{W}_k = \oint_{\gamma} w_k(x, y, x_0(s), y_0(s)) e^{2ik\pi(s-at)/L} ds$. Using the well-known formulas of the thin plate theory and

the formula obtained from the above relations determining the deflection W (2), we can calculate the displacements u_x , u_y and the stresses σ_x , σ_y and σ_{xy} at any point on the plate.

For large k , it is necessary to calculate the integral of fast oscillating functions. For this, a quadrature formula based on replacing the weakly oscillating part of the integrand by a cubic spline was used, and the highly oscillating factor $e^{2ik\pi y/L}$ was considered as a weight function [15].

Research Results. So, an infinite plate lies on an elastic Winkler base. A normal force acts on it moving along the trajectory shown in Fig. 1.

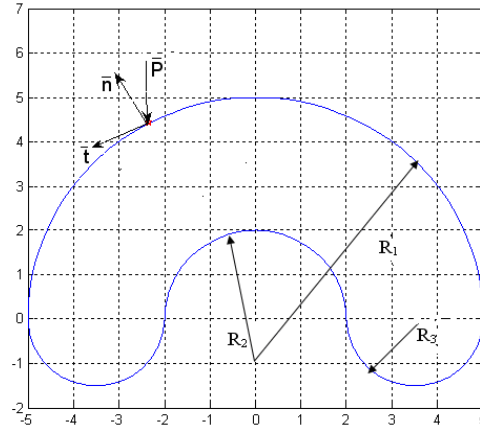


Fig. 1. Load motion trajectory

The computation was performed at the following initial data: $h = 0.25$ m; $s = 221$ m/s; $E = 232469 \cdot 10$ N/m²; $\nu = 0.36$. Fig. 2 shows the calculation results corresponding to $K = 1.864$ m⁻⁴ and $a = 125$ m/s.

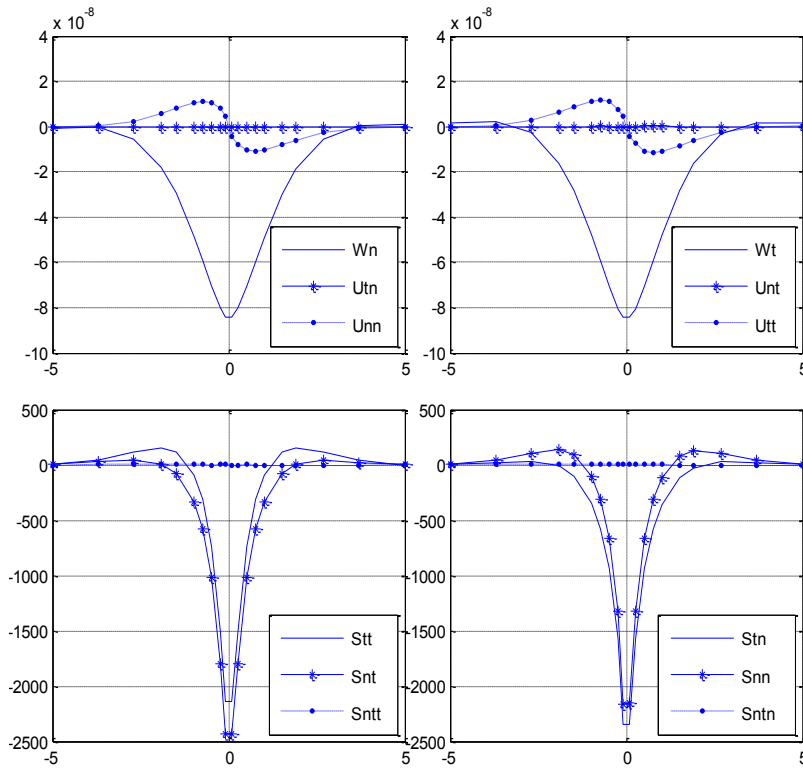


Fig. 2. Variation of displacements and stresses

These graphs describe changes in displacements and stresses in the coordinate system associated with the point of application of the moving force P . The t axis is directed tangentially to the motion path \bar{t} , and the n axis is directed along the external normal to the region bounded by the path \bar{n} (see Fig. 1) at $z = h/2$.

In this case, the displacement vector and stress tensor, respectively, were represented as:

$$\bar{U} = U_t \cdot \bar{t} + U_n \cdot \bar{n} + W \cdot \bar{k}, \quad \bar{S} = S_t \cdot \bar{t}\bar{t} + S_n \cdot \bar{n}\bar{n} + S_{tn} \cdot (\bar{t}\bar{n} + \bar{n}\bar{t}),$$

where \bar{k} is normal to the plate.

Fig. 2 shows the change along the t axis of the displacement vector components W_t, U_{tt}, U_{nt} , the stress tensor S_{tt}, S_{nt}, S_{tn} , and the variation of these values along the n axis— W_n, U_{tn}, U_{nn} and S_{tn}, S_{nn}, S_{nn} .

According to the calculations, the behavior of these values at all points of the trajectory remains unchanged. The computation also showed that with a change in the velocity of the load a in the range from 0 to 125 m/s, the components of the displacement vector and the stress tensor increased moderately (by 3-4%).

To study the elastic energy propagation, the components of the Umov-Poynting vector $e_i = -S_{ij} \cdot \partial_j u_i$ (S_{ij} are the components of the stress tensor, u_i are the coordinates of the displacement vector) whose direction indicates the direction of energy propagation, and the length describes the amount of energy transferred through a surface unit perpendicular to this vector line per unit time.

Fig. 3 shows the elastic energy propagation near a moving concentrated force (the position of the force is marked with a red asterisk).

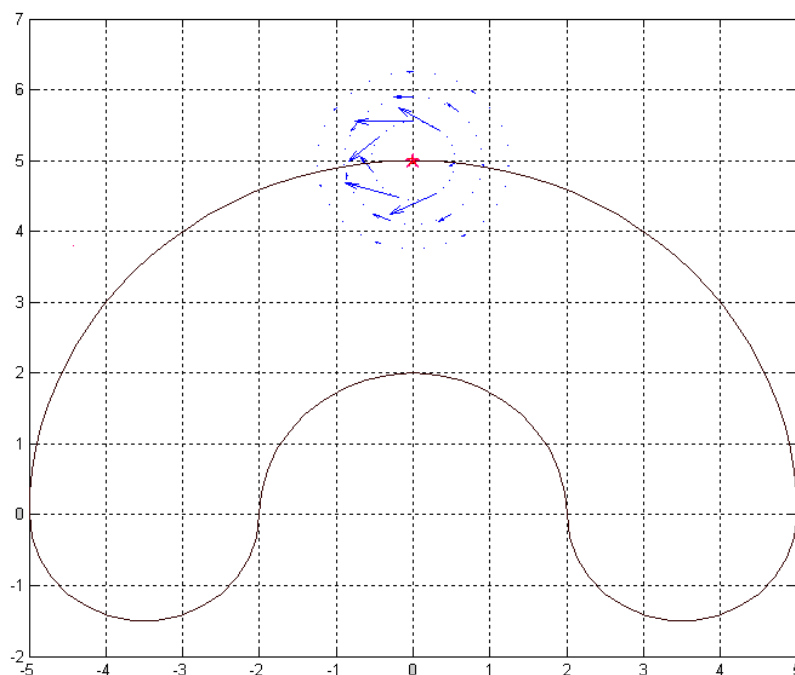


Fig. 3 Elastic energy propagation

Discussion and Conclusions. The analysis of the results obtained shows the following: at the speed variation limits indicated above, the length of the Umov-Poynting vector is almost proportional to the load speed and a sound energy pattern near the force changes slightly during the movement. The behavior of the displacements and stresses calculated above at all points of the trajectory remains unchanged, and their values weakly depend on the load speed a when this velocity varies from 0 to 125 m/s.

Application of the proposed method to an infinite plate lying on an elastic base does not exhaust its possibilities. It can be used when considering more complex objects (plates of complex shape, layered plates, viscoelastic plates). The considered method differs from the mentioned above in greater efficiency since it uses the known problem solving to construct the solution. The final decision is expressed in a convenient form – as a sum of curvilinear integrals.

The results can be used in the road design process. Studying the elastic energy propagation from moving vehicles will provide evaluating the impact of these waves on buildings near the road. The wear of the pavement is estimated considering data on the behavior of displacements and stresses

References

1. Aleksandrov, V.M., Mark, A.V. Dvizhenie s postoyannoy skorost'yu zhestkogo shtampa po granitse vyazkouprugoy poluploskosti. [Motion of rigid punch over boundary of viscoelastic half-plane at constant velocity.] Journal of Friction and Wear, 2006, vol. 27, no. 1, pp. 5–11 (in Russian).
2. Ege, N., Sahin, O., Erbas, B. Response of a 3D elastic half-space to a distributed moving load. Hacettepe Journal of Mathematics and Statistics, 2017, vol. 46 (5), pp. 817–828. DOI: 10.15672 /HJMS.2017.434.
3. Kaplunov, J., et al. On a 3D moving load problem for an elastic half space. Wave Motion, 2013, vol. 50, pp. 1229–1238. DOI:10.1016/j.wavemoti.2012.12.008.

4. Kalinchuk, V.V., et al. Dinamika sloistogo poluprostranstva pod deystviem dvizhushcheysya i ostsilliruyushchey nagruzki. [Dynamics of layered half-space under the action of moving and oscillating load.] Vestnik SSC RAS, 2005, vol. 1, no. 1, pp. 3–11 (in Russian).
5. Prikazchikov, D.A. Okolorezonansnye rezhimy v statsionarnoy zadache o podvizhnoy nagruzke v sluchae transversal'no izotropnoy uprugoy poluploskosti. [Near-resonant regimes of a steady-state moving load on a transversely isotropic elastic half-plane.] Izvestiya of Saratov University, 2015, vol. 15, no. 2, pp. 215–221 (in Russian).
6. Chen, Y., Beskou, N.D., Qian, J. Dynamic response of an elastic plate on a cross-anisotropic poroelastic halfplane to a load moving on its surface. Soil Dynamics and Earthquake Engineering, 2018, vol. 107, pp. 292–302.
7. Beskou, N.D., Chen, Y., Qian, J. Dynamic response of an elastic plate on a cross-anisotropic elastic half-plane to a load moving on its surface. Transportation Geotechnics, 2018, vol. 14, pp. 98–106.
8. Oblakova, T.V., Prikazchikov, D.A. O rezonansnom rezhime v nestatsionarnoy zadache o podvizhnoy nagruzke dlya uprugogo poluprostranstva. [On the resonant regime of a transient moving load problem for an elastic half-space.] Engineering Journal: Science and Innovation, 2013, vol. 9, pp. 1–8 (in Russian).
9. Kaplunov, J., et al. The edge wave on an elastically supported Kirchhoff plate. The Journal of the Acoustical Society of America, 2014, vol. 136, no. 4, pp. 1487–1490. DOI: 10.1121/1.4894795.
10. Glukhov, Yu.P. Dinamicheskaya zadacha dlya dvukhsloynnoy polosy na zhestkom osnovanii. [Dynamic problem for two-layered stripe on the rigid basis.] Proceedings of Odessa Polytechnic University, 2014, iss. 2, pp. 9–14 (in Russian).
11. Yegorychev, O.O. Vozdeystvie podvizhnoy nagruzki na mnogosloynnyuyu vyazkoupruguyu plastinu, lezhashchuyu na vyazkouprugom osnovanii. [Impact of a moving load on a multilayer viscoelastic plate lying on a viscoelastic base.] Vestnik MGSU, 2007, iss. 1, pp. 39–42 (in Russian).
12. Doszhanov, M.Zh., et al. Dinamicheskoe povedenie bezgranichnoy uprugoy plastinki pri vozdeystvii podvizhnoy (begushchey) nagruzki. [Dynamic behaviour of infinite elastic plane affected by mobile load.] The Way of Science, 2016, vol. 1, no. 11 (33), pp. 26–28 (in Russian).
13. Shishmarev, K.A. Postanovka zadachi o vyazkouprugikh kolebaniyakh ledovoy plastiny v kanale v rezul'tate dvizheniya nagruzki. [Problem formulation of ice plate viscoelastic oscillations in a channel caused by a moving load.] Izvestia of Altai State University, 2015, no. 1/2 (85), pp. 189–194. DOI 10.14258/izvasu(2015) 1.2–35 (in Russian).
14. Dyniewicz, B., Pisarski, D., Bajer, C. Vibrations of a Mindlin plate subjected to a pair of inertial loads moving in opposite directions. Journal of Sound and Vibration, 2017, vol. 386, pp. 265–282 (in Russian).
15. Esen, I. A new finite element for transverse vibration of rectangular thin plates under a moving mass. Finite Elements in Analysis and Design, 2013, vol. 66, pp. 26–35.
16. Song, Q., Shi, J., Liu, Z. Vibration analysis of functionally graded plate with a moving mass. Applied Mathematical Modelling, 2017, vol. 46, pp. 141–160.
17. Parametric study of dynamic response of sandwich plate under moving loads / Q. Song [et al.] // Thin-Walled Structures. — 2018. — Vol. 123. — C. 82–99.
18. Qu, Y., et al. Time-domain structural-acoustic analysis of composite plates subjected to moving dynamic loads. Composite Structures, 2019, vol. 208, pp. 574–584.
19. Foyouzat, M.A., Estekanchi, H.E., Mofid, M. An analytical-numerical solution to assess the dynamic response of viscoelastic plates to a moving mass. Applied Mathematical Modelling, 2018, vol. 54, pp. 670–696.
20. Galaburdin, A.V. Primenenie metoda granichnykh integral'nykh uravneniy k resheniyu svyaznykh zadach termouprugosti s podvizhnoy nagruzkoy. [Applying of boundary integral equation method to the decision of flat problems of thermoelasticity with mobile load.] Izvestiya vuzov. Severo-Kavkazskiy region. Natural Sciences. 2012, no. 4, pp. 29–31 (in Russian).
21. Galaburdin, A.V. Primenenie metoda granichnykh integral'nykh uravneniy k resheniyu zadach o dvizhushcheysya nagruzke. [Application of a method of the of boundary integral equations to the decision of problems on moving loading.] Izvestiya vuzov. Severo-Kavkazskiy region. Natural Sciences, 2015, no. 1, pp. 9–11 (in Russian).
22. Rekach, V.G. Rukovodstvo k resheniyu zadach prikladnoy teorii uprugosti. [Guide to solving problems of the applied theory of elasticity.] Moscow: Vysshaya shkola, 1973, 384 p. (in Russian).
23. Zavyalov, Yu.S., Kvasov, B.I., Miroshnichenko, A.L. Metody splayn-funktsii. [Spline Function Methods.] Moscow: Nauka, 1980, 352 p. (in Russian).

MACHINE BUILDING AND MACHINE SCIENCE МАШИНОСТРОЕНИЕ И МАШИНОВЕДЕНИЕ



UDC 621.9.048:539.3

<https://doi.org/10.23947/1992-5980-2019-19-2-214-220>

Finite element modeling method of centrifugal rotary processing *

A. N. Soloviev¹, M. A. Tamarkin², Nguyen Van Tho^{3**}

^{1,2,3} Don State Technical University, Rostov-on-Don, Russian Federation

³ Hai Phong University, Hai Phong City, Socialist Republic of Vietnam

Метод конечных элементов в моделировании центробежно-ротационной обработки ***

А. Н. Соловьев¹, М. А. Тамаркин², Нгуен Ван Тхо^{3**}

^{1,2,3} Донской государственный технический университет, г. Ростов-на-Дону, Российская Федерация

³ Университет Хайфона, г. Хайфон, Социалистическая Республика Вьетнам

Introduction. In modern production, when performing finishing operations, centrifugal rotary processing in the medium of abrasive plays an important role. High productivity, low costs and extensive technological capabilities are the main advantages of these cleaning and finishing operations. This paper considers the process of abrasive particle – workpiece surface interaction within the framework of the static contact problem of the elasticity theory. Thus, plastic deformation in the contact area comes into account.

Materials and Methods. The abrasive particle (corundum) is simulated with a linearly elastic body, whose Young's modulus is significantly larger than that of the work material. The process material (steel) is simulated with an elastoplastic bilinear body using the von Mises yield criterion.

Research Results. Finite element modeling of the structures under consideration was performed in the ANSYS CAE package. The process of abrasive particle – workpiece surface interaction was simulated; its stress-strain state was analyzed. The results of numerical experiments are presented. They have determined how equivalent plastic strains are distributed at depths of the cone penetration of 0.01 mm and 0.05 mm. The data obtained, as well as the areas of plastic strain values of more than 1%, are visualized in the ANSYS CAE package.

Discussion and Conclusions. It is established that the equivalent plastic deformation is proportional to the depth of penetration (DP). It reaches a minimum value of 0.158 at DP = 0.01 mm, and a maximum of 0.825 at DP = 0.05 mm. The dependences of the plastic region sizes on DP are determined for cases when the plastic deformation exceeds 1%. At the maximum penetration (0.05 mm), the deformation radius is 1 mm, and the depth is 0.8 mm.

On the basis of the data obtained as a result of the conducted

Введение. В современном производстве при выполнении финишных операций важную роль играет центробежно-ротационная обработка в среде абразива. Основные преимущества этого метода отделочно-зачистной обработки: высокая производительность, низкая себестоимость и широкие технологические возможности. В данном исследовании рассматривается процесс взаимодействия абразивной частицы с поверхностью детали в рамках статической контактной задачи теории упругости. При этом учитывается пластическая деформация в области контакта.

Материалы и методы. Абразивная частица (корунд) моделируется линейно упругим телом, модуль Юнга которого значительно больше, чем у обрабатываемого материала. Обрабатываемый материал (сталь) моделируется упруго пластическим билинейным телом с применением критерия пластичности Мизеса.

Результаты исследования. Выполнено конечноэлементное моделирование рассматриваемых конструкций в САЕ-пакете ANSYS. Смоделирован процесс взаимодействия абразивной частицы и поверхности детали, проанализировано ее напряженно-деформированное состояние. Представлены результаты численных экспериментов, которые позволили установить, как распределяются эквивалентные пластические деформации при глубинах внедрения конуса 0,01 мм и 0,05 мм. Полученные данные, а также области значений пластической деформации более 1 % визуализированы в САЕ-пакете ANSYS.

Обсуждение и заключения. Установлено, что эквивалентная пластическая деформация пропорциональна глубине внедрения (ГВ). Она достигает минимального значения 0,158 при ГВ = 0,01 мм, максимального 0,825 — при ГВ = 0,05 мм. Определены зависимости размеров области пластической деформации от ГВ для случаев, когда пластическая деформация превышает 1 %. При максимальном внедрении (0,05 мм) радиус деформации составляет 1 мм, глубина — 0,8 мм. На основе данных, полученных в результате проведенного исследования, могут быть выбраны

* The research is done within the frame of the independent R&D.

**E-mail: solovievarc@gmail.com, tehn_rostov@gmail.ru, thonguyen239@gmail.com

*** Работа выполнена в рамках инициативной НИР.



research, the parameters of the technological process (rotational speed, size of the abrasive surface, mass of abrasive particles) that affect the workpiece – abrasive particle interaction can be selected. A judicious choice of these parameters will increase the processing efficiency.

Keywords: centrifugal rotary processing, abrasive treatment, contact problem, plasticity, finite element method.

For citation: A.N. Soloviev, et al. Finite element modeling method of centrifugal rotary processing. Vestnik of DSTU, 2019, vol. 19, no. 3, pp. 214–220. <https://doi.org/10.23947/1992-5980-2019-19-2-214-220>

параметры технологического процесса (скорость вращения, размер абразивной поверхности, масса абразивных частиц), которые влияют на взаимодействие между деталью и абразивной частицей. Рациональный выбор этих параметров позволит повысить эффективность обработки.

Ключевые слова: центробежно-ротационной обработки, абразивная обработка, контактная задача, пластичность, метод конечных элементов.

Образец для цитирования: Соловьев, А. Н. Метод конечных элементов в моделировании центробежно-ротационной обработки / А. Н. Соловьев, М. А. Тамаркин, Нгуен Ван Тхо // Вестник Дон. гос. техн. ун-та. — 2019. — Т. 19, № 3. — С. 214–220. <https://doi.org/10.23947/1992-5980-2019-19-2-214-220>

Introduction. In modern production, when performing finishing operations, an important role is played by centrifugal rotary processing (CRP) in an abrasive medium. The primary advantages of this method of finishing – clearing operation are high productivity, low cost and wide technological capabilities. This study discusses the process of interaction of an abrasive particle and a workpiece surface in the framework of the static problem of the elasticity theory. In this case, plastic deformation in the contact area is taken into account. An abrasive grain element in the form of a truncated cone (more precisely: a circle of a minor diameter of this cone) interacts with the workpiece surface. In this case, friction and plastic deformation of this surface should be considered. Kinematic or force boundary conditions are applied to a larger diameter circle. In case of kinematic conditions, normal and tangential displacements of the circle and its rotation are specified. In case of force conditions, force and torque are set. The stress fields and equivalent plastic deformations near the contact area are investigated.

Modeling the geometry of an abrasive particle of a centrifugal rotary processing. The summary of the CRP method is that the abrasive particles 3 and the workpiece 4 (Fig. 1 [1]) are loaded into the working chamber and rotated about the vertical axis so that the entire mass of the load becomes a torus [2, 3] in which particles move along spiral paths.

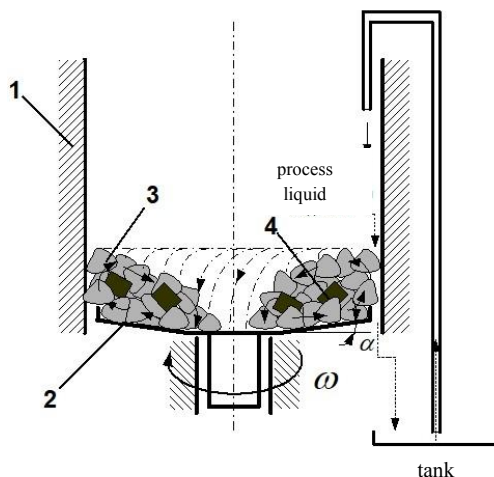


Fig. 1. Centrifugal rotary processing in abrasive medium:
 1 is fixed cylindrical ring; 2 is rotor; 3 is abrasive grain; 4 is workpieces

The toroidal helical flow is ensured through the design of the machine working chamber consisting of a fixed cylindrical ring 1 and a rotating bottom (rotor) 2 adjacent to it, having a common plate shape. Workpieces 4 are loaded into the working chamber in bulk together with abrasive particles 3. To reduce wear, the inner surfaces of the bottom and the fixed part of the working chamber are coated with a wear-resistant material. Rubber or polyurethane coatings are most commonly used.

The scheme for constructing an indenter (in the form of a truncated cone) penetration model suggests a spherical shape of an abrasive granule with a set of truncated cones [3]. An approximate idea of the geometry of a spherical abrasive particle is shown in Fig. 2 [4].

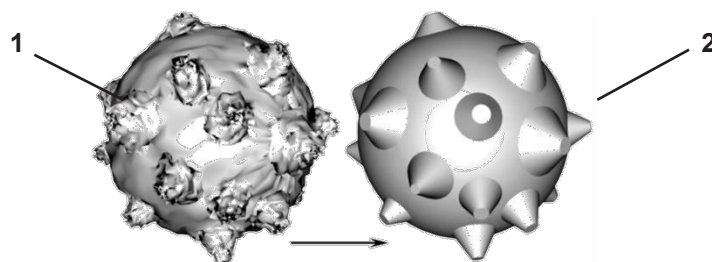


Fig. 2. Geometry of a spherical abrasive granule:
 1 is approximate to actual one; 2 is simulated one

According to the model, the abrasive grain has a shape of a truncated cone. This model considers the always occurring blunting of abrasive grains. Fig. 3 presents a diagram of interaction of the abrasive particles and workpieces [5].

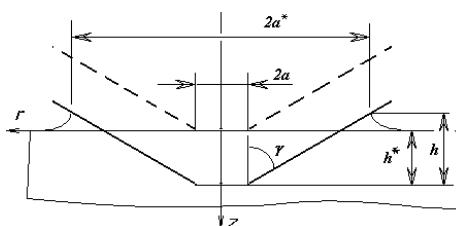


Fig 3. Scheme of conical indenter penetration

In the force acting on the indenter, normal and tangent components are distinguished [2]. According to the work of A. N. Beskopylny [5], a normal component of the cutting force is:

$$P = \begin{cases} 2ah^*E^*, & h^* \leq h_{cr}^* \\ \chi \left(\frac{h^* + C_1}{C} \right)^2, & h^* > h_{cr}^* \end{cases}$$

where $C = (1 - \delta^*) \operatorname{ctg}(\gamma) + \chi \frac{(1 - 2/\pi)}{2E^*}$; $C_1 = a(1 - \delta^*) \operatorname{ctg}(\gamma)$; δ^* is the relative height of influx; E^* is the re-

duced modulus of elasticity; h^* is the depth of grain indentation; $\chi = \frac{\pi}{2} \lambda \sigma_T$ is the plasticity parameter.

Mathematical model. Optimization of the abrasion process requires the development of improved models of frictional interaction between abrasive particles and the surface of a metal component. In this model, it is required to require heating and surface wear due to the impact and sliding of an abrasive particle.

Under the abrasive processing, contact interaction occurs, which leads to wear and heating of the workpiece surface. The basic data on the processes of friction and wear are shown in [6]. Processing in a rotation chamber is described by M.A. Tamarkin and his disciples [1–5]. The features of this process are discussed in [7–9].

In the presented paper, the contact interaction of an abrasive particle and the workpiece surface is considered in the framework of axisymmetric deformation of an abrasive particle fragment and the workpiece surface. The abrasive particle fragment is a truncated cone, the smaller base of which interacts with the workpiece surface (Fig. 4).

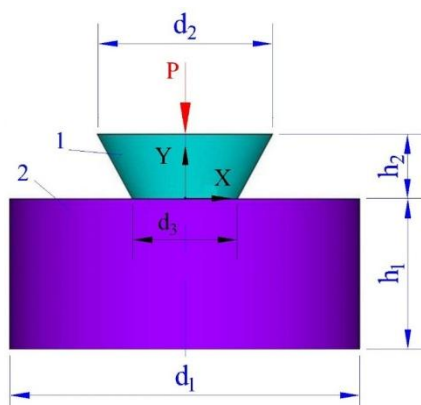


Fig. 4. Particle and workpiece model: 1 is abrasive particle; 2 is workpiece

According to the model, an abrasive particle (corundum) is a linearly elastic body, whose Young's modulus is much larger than that of the processed material. The processed material (steel) is modeled as an elastically plastic bilinear body. The Mises yield criterion [10] is applied.

The abrasive particle and the workpiece are in contact without friction. Contact surfaces are the upper plane of the workpiece, the smaller base and the side surface of the cone. The lower plane and the side surface of the workpiece are fixed normal. On the larger base of the truncated cone, boundary conditions are specified: power (uniformly distributed pressure) or kinematic (vertical displacement). The indentation of a particle into a workpiece is considered, the zone of plastic deformations and their maximum values are investigated.

Solution method. To solve the described boundary-value problems, the finite element method implemented in the ANSYS CAE package is used. Fig. 5 shows the finite element mesh of the first problem.

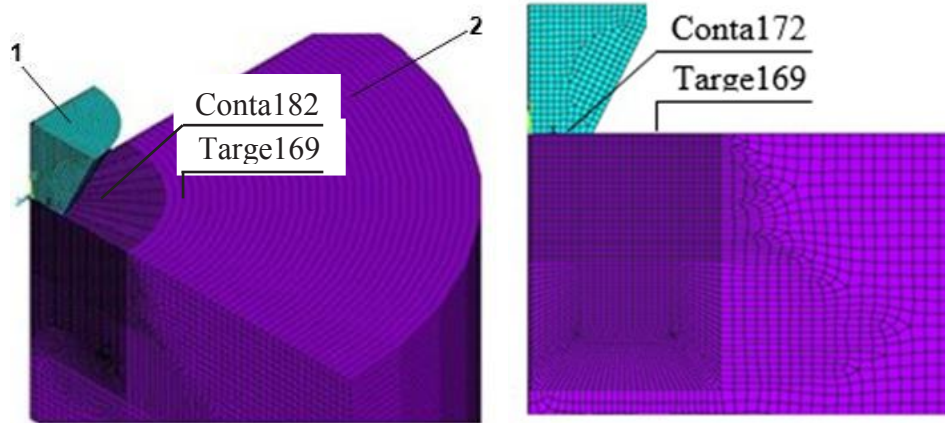


Fig. 5. Finite-element segmentation in the contact problem: 1 is abrasive particle; 2 is workpiece

In the contact area and possible plastic deformation, the grid is condensed. The end elements PLANE183 (material 1), PLANE182 (material 2) and TARGE169, CONTA172 are used for the contact surfaces. The abrasive particle and the workpiece are symmetrical; therefore, half the axial section is considered (see Fig. 5).

Results of numerical experiments. In the numerical calculations, the following data were used in the problem: the radii of a truncated cone were 0.5 mm and 1 mm; cone height was 1 mm; part radius was 5 mm; thickness was 3 mm. Young's modulus of the material 1 was equal to 2×10^6 GPa; Poisson's ratio was 0.3. Young's modulus of material 2 was equal to 2×10^2 GPa; Poisson's ratio was 0.28. The yield stress was 0.22 GPa. Fig. 6 shows the distribution of equivalent plastic deformations at a cone penetration depth of 0.01 mm (Fig. 6, a) and 0.05 mm (Fig. 6, b).

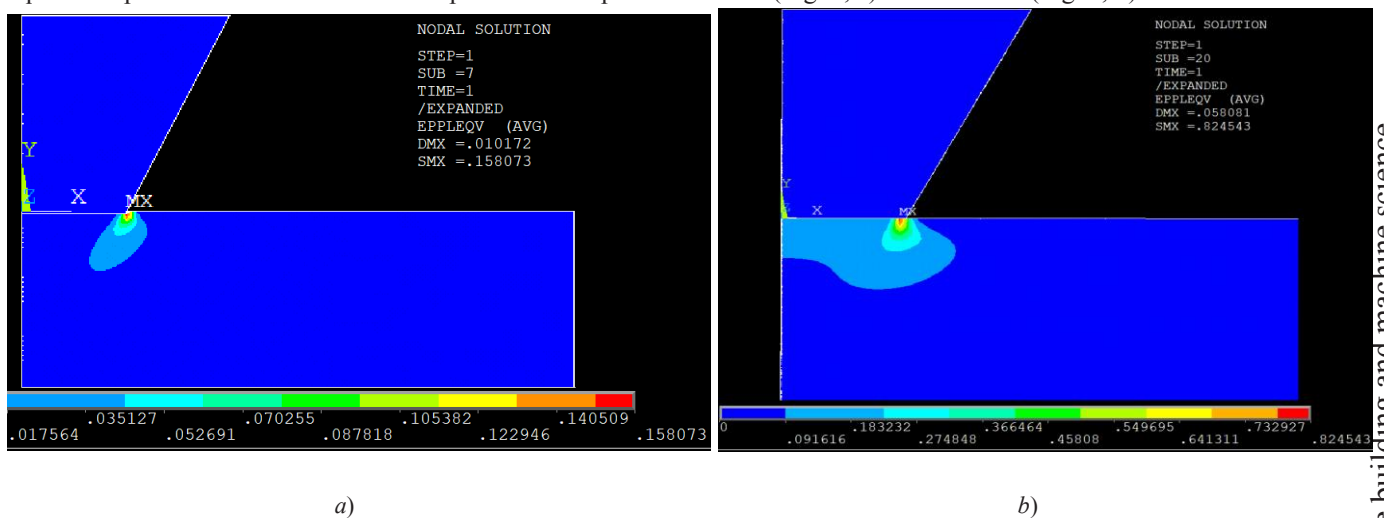


Fig. 6. Distribution of equivalent plastic deformations at cone penetration depth of 0.01 mm (a); 0.05 mm (b)

Fig. 7 shows the dependences of the maximum value of equivalent plastic deformation on the depth penetration (DP).

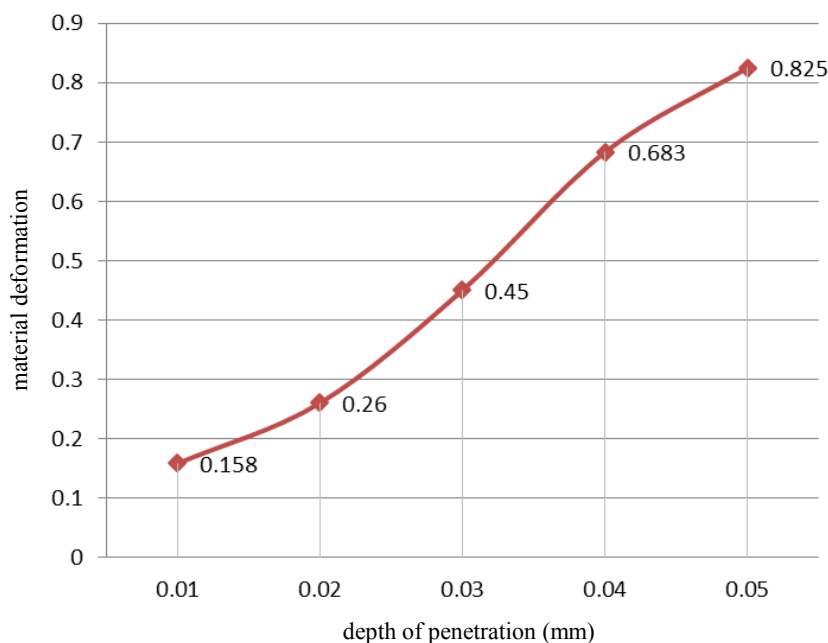


Fig. 7. Peak plastic deformations depending on the depth of penetration

In modeling experiments, the authors have found that equivalent plastic deformation is proportional to the penetration depth. Equivalent plastic deformation reaches a minimum value of 0.158 at a GV = 0.01 mm, a maximum of 0.825 at DP = 0.05 mm. The dependences of the sizes of the plastic deformation region on the penetration depth were determined for the cases when plastic deformation exceeded 1% (Fig. 8–10). Areas of plastic strain greater than 1% are selected using ANSYS software. In this case, the depth (H) and radius (L) of the deformation zone are determined.

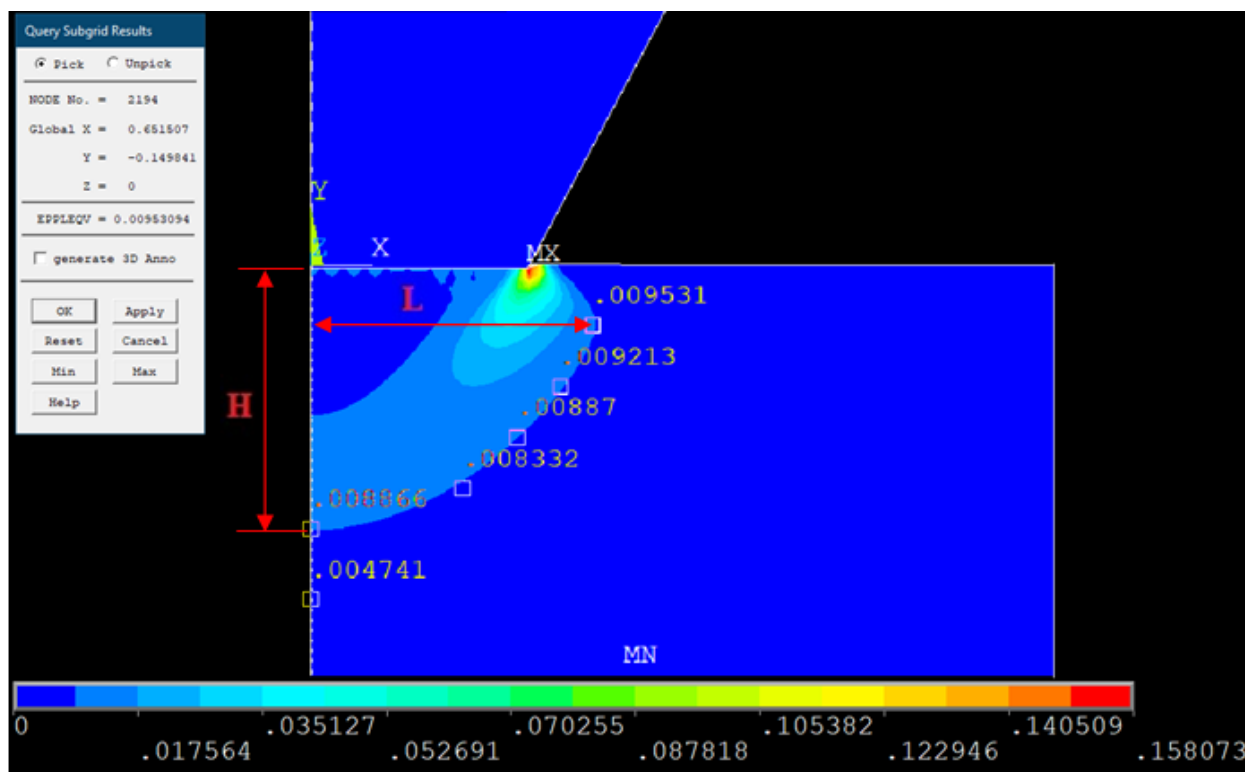


Fig. 8. Sizes of the plastic deformation region

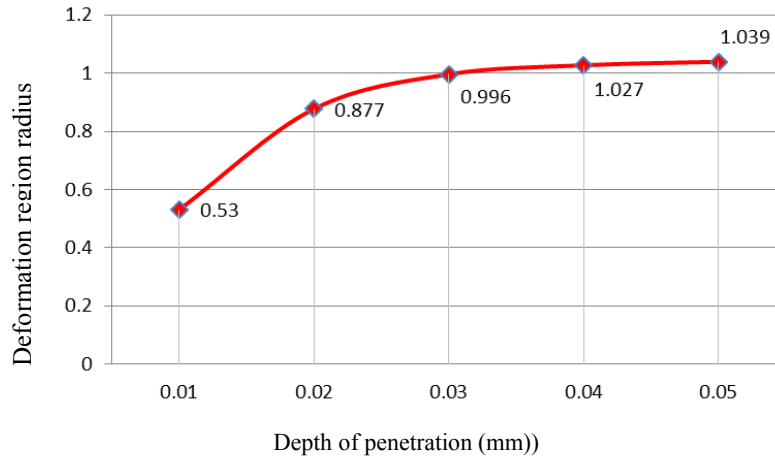


Fig. 9. Dependence of radius of plastic deformation region on penetration depth

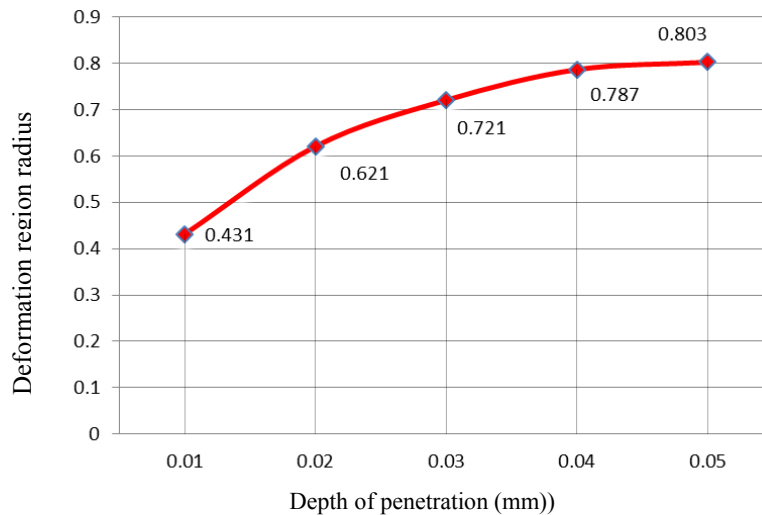


Fig. 10. Dependence of depth of plastic deformation region on penetration depth

The dependence of the cone penetration depth on the uniform pressure acting on its larger base is determined. This dependence is presented in Table 1.

Table 1

Dependence of cone depth penetration on pressure					
Voltage (N/mm ²)	100	150	200	250	300
Displacement (mm)	−0.059	−0.119	−0.237	−0.354	−0.530

The results of numerical experiments make it possible to determine the regions of plastic deformations and their magnitude depending on the penetration depth. The data in Table 1 relate them to the force that should be applied to the abrasive particle. This effort can be determined through the parameters of the process.

Discussion and Conclusions. In this work, we have performed:

- finite element modeling of the interaction of an abrasive particle and the workpiece surface;
- analysis of the stress-strain state of the surface.

The dependence of the peak plastic deformation on the cone penetration depth (0.01 mm - 0.05 mm) is determined. It is found that this value varies from 0.158 to 0.825.

The dependences of the sizes of the plastic deformation region on the penetration depth are determined for the cases when the plastic deformation exceeds 1%. At maximum penetration (0.05 mm), the deformation radius is 1 mm and the depth is 0.8 mm.

Based on these data, the process parameters (rotation speed, abrasive surface size, mass of abrasive particles) that affect the interaction between the workpiece and the abrasive particle can be selected. The rational choice of these parameters will improve the processing efficiency.

References

1. Tamarkin, M.A., Tishchenko, E.E., Drupov, V.V. Issledovanie udaleniya metalla pri tsentrobezhno-rotornoy obrabotke v abrazivnoy srede. [Study on metal removal during centrifugal rotor treatment in an abrasive medium.] Vestnik of P.A. Soloviyov Rybinsk State Aviation Technical University, 2007, no. 1 (11), pp. 169–186 (in Russian).
2. Tamarkin, M.A., et al. Teoreticheskie i eksperimental'nye issledovaniya protsessov obrabotki fazonnykh poverkhnostey detaley svobodnym abrazivom. [Theoretical and experimental study of process of shaped parts surfaces loose abrasive.] Strengthening Technologies and Coatings, 2011, no. 11, pp. 27–31 (in Russian).
3. Tamarkin, M.A., Tishchenko, E.E., Drupov, V.V. Formirovanie parametrov kachestva poverkhnosti dlya tsentrobezhno-rotornoy obrabotki v abrazivnoy srede. [Formation of parameters of quality of surface at centrifugal-rotational processing in the environment of the abrasive.] Strengthening Technologies and Coatings, 2007, no. 10, pp. 19–23 (in Russian).
4. Korolkov, Yu.V. Obespechenie nadezhnosti tekhnologicheskikh protsessov tsentrobezhno-rotatsionnoy obrabotki svobodnym abrazivom. [Reliability control of production processes of centrifugal-rotary treatment by loose abrasive.] Vestnik of DSTU, 2011, 8, pp. 1247–1254 (in Russian).
5. Shvedova, A.S., Kazakov, D.V. Obespechenie nadezhnosti tekhnologicheskogo protsessa tsentrobezhno-rotatsionnoy otdelochno-uprochnyayushchey obrabotki. [Software of reliability technology process of centrifugal rotary finishing-hardening treatment.] Vestnik of DSTU, 2014, no. 4, pp. 69–83 (in Russian).
6. Kragelskiy, I.V. Trenie i iznos. [Friction and wear.] Moscow: Mashinostroyeniye, 1968, 480 p. (in Russian).
7. Grützmacher, Ph.G. The influence of centrifugal forces on friction and wear in rotational sliding. Tribology International, 2017, no. 116, pp. 256–263. DOI: [org/10.1016/j.triboint.2017.07.021](https://doi.org/10.1016/j.triboint.2017.07.021).
8. Wenhui Li, et al. Theoretical and Simulation Analysis of Abrasive Particles in Centrifugal Barrel Finishing: Kinematics Mechanism and Distribution Characteristics. Powder Technology, 2017, no. 318, pp. 518–527. DOI: [10.1016/j.powtec.2017.06.033](https://doi.org/10.1016/j.powtec.2017.06.033).
9. Aurich, J.C., Hauschild, M., Carrella, M. Sustainability of abrasive processes. CIRP Annals. Manufacturing Technology, 2013, no. 62, pp. 653–672.
10. Silori, P., et al. Finite Element Analysis of Traction Gear Using ANSYS. Materialstoday Proceedings, 2015, vol. 2, pp. 2236–2245. DOI: [org/10.1016/j.matpr.2015.07.243](https://doi.org/10.1016/j.matpr.2015.07.243)

Submitted 25.02.2019

Scheduled in the issue 05.04.2019

Authors:

Soloviev, Arkady N.,

professor, Head of the Theoretical and Applied Mechanics Department, Don State Technical University

(1, Gagarin Square, Rostov-on-Don, 344000, RF), Dr.Sci. (Eng.), professor,

ORCID: <http://orcid.org/0000-0001-8465-5554>

solovievarc@gmail.com

Tamarkin, Mikhail A.,

Head of the Engineering Technology Department, Don State Technical University

(1, Gagarin Square, Rostov-on-Don, 344000, RF), Dr.Sci. (Eng.), professor,

ORCID: <http://orcid.org/0000-0001-9558-8625>

tehn_rostov@mail.ru

Nguyen Van Tho,

Researcher of the Electrical and Mechanical Engineering, Haiphong University

(117, Phan Dang Luu sq., Haiphong, 180000, Vietnam),

ORCID: <https://orcid.org/0000-0002-9105-7701>

thonguyen239@gmail.com

MACHINE BUILDING AND MACHINE SCIENCE МАШИНОСТРОЕНИЕ И МАШИНОВЕДЕНИЕ



UDC 678.549

<https://doi.org/10.23947/1992-5980-2019-19-3-221-230>

Efficient optimum safety factor approach for system reliability-based design optimization with application to composite yarns*

Ghias Kharmanda¹, Imad R. Antypas^{2**}

¹ France INSA Rouen Normandie, Saint-Etienne-du-Rouvray, France

² Don State Technical University, Rostov-on-Don, Russian Federation

Эффективность оптимизации проектирования на основе надёжности системы применительно к составным нитям^{3***}

Харманда М. Г.¹, Антибас И. Р.^{2**}

¹ France INSA Rouen Normandie, Saint-Etienne-du-Rouvray, Нормандия, Франция

² Донской государственный технический университет, г. Ростов-на-Дону, Российская Федерация

Introduction. The integration of reliability and optimization concepts seeks to design structures that should be both economic and reliable. This model is called Reliability-Based Design Optimization (RBDO). In fact, the coupling between the mechanical modelling, the reliability analyses and the optimization methods leads to very high computational cost and weak convergence stability.

Materials and Methods. Several methods have been developed to overcome these difficulties. The methods called Reliability Index Approach (RIA) and Performance Measure Approach (PMA) are two alternative methods. RIA describes the probabilistic constraint as a reliability index while PMA was proposed by converting the probability measure to a performance measure. An Optimum Safety Factor (OSF) method is proposed to compute safety factors satisfying a required reliability level without demanding additional computing cost for the reliability evaluation. The OSF equations are formulated considering RIA and PMA and extended to multiple failure case.

Research Results. Several linear and nonlinear distribution laws are applied to composite yarns studies and then extended to multiple failure modes. It has been shown that the idea of the OSF method is to avoid the reliability constraint evaluation with a particular optimization process.

Discussion and Conclusions. The simplified implementation framework of the OSF strategy consists of decoupling the optimization and the reliability analyses. It provides designers with efficient solutions that should be economic satisfying a required reliability level. It is demonstrated that the RBDO

Введение. Интеграция концепций надёжности и оптимизации направлена на разработку структур, которые должны быть экономичными и надёжными. Эта модель называется Оптимизация проектирования на основе надёжности (RBDO). Фактически связь между механическим моделированием, анализом надёжности и методами оптимизации приводит к очень высоким вычислительным затратам и слабой стабильности конвергенции.

Материалы и методы. Для преодоления этих трудностей было разработано несколько методов. Методы под названием «Индекс показателя надёжности» (RIA) и «Метод оценки эффективности» (PMA) – это два альтернативных метода. RIA описывает вероятностное ограничение как индекс надёжности, в то время как PMA был предложен как путь преобразования вероятностной меры эффективности. Предложен метод оптимального коэффициента безопасности (OSF) для расчета коэффициентов безопасности, удовлетворяющих требуемому уровню надёжности, без дополнительных вычислительных затрат для оценки надёжности. Уравнения OSF сформулированы с учетом RIA и PMA и расширены до случая с несколькими отказами.

Результаты исследования. Несколько линейных и нелинейных законов распределения применяются к исследованиям композиционных нитей, а затем распространяются на множественные режимы отказа. Было показано, что идея метода OSF заключается в том, чтобы избежать оценки ограничения надёжности с помощью конкретного процесса оптимизации.

Обсуждение и выводы. Упрощенная структура реализации стратегии OSF заключается в разделении анализа оптимизации и надёжности. Она предоставляет проектировщикам эффективные решения, которые должны экономически удовлетворять требуемый уровень

* The research is done within the frame of the independent R&D.

** E-mail: ghias.kharmanda@bme.lth.se, imad.antypas@mail.ru

*** Работа выполнена в рамках инициативной НИР.



compared to OSF has several advantages: small number of optimization variables, good convergence stability, small computing time, satisfaction of the required reliability levels.

Keywords: Reliability-Based Design Optimization, Structural Reliability, Safety Factors, Fatigue Damage Analysis, Multi Failure Scenarios.

For citation: Kharmanda Ghias, Antypas Imad R.. Efficient optimum safety factor approach for system reliability-based design optimization with application to composite yarns. Vestnik of DSTU, 2019, vol. 19, no.3, pp. 221–230. <https://doi.org/10.23947/1992-5980-2019-19-3-221-230>

надежности. Показано, что RBDO в сравнении с OSF имеет ряд преимуществ: небольшое число переменных оптимизации, хорошая стабильность сходимости, малое время вычислений, удовлетворение требуемым уровням надежности.

Ключевые слова: оптимизация на основе надежности, структурная надежность, факторы безопасности, анализ ущерба от изношенности, сценарии множественных отказов.

Образец для цитирования: Харманда, М. Г. Эффективность оптимизации проектирования на основе надежности системы применительно к составным нитям / М. Г. Харманда, И. Р. Антипас // Вестник Дон. гос. техн. ун-та. — 2019. — Т.19, №3. С. 221–230. <https://doi.org/10.23947/1992-5980-2019-19-3-221-230>

1. Introduction

When Deterministic Design Optimization (DDO) methods are used, deterministic optimum designs are usually pushed to the design constraint boundary, leaving little or no room for tolerances (or uncertainties) in design, manufacture, and operating processes. So deterministic optimum designs obtained without consideration of uncertainties could lead to unreliable designs, therefore calling for Reliability-Based Design Optimization (RBDO). It is the objective of RBDO to design structures that should be both economic and reliable. However, the coupling between the mechanical modeling, the reliability analyses and the optimization methods leads to very high computational cost and weak convergence stability. To overcome these difficulties, two points of view have been considered. From a reliability view point, RBDO involves the evaluation of probabilistic constraints, which can be executed in two different ways: either using the Reliability Index Approach (RIA) or the Performance Measure Approach (PMA) [1]. The major difficulty lies in the evaluation of the probabilistic constraints, which is prohibitively expensive and even diverges for many applications. However, from an optimization view point, a hybrid method based on simultaneous solution of the reliability and the optimization problem has successfully reduced the computational time problem. However, the hybrid RBDO problem is more complex than that of deterministic design and may not lead to local optima. To overcome both drawbacks, an Optimum Safety Factor (OSF) method has been proposed to compute safety factors satisfying a required reliability level without demanding additional computing cost for the reliability evaluation. The efficiency of the OSF method has been demonstrated relative to the hybrid one for a linear distribution law [2]. In this work, the OSF is reformulated considering RIA and PMA. Next, an extension to multiple failure modes is carried out. Finally, an application on composite yarns is carried out for linear and nonlinear distribution laws and multiple failure modes (scenarios).

2. Reliability-Based Design Optimization

The reliability-based design optimization problem is performed by nesting two sub-problems [3, 4]:

1: Optimization problem: The objective is to minimize an objective function $f(x)$ subject to deterministic constraints $g_k(x) \leq 0$ and a required reliability level $\beta(x, u) \geq \beta_t$ as follows:

$$\min : f(x) \quad \text{subject to } g_k(x) \leq 0 \text{ and } \beta(x, u) \geq \beta_t \quad (1)$$

2: Reliability problem: The objective is to find the minimum distance between the origin of the normalized space and the MPP (Most Probable failure Point or design point) on the limit state function (Fig. 1). The problem can be written as follows:

$$\beta = \min d(u) = \sqrt{\sum_{i=1}^n u_i^2} \quad \text{subject to } H(x, u) \leq 0 \quad (2)$$

For more details about reliability analysis, readers can see [5]. These two sub-problems are carried in two different spaces: physical and normalized spaces (Fig. 1).

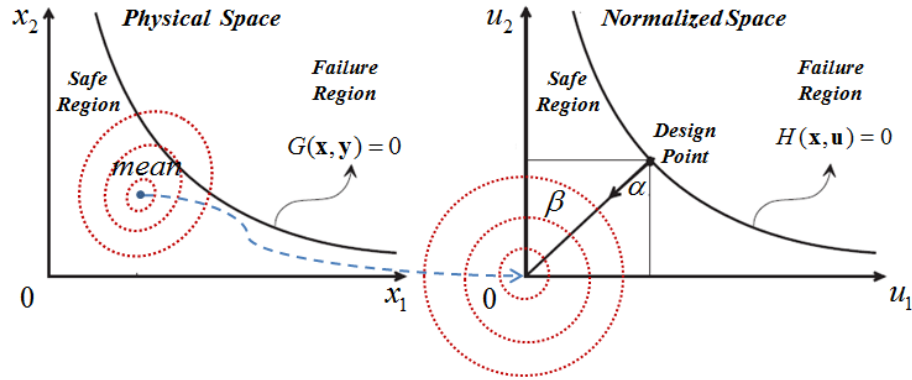


Fig. 1. Physical and normalized spaces [3, 4]

These nested problems require a high computing time, however, the Optimum Safety Factor (OSF) is used to solve these numerical difficulties.

3. OSF developments

In the RIA and PMA, the major difficulty lies in the evaluation of the probabilistic (reliability) constraints; this is prohibitively expensive and even diverges for many applications [6]. RIA describes the probabilistic constraint as a reliability index while PMA was proposed by converting the probability measure to a performance measure. It has been found in the literature that PMA is more efficient and stable than RIA in the RBDO process [1]. Furthermore, PMA converges to different optimum solutions when starting from different initial designs [7]. In this section, it is shown that the OSF formulations can be deduced from both approaches (RIA & PMA).

3.1 OSF considering RIA and PMA

3.1.1 OSF based on RIA

The probabilistic constraint in RIA can be evaluated by solving the first-order reliability analysis to calculate the design point P^* , which is formulated as an optimization problem with an equality constraint $H(\mathbf{u}) = 0$, in the normalized space:

$$\begin{aligned} \min_{\mathbf{u}} \quad & d(\mathbf{u}) \\ \text{subject to:} \quad & H(\mathbf{u}) = 0 \end{aligned} \quad (3a)$$

and can be also written as:

$$\begin{aligned} \min_{\mathbf{u}} \quad & d^2(\mathbf{u}) \\ \text{subject to:} \quad & H(\mathbf{u}) = 0 \end{aligned} \quad (3b)$$

The Lagrangian function for the problem (3b) can be written as

$$L(\mathbf{u}, \lambda) = d^2(\mathbf{u}) + \lambda \cdot H(\mathbf{u}) \quad (4)$$

The optimality conditions for the Lagrangian function are:

$$\frac{\partial L}{\partial u_i} = \frac{\partial d^2}{\partial u_i} + \lambda \frac{\partial H}{\partial u_i} = 0 \quad , \quad i = 1, \dots, n \quad (5a)$$

$$\frac{\partial L}{\partial \lambda} = H(\mathbf{u}) = 0 \quad (5b)$$

Using the expression for the square distance d^2 in the equation (3b), we get:

$$u_i = -\frac{\lambda}{2} \frac{\partial H}{\partial u_i}, \quad i = 1, \dots, n \quad (6)$$

3.1.2 OSF based on PMA

The evaluation of the probabilistic constraint in PMA requires an inverse reliability analysis, which corresponds to the inverse problem of the reliability analysis to calculate the design point P^* , which is formulated as an optimization problem with an equality constraint $d^2(\mathbf{u}) = \beta_t^2$, in normalized space:

$$\begin{aligned} \min_{\mathbf{u}} \quad & H(\mathbf{u}) \\ \text{subject to:} \quad & d(\mathbf{u}) = \beta_t \end{aligned} \quad (7a)$$

and can be also written as:

$$\begin{aligned} \min_u & : H(u) \\ \text{subject to: } & d^2(u) = \beta_t^2 \end{aligned} \quad (7b)$$

The Lagrangian function for the problem (7b) can be written as

$$L(u, \lambda, s) = H(u) + \lambda \cdot [d^2(u) - \beta_t^2] \quad (8)$$

The optimality conditions for the Lagrangian function are:

$$\frac{\partial L}{\partial u_i} = \frac{\partial H}{\partial u_i} + \lambda \frac{\partial d^2}{\partial u_i} = 0, \quad i = 1, \dots, n \quad (9a)$$

$$\frac{\partial L}{\partial \lambda} = d^2(u) - \beta_t^2 = 0 \quad (9b)$$

Using the expression for the square distance d^2 in the equation (7b), we get:

$$u_i = -\frac{1}{2\lambda} \frac{\partial H}{\partial u_i}, \quad i = 1, \dots, n \quad (10)$$

According to equations 6 and 10, the resulting normalized vector u can be written in term of the same derivative $\partial H / \partial u_i$.

3.2 OSF for component RBDO

Let us consider now the case of $n=2$ normalized variables $i = 1, 2$ (see Fig. 2). The tangent of α is given by: $\tan \alpha = u_2 / u_1$. Using (6) and (10), we get the same formulations as follows:

$$\tan \alpha = \frac{\frac{\partial H}{\partial u_2}}{\frac{\partial H}{\partial u_1}} \quad (11)$$

The formulation (11) shows that there is no difference between RIA and PMA for the following OSF developments. The problems (3) and (7) give us the reliability index β as the minimum distance between the limit state surface and the origin [8]. This means that the resulting reliability index may be lower or higher than the target reliability index β_t . As we wish to satisfy a required target reliability level for the optimization problem, we can write

$$\beta_t^2 = \sum_{i=1}^n u_i^2 \quad (12)$$

Thus, the general expression for the normalized variable u_i when using RIA or PMA, is

$$u_i = \pm \beta_t \sqrt{\frac{\left(\frac{\partial H}{\partial u_i}\right)^2}{\sum_{j=1}^n \left(\frac{\partial H}{\partial u_j}\right)^2}}, \quad i = 1, \dots, n \quad (13)$$

The calculation of the normalized gradient $\partial H / \partial u$ is not directly accessible because the mechanical analysis is carried out in the physical space rather than in the standard space [9, 10]. However, using theory of statistics, we can derive the following expression from which the computation of the normalized gradient can be carried out by applying the chain rule on the physical gradient $\partial G / \partial y$:

$$\frac{\partial H}{\partial u_i} = \frac{\partial G}{\partial y_k} \frac{\partial T_k^{-1}(x, u)}{\partial u_i}, \quad i = 1, \dots, n, \quad k = 1, \dots, K \quad (14)$$

where $T^{-1}(x, u)$ is the inverted probabilistic transformation function. We find that the normalized gradient can be expressed as

$$\frac{\partial H}{\partial u_i} = \sqrt{\frac{\partial G}{\partial y_i}} \quad , \quad i = 1, \dots, n \quad (15)$$

To summarize, we satisfy the required target reliability index as follows:

$$d_\beta = \beta_t = \sqrt{\sum_{i=1}^n (u_i^*)^2} \quad , \quad i = 1, \dots, n \quad (16)$$

Thus, we compute the optimum safety factors subject to the optimum values of the normalized variables u_i^* . According to (13) and (15), it has been demonstrated that the optimum values of u_i^* can be written in the following form:

$$u_i^* = \pm \beta_t \sqrt{\frac{\left| \frac{\partial G}{\partial y_i} \right|}{\sum_{j=1}^n \left| \frac{\partial G}{\partial y_j} \right|}} \quad , \quad i = 1, \dots, n \quad (17)$$

where the sign of \pm depends on the sign of the derivative, i.e.:

$$\frac{\partial G}{\partial y_i} > 0 \Leftrightarrow u_i^* > 0 \quad \text{and} \quad \frac{\partial G}{\partial y_i} < 0 \Leftrightarrow u_i^* < 0 \quad , \quad i = 1, \dots, n \quad (18)$$

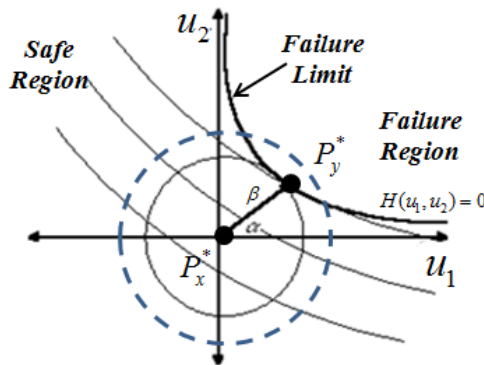


Fig. 2. Design point modeling in a double normalized variable space

The efficiency of the OSF is to transfer the reliability problem into an analytical formulation (17). This formulation has been extended to several distribution laws (normal, lognormal, uniform Weibull, and Gumbel laws) for single failure mode cases considering only RIA [11]. However, in this work, both RIA and PMA are used to show the efficiency of the OSF formulation, and an extension to multiple failure case is carried out in the next section.

3.3 OSF for system RBDO

The system reliability problem can be written as:

$$\beta_{system} = \min d(u_i) = \sqrt{u_1^2 + u_2^2 + \dots + u_n^2} \quad \text{s.t.:} \quad H_j(u_1, u_2, \dots, u_m) \leq 0 \quad (19)$$

where $d(u_i)$ is the minimum distance between the Most Probable failure Point (MPP) and the optimal solution in the normalized space (Fig. 1). And $H_j(u_i) \leq 0$ represent the different failure modes. Using similar way, the analytical formulation using OSF for a system RBDO can be written as follows:

$$u_i^* = \pm \beta_t \sqrt{\frac{\left| \sum_{j=1}^m \frac{\partial G_j}{\partial y_i} \right|}{\sum_{i=1}^n \left| \sum_{j=1}^m \frac{\partial G_j}{\partial y_i} \right|}} \quad (20)$$

The formulation (20) provides different optimum values of the normalized variables at the failure point and taking into account several failure modes.

4. Numerical Application on composite yarns

Composite materials have been used in structures for centuries. In recent times, composite parts have been used extensively in aircraft structures, automobiles, sporting goods, and many consumer products. Composite materials are those containing more than one bonded material, each with different structural properties. The main advantage of composite materials is the potential for a high ratio of stiffness to weight. To solve the composite yarns structures (or systems), a stress unilateral study is required.

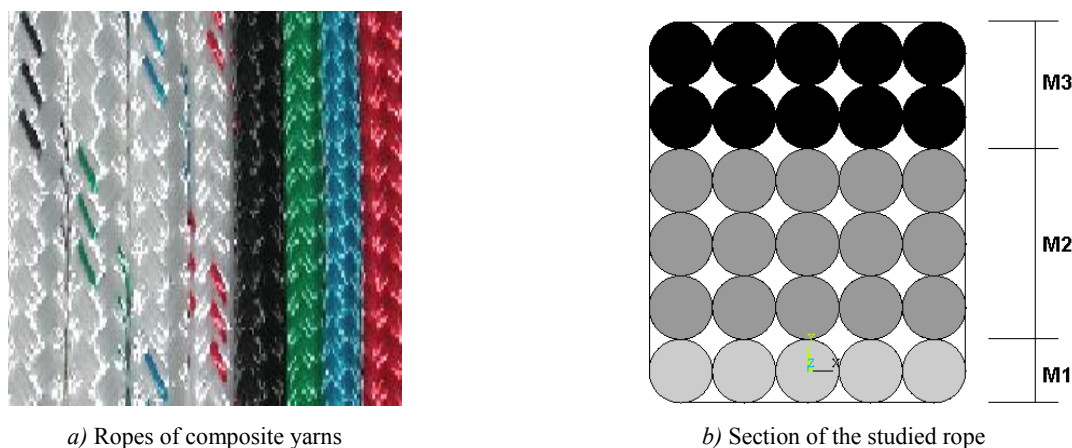


Fig. 3. Material structure

4.1 Problem description

For tri-material structure illustrated in Fig. 3, the number of yarns n_i , the section S_i , the Young's modulus E_i , the Poisson's ratio ν_i and material density ρ_i are given according to each material as shown in Table 1.

Table 1

Material properties of different used yarns					
Material number	n_i	S_i (m ²)	E_i (Pa)	ν_i	ρ_i (Kg/m ³)
M1	5	10e-8	5.8e6	0.4	4.0
M2	15	10e-8	8e6	0.3	5.0
M3	10	10e-8	9e6	0.2	6.0

4.1 Single yarn behavior

A stress unilateral structure is not capable of transmitting compression, i.e. negative stress: all its internal efforts are traction. The formulation of this problem is complex and may lead to non-existence of solutions or several approximate solutions. Some methods have been developed to determine a solution among all resulting configurations [12].

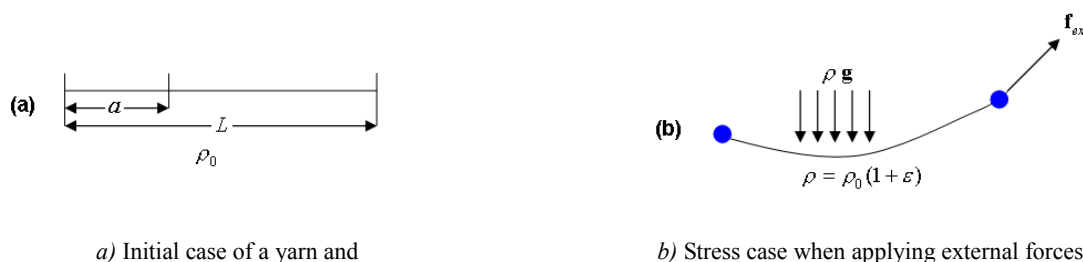


Fig. 4. The tension on the yarn

The behaviour of an elastic file is not defined by the single Hooke's law; even in the frame of the linear elasticity, we have

$$\varepsilon = \frac{T}{K} \quad \text{and} \quad T \geq 0 \quad (21)$$

where $K > 0$ is the constant of elasticity and T is the tension which defines the internal efforts of the studied yarn. The total section is given by

$$S = \sum_{i=1}^{n_1} S_{1,i} + \sum_{j=1}^{n_2} S_{2,j} + \sum_{k=1}^{n_3} S_{3,k} \quad (22)$$

and the total tension is given by

$$T = \sum_{i=1}^{n_1} T_{1,i} + \sum_{j=1}^{n_2} T_{2,j} + \sum_{k=1}^{n_3} T_{3,k} \quad (23)$$

with

$$T_{1,i} = \frac{S_{1,i}}{S} T, \quad T_{2,j} = \frac{S_{2,j}}{S} T \quad \text{and} \quad T_{3,k} = \frac{S_{3,k}}{S} T$$

Fig. 4a shows the initial case of a yarn in which the volume mass $= \rho_0$. When applying an external force and considering the gravity force (see Fig. 4b), the equilibrium vector equation can be written as

$$\frac{dT}{da} + \rho_0 g = 0, \quad (24)$$

with $\rho = \rho_0(1 + \varepsilon)$.

For our studied rope, there is a non gravity force $\rho_0 g = 0$. So, we get

$$T(L) = f_{ext} \quad (25)$$

This way, the tension is a proportional value of the external force as follows

$$T_{1,i} = \frac{S_{1,i}}{S} f_{ex}, \quad T_{2,j} = \frac{S_{2,j}}{S} f_{ex} \quad \text{and} \quad T_{3,k} = \frac{S_{3,k}}{S} f_{ex} \quad (26)$$

Here, the failure conditions are written as follows:

$$\varepsilon_{1,i} \leq \varepsilon_{1,\max}, \quad \varepsilon_{2,j} \leq \varepsilon_{2,\max} \quad \text{and} \quad \varepsilon_{3,k} \leq \varepsilon_{3,\max} \quad (27)$$

In order to compute the maximum strain of each material, we have

$$\varepsilon_{1,i} = \frac{T_{1,i}}{K_{1,i}}, \quad \varepsilon_{2,j} = \frac{T_{2,j}}{K_{2,j}} \quad \text{and} \quad \varepsilon_{3,k} = \frac{T_{3,k}}{K_{3,k}} \quad (28)$$

4.3 Procedures

DDO procedure:

The optimization problem is to minimize the mass subject to the allowable strain ε_w and taking a global safety factor S_f . This optimization problem must be followed by the reliability analysis as follows:

1- Optimization problem

$$\min \quad mass(x) \quad \text{subject to} \quad \varepsilon(x) \leq \varepsilon_w = \varepsilon_{lim} / S_f \quad (28)$$

2- Reliability analysis

$$\beta = \min d(u) = \sqrt{\sum_{i=1}^n u_i^2} \quad \text{subject to} \quad \varepsilon(u) \leq \varepsilon_{lim} \quad (29)$$

RBDO procedure

Using OSF method, the RBDO procedure contains three main steps:

1- The first step is to obtain the design point (MPP). It is the objective to minimize the volume subject to the design constraints without consideration of the safety factors. This way, the optimization problem for a single failure mode is simply written as:

$$\min \quad mass(y) \quad \text{subject to} \quad \varepsilon(y) \leq \varepsilon_{lim} \quad (30)$$

and for a multiple (double) failure mode as follows:

$$\min \quad mass(y) \quad \text{subject to} \quad \varepsilon(y) \leq \varepsilon_{lim} \quad (31)$$

$$T(y) \leq T_{lim}$$

2- The second step is to compute the optimum safety factors using linear and nonlinear distributions [9] when the number of the deterministic variables is equal to that of the random ones. During the optimization process, we obtain the sensitivity values of the limit state with respect to all variables.

3- The third step is to calculate the optimum solution. This encompasses inclusion of the resulting values of the safety factors into the design variables in order to evaluate the optimum solution.

4.4 Numerical results

4.4.1 Component RBDO

According to Table 2, the DDO procedure leads to a high reliability index, while the RBDO one satisfies the required reliability level for the linear and nonlinear distribution laws. The resulting reliability index is: $\beta = 3$ that corresponds to a probability of failure ($P_f \approx 0.1\%$).

Table 2

DDO and RBDO results for a single failure mode

Parameters	Design Point	Optimum Solution				
		DDO	RBDO			
		Normal	Normal	Lognormal	Uniform	Weibull
S1	0.2900	0.4400	0.3415	0.3387	0.3413	0.3455
S2	0.4750	0.8500	0.5774	0.5698	0.5655	0.5922
S3	0.5550	1.2300	0.6846	0.6737	0.6632	0.7072
ε_{\max}	0.0095	0.0048	0.0078	0.0079	0.0080	0.0076
Mass	0.034	0.0669	0.042	0.041	0.041	0.043
β	--	7.8231	3.00	3.00	3.00	3.00
S_{f1}	--	--	0.849274	0.856135	0.849613	0.839352
S_{f2}	--	--	0.822641	0.833690	0.839981	0.802099
S_{f3}	--	--	0.810724	0.823839	0.836908	0.784831

4.4.2 System RBDO

It is easy to study structures under the most critical mode but it may provide inaccurate results for structural reliability analysis. When dealing with several failure modes, the sensitivity study of each failure mode with respect to all parameters may lead to strange results for the role of certain parameters. The required reliability for both failure modes (tension and strain) is considered to be: $\beta_t = 3$ that leads to a system reliability index $\beta_{\text{System}} \geq \beta_t$. The system reliability index should be bigger or equal to the minimum required reliability index of all failure modes $\beta_{\text{System}} \geq \min(\beta_j)$. Table 3 shows Linear and nonlinear RBDO results for the same target reliability index for both failure modes.

Table 3

Linear and nonlinear RBDO results for multiple failure modes

Parameters	Design Point	Optimum Solution			
		Normal	Lognormal	Uniform	Weibull
S1	0.2900	0.3432	0.3402	0.3421	0.3479
S2	0.4750	0.5774	0.5698	0.5655	0.5922
S3	0.5550	0.6850	0.6740	0.6632	0.7078
ε	0.0095	0.0078	0.0079	0.0080	0.0076
T	66335	58956	59526	59909	57830
Mass	0.0343	0.0418	0.0413	0.0409	0.0430
β_{system}	0.0000	3.0242	3.0242	3.0241	3.0183
S_{f1}	0.00	0.845081	0.852562	0.847811	0.833615
S_{f2}	0.00	0.822641	0.833690	0.839981	0.802099
S_{f3}	0.00	0.810263	0.823460	0.836803	0.784156

6. Conclusions

In this paper, the OSF method is shown as a distinctive tool for RBDO problems. This method is based on the sensitivity of the limit-state function with object of determining the role of each studied parameter relative to the failure mode (or modes). First of all, it has been shown that the idea of the OSF method is to avoid the reliability constraint evaluation with a particular optimization process. In addition to its simplified implementation framework to completely decouple the optimization and the reliability analyses, it provides designers with efficient solutions that should be economic satisfying a required reliability level. The developed equation of OSF basing on both of RIA and PMA leads to the same formulations. The OSF procedure needs only single optimization process for the design point without additional computing time because it has a single variable vector. Finally, the developments based on the reliability view point are less efficient than those based on the optimization view point because the second provides us with reliability-based optimum designs without additional computing cost for probabilistic (reliability) constraints and can lead to global optima. It is shown that the RBDO compared to OSF has several advantages: small number of optimization variables, good convergence stability, small computing time, satisfaction of the required reliability levels. For composite structures, the RBDO problems are more difficult than for simple structures because we deal with several related limit state functions.

References

1. Youn, B.D. and Choi, K.K. Selecting Probabilistic Approaches for Reliability-Based Design Optimization, AIAA Journal, January 2004, vol. 42, no. 1.
2. Kharmanda, G., Sharabaty, S., Ibrahim, H., Makhoulfi, A.H., El Hami, A. Reliability-based design optimization using semi-numerical methods for different engineering application. International Journal of CAD/CAM, 2009, vol. 9, pp. 1-16.
3. Lopez, R.H., Beck A.T. Reliability-Based Design Optimization Strategies Based on FORM: A Review. J. of the Braz. Soc. of Mech. Sci. & Eng., 2012, vol. 34 (4), pp. 506-514.
4. Steenackers, G., Versluys, R., Runacres, M., Guillaume, P. Reliability-based design optimization of computation-intensive models making use of response surface models. Quality and Reliability Engineering International, 2011, vol. 27 (4), pp. 555–568.
5. Kharmanda, G., Antypas, I. Integration of Reliability Concept into Soil Tillage Machine Design. Vestnik of DSTU, 2015, vol. 15, no. 2 (81), pp. 22-31. DOI: 10.12737/11610. ISSN 1992-5980.
6. Kharmanda, G., Antypas, I. Integration of reliability and optimization concepts into composite yarns. Current Status and Prospects of Agricultural Engineering, Interagromash-2017: Proc. 10-th Int. Sci.-Pract. Conf. (Borisova, L., et al., eds.), DSTU Publ. Centre, Rostov-on-Don, Russia, 1-3 March, 2017, pp. 174-176.
7. Yang, R.J., Chuang, C., Gu, L., Li, G. Experience with approximate reliability-based optimization methods II: an exhaust system problem. Structural and Multidisciplinary Optimization, 2005, vol. 29, pp. 488-497.
8. Hasofer, A.M., Lind, N.C. An exact and invariant first order reliability format. J. Eng. Mech, ASCE, EM1, 1974, vol. 100, pp. 111-121.
9. Kharmanda, G., Antypas, I. Reliability-Based Design Optimization Strategy for Soil Tillage Equipment Considering Soil Parameter Uncertainty. Vestnik of DSTU, 2016, vol. 16, no. 2 (85), pp. 136-147. ISSN 1992-5980.
10. Du, X., Chen, W. Sequential Optimization and Reliability Assessment method for Efficient Probabilistic Design. ASME J. Mech. Des., 2004, vol. 126(2), pp. 225-233.
11. Kharmanda, G., Antypas, I. System reliability-based design optimization using optimum safety factor with application to multi failure fatigue analysis. Current Status and Prospects of Agricultural Engineering, Interagromash-2017: Proc. 10-th Int. Sci.-Pract. Conf. (Borisova, L., et al., eds.), DSTU Publ. Centre, Rostov-on-Don, Russia, 1-3 March, 2017, pp. 174-176.
12. Souza de Cursi E. Stress unilateral analysis of mooring cables. International Journal for Numerical Methods in Engineering, 1992, vol. 34, pp. 279-302.

Submitted 29.02.2018

Scheduled in the issue 26.06.2019

Authors:

Kharmanda Ghias,

guest Researcher, Institut National des Sciences Appliquées de Rouen (INSA Rouen Normandie),
France (France 76801 Saint - Etienne- du- Rouvray St. 685 avenue de l universite BP08
LMN, INSA Rouen Normandie), H.D.R. European Dr. Eng. (Docent Degree of Habilitation),
ORCID: <http://orcid.org/0000-0002-8344-9270>
g.karamanda@gmail.com

Antypas, Imad Rizakalla,

associate professor of the Machine Design Principles Department, Don State Technical University
(1, Gagarin sq., Rostov-on-Don, 344000, RF), Cand.Sci. (Eng.), associate professor,
ORCID: <http://orcid.org/0000-0002-8141-9529>
Imad.antypas@mail.ru

MACHINE BUILDING AND MACHINE SCIENCE МАШИНОСТРОЕНИЕ И МАШИНОВЕДЕНИЕ



UDC 621.824.32

<https://doi.org/10.23947/1992-5980-2019-19-3-231-241>

Micrometric research results of vacuum dough divider components*

E. G. Martynova¹, S. A. Velichko², A. V. Martynov^{3**}

^{1,2,3} Ogarev Mordovia State University, Saransk, Russian Federation

Результаты микрометрических исследований деталей тестоделительных машин вакуумного типа***

Е. Г. Мартынова¹, С. А. Величко², А. В. Мартынов^{3**}

^{1,2,3} Национальный исследовательский Мордовский государственный университет, г. Саранск, Российская Федерация

Introduction. Nowadays, vacuum-type dough dividers are used in industries with a production volume of up to 4,000 loaves per day. In the dough divider operation, due to wear of the working surfaces of the piston, chamber, and drum, the gap between them goes beyond the value equal to 50 microns, which provides vacuum in the suction chamber. As a result, the suction process becomes unstable; the dough divider disturbs the weight accuracy of bakery goods. Repair of such equipment is carried out mainly through a full or partial replacement of worn parts and assemblies with new ones. To increase their durability, there is a need to develop a new highly efficient technology with the restoration of worn part surfaces using the welding and surfacing methods.

Materials and Methods. A new technique of determining the number of objects for research using the “STATISTICA” program is presented. Wear surfaces of the vacuum dough divider parts are determined.

Research Results. Micrometric studies of the dough divider components were carried out. They showed the presence of appreciable size distortions due to the local wear of the working surfaces. In this case, a side gap between the suction chamber and the main piston and between the drum and the suction chamber is 6 times higher than the permissible one, and a vertical gap between the division box and the piston exceeds the permissible gap by more than 10 times. Wear of the working surfaces of the dough divider parts is local in nature, while the range of values is as follows: for the main piston, it is 10–200 microns; for the gaging piston, it is 250–900 microns; for the suction chamber and division box, it is 300–400 microns; for the drum surfaces, it is 280–300 microns.

Введение. В настоящее время на производствах с объемом выпуска до 4 000 булок в день используются тестоделительные машины вакуумного типа. В процессе эксплуатации тестоделительного устройства из-за износов рабочих поверхностей поршня, камеры, барабана зазор между ними выходит за величину, равную 50 мкм, при которой обеспечивается вакуум во всасывающей камере. В результате этого процесс всасывания становится нестабильным, тестоделительное устройство нарушает точность развесовки хлебобулочных изделий. Ремонт такого оборудования проводится в основном с использованием полной или частичной замены изношенных деталей и узлов на новые. Для повышения их долговечности возникает потребность в разработке новой высокоэффективной технологии с восстановлением изношенных поверхностей деталей сварочно-наплавочными методами.

Материалы и методы. Представлена новая методика определения количества объектов для исследования с использованием программы «Статистика». Определены поверхности износа деталей тестоделительных машин вакуумного типа.

Результаты исследования. Проведены микрометрические исследования деталей тестоделительных устройств, которые показали наличие у них значительных искажений размеров из-за локального износа рабочих поверхностей. При этом боковой зазор между всасывающей камерой и главным поршнем, барабаном и всасывающей камерой в 6 раз превышает допустимый, а вертикальный зазор между мерной камерой и поршнем превышает допустимый зазор более чем в 10 раз. Износы рабочих поверхностей деталей тестоделительных машин носят локальный характер, при этом диапазон значений составляет: для главного поршня — 10–200 мкм; мерного поршня — 250–900 мкм; всасывающих и мерных камер — 300–400 мкм; поверхностей барабана — 280–300 мкм.



* The research is done within the frame of Contract No. 18-43130003/18.

** E-mail: el.mart2012@yandex.ru, Velichko2005@yandex.ru, Martynov-230685@yandex.ru

*** Работа выполнена по договору №18-43130003/18.

Discussion and Conclusions. The conducted micrometric studies showed the presence of appreciable size distortions due to the local wear of the working surfaces. Based on the results obtained, it can be argued that the most productive and economically viable technique for the restoration of worn surfaces of dough divider parts is, for example, the electrospark machining.

Keywords: dough divider, dough weight distribution, wear of dough divider parts, measurement diagram, gaps in mobile interfaces of dough divider.

For citation: E.G. Martynova, et al. Micrometric research results of vacuum dough divider components. Vestnik of DSTU, 2019, vol. 19, no. 3, pp. 231–241. <https://doi.org/10.23947/1992-5980-2019-19-3-231-241>

Обсуждение и заключения. Проведенные микрометрические исследования деталей тестоделительных устройств показали наличие у них значительных искажений размеров из-за локального износа рабочих поверхностей. Основываясь на полученных результатах, можно утверждать, что наиболее технологичным и экономически целесообразным для восстановления изношенных поверхностей деталей тестоделительных машин является метод электроискровой обработки.

Ключевые слова: тестоделительное устройство, развесовка теста, износы деталей тестоделительного устройства, схема измерения, зазоры в подвижных сопряжениях тестоделительных устройств.

Образец для цитирования: Мартынова, Е. Г. Результаты микрометрических исследований деталей тестоделительных машин вакуумного типа / Е. Г. Мартынова, С. А. Величко, А. В. Мартынов // Вестник Дон. гос. техн. ун-та. — 2019. — Т.19, №.3. — С. 231–241. <https://doi.org/10.23947/1992-5980-2019-19-3-231-241>

Introduction. Bread baking holds a specific place in the food industry. Products of enterprises of this specialization are top requested. However, despite high demand for bread and bakegoods, in some cases, such production may be wasteful. This is due to the insufficient mechanization of the baking process and the complexity of its maintenance. To make an enterprise of such specialization profitable, it is necessary to use high-tech equipment in the process of making bread, which includes, for example, dough-dividing machines [1].

Dough dividers are designed for mechanical processing of dough through dividing it into portioned pieces of a certain weight and shape. Dough dividers are most often used in bakeries that supply bread, loaves, rolls, etc. to the market.

At the bread factories and in bakeries, dough-making machines of domestic production “Voskhod”, “GORIZONT” and of foreign manufacture - “PARTA U2”, “Kumkaya”, “CRV” are mostly often used [2, 3]. Imported equipment is although more functional than domestic analog models, but, it costs 1.5–2.5 times as much.

The main unit of the dough divider that performs the key function is a dividing device (Fig. 1) which consists of hopper *A*; bin hopper *B*; suction chamber body *C*; dividing knife *D*; main piston *E*; suction chamber *F*; measuring piston *G*; drum-type tail gate *I* (hereinafter referred to as the drum) with division box *H* [4].

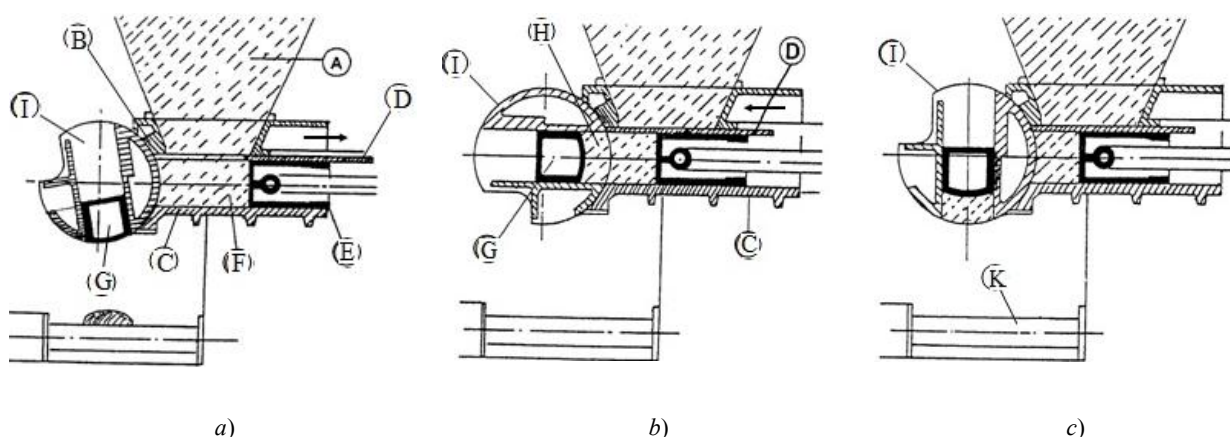


Fig. 1. Structure diagram of vacuum-type dough divider: *A* is hopper; *B* is bin hopper; *C* is suction chamber body; *D* is dividing knife; *E* is main piston; *F* is suction chamber; *G* is measuring piston; *H* is division box; *I* is tail gate (drum); *K* is conveyer belt.

When in operation, the working surfaces of the main piston (Fig. 2 a), the suction chamber body (Fig. 2 b), the drum (Fig. 2 c), etc., wear out.

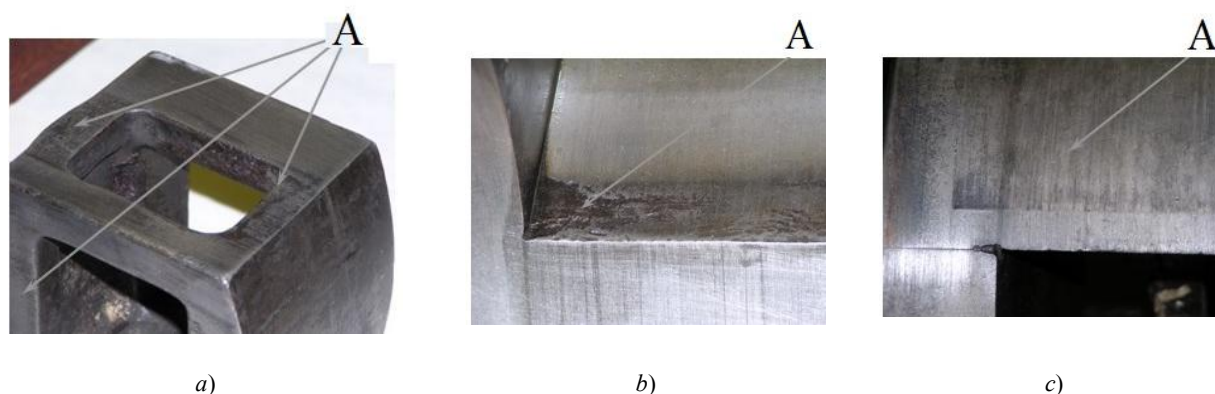


Fig. 2. General view of dough divider components: (A is maximum wear region): *a* is measuring piston; *b* is suction chamber body; *c* is drum

As a result, gaps between them go beyond the value at which vacuum is maintained in the suction chamber; the suction process goes out of control, and the dough divider disturbs the weight distribution accuracy of bakery goods [5].

Till now, repair of such equipment is carried out by 70–80% using spare parts priced from 200 to 300 thousand rubles. The component parts of foreign equipment are particularly expensive [6].

At a number of technical service enterprises, the restoration of components is carried out through the building-up of cast iron, stainless steel and non-ferrous metal on worn surfaces, and then through machining according to the allowance and technical requirements of the maker [6, 7]. However, this technique is unsustainable, time-consuming, and it has high cost.

To increase the durability of such machines, a new highly efficient technology is needed, which provides restoring components through coating with the desired physical and mechanical properties. One of the main criteria for selecting a technique of restoring worn parts is evaluation of the part surface wear that determines the required thickness of metal coatings.

In this regard, the work objective is to assess average values of gaps and wear of dough divider components according to the micrometric study results.

Materials and Methods. The number of dough dividing devices for micrometric studies was selected using the *chi*-square test. When using this criterion, the critical power value $p_{kp} = 0.80$ [8] and the value of the one-sided probability belief $p_d = 0.80$ [9] were set.

The determination of the number of objects is carried out according to the hypothesis: for a given value of the significance level $\alpha = 0.05$. According to the null hypothesis, the number of objects is enough for research, according to the alternative one, it is not enough. If the significance level of the current value α_i is higher than the accepted value of 0.05 and the current value of the *chi*-square p_{xi} criterion power is higher than the critical value of 0.80, then the null hypothesis is valid, and vice versa.

For the accepted parameter values, the dependency graph of the number of objects N and the one-sided confidence probability p_d of the *chi*-square criterion is shown in Fig. 3.

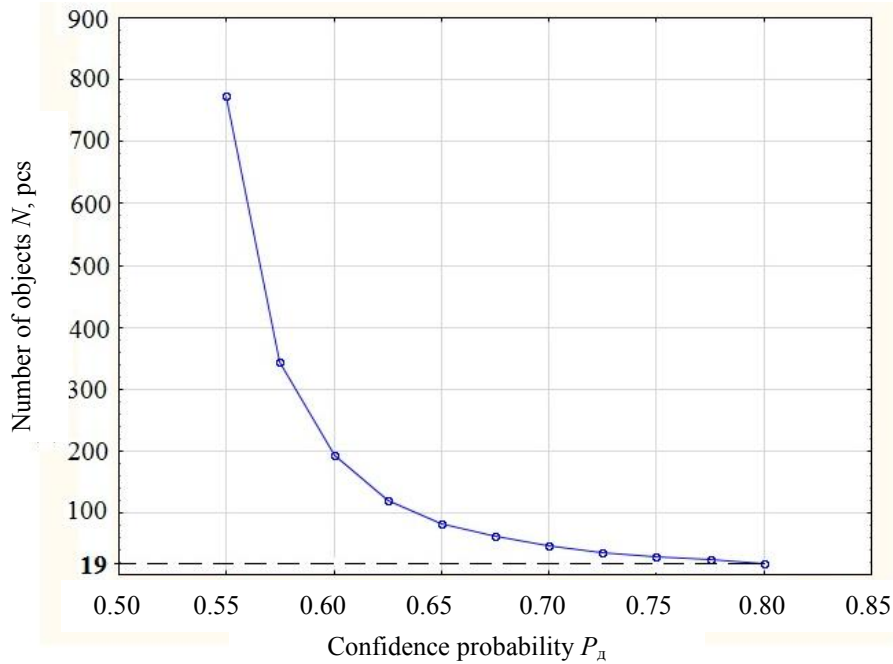


Fig. 3. Dependency graph of number of objects N and the one-sided confidence probability of χ^2 -criterion

The graph shows that for the accepted one-sided confidence probability $p_d = 0.80$, the number of objects for the experiment is $N = 19$ pcs.

The calculation results in the *STATISTICA* program show that the design value of the significance level of the χ^2 -square test $\alpha_i = 0.064$ is higher than the accepted 0.05, and the actual power of the criterion $p_{st} = 0.84$ is higher than the critical value 0.80 [8]. The results obtained validate the null hypothesis with a certain number of dough divider devices $N = 19$ pcs.

Under the micrometric studies at the first stage, gaps in the interfaces were measured.

According to Fig. 1, a divider consists of a suction chamber and a division box, inside which the main piston and the measuring one, respectively, are moving.

When measuring the gap in the horizontal plane of these joints, the piston 1 is shifted all the way to the fixed chamber 2 and, on the opposite side, the gap Z_1 is measured in different sections (Fig. 4,a). Also, in this position of the piston 1, the gap Z_2 in the vertical plane is measured.

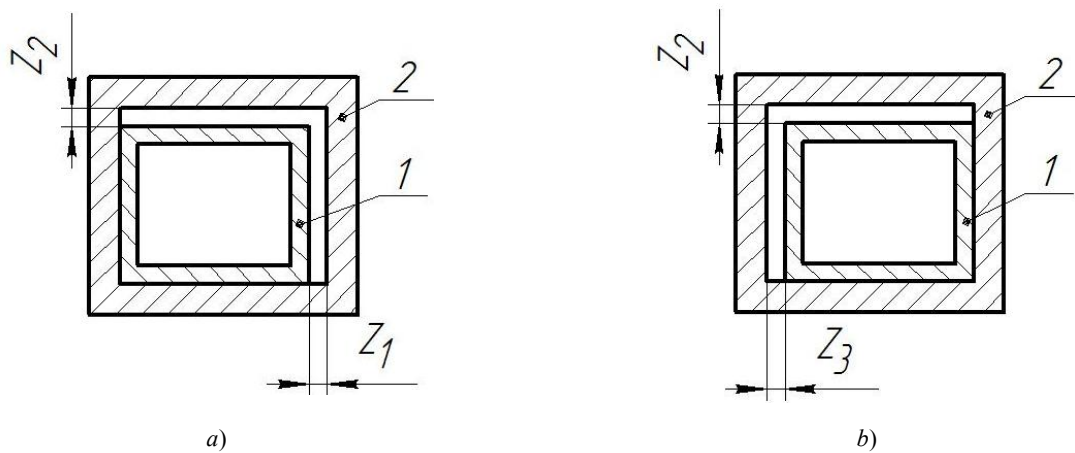


Fig. 4. Measurements of gap in sliding joints of dough dividers

Then piston 1 is shifted to the opposite direction (Fig. 4, b), and the measurement algorithm is repeated. Such measurements were carried out in the extreme and middle working position of the main and measuring piston 1 (Fig. 1).

The tail gate-drum coupling is structurally made of two parts — a housing with a division box and a faceplate. The gap in this coupling is measured between the drum and the suction chamber.

If a gap in the joints is more than 0.05 mm, the wear of the part working surfaces is measured. When the dough divider is operating in the joints, the main piston is a suction chamber, the measuring piston is a division box, and the drum is a suction chamber (Fig. 1). The unworn surface of the parts is absent, their relative wear is measured according to [10, 11].

The relative wear of the outer part surfaces in the i -th section is calculated from the formula

$$U_i^H = d_{\max} - d_i,$$

where d_{\max} is maximum part size, microns; d_i is the part size in the i -th section, microns.

The relative wear of the internal part surfaces in the i -th section is calculated from the formula

$$U_i^B = D_i - D_{\min},$$

where D_i is the part size in the i -th section, microns; D_{\min} is the minimum part size, microns.

When measuring, the sections of the chamber parts of the dough dividers are selected according to the working stroke of the pistons in those places where the working surfaces are in contact (Fig. 1).

The relative wear of the drum surface is measured through radial deviation of the fixed points of the drum surface relating to the center holes of the bearing trunnions. A measurement circuit of the drum working surface is shown in Fig. 5.

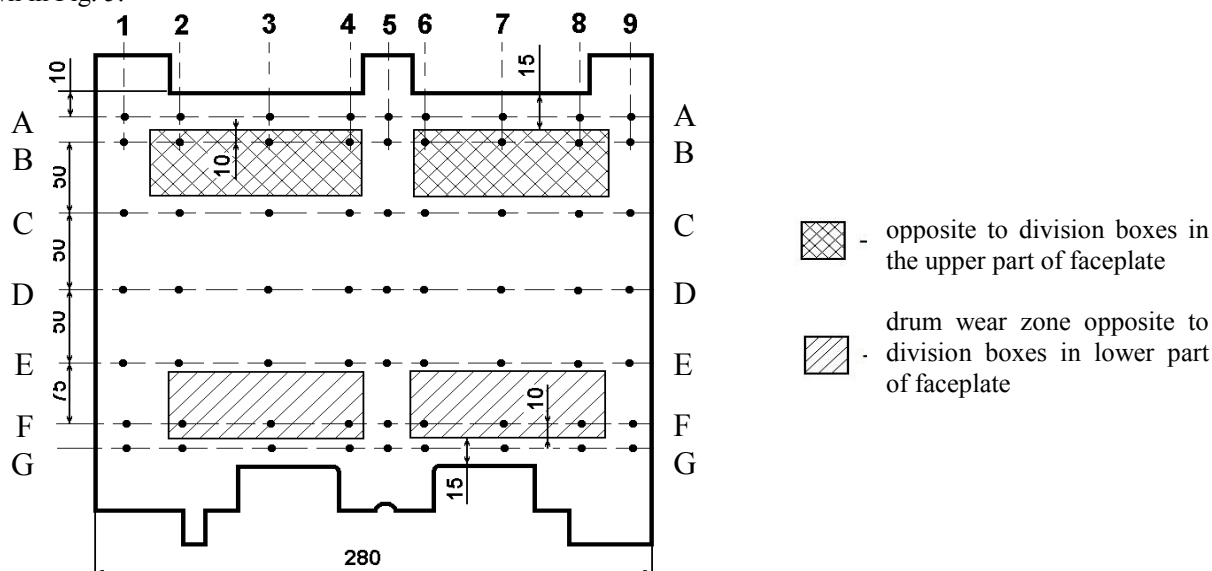


Fig. 5. Measurement circuit of the drum working surface

For measurements, the drum is installed in the centers of the lathe. Measurements during a longitudinal movement are made by the detecting head along the drum in different planes, but without changing the position of this head in the radial direction.

To measure the external components of the dough dividers, MP02102 micrometer with an accuracy of 0.003 mm in 0.002 is used. For internal parts – GOST 868 indicating hole gage NI-100M, whose measurement error is 0.015 mm, with GOST 577 ICH10 mercer clock gauge head, 1 accuracy class in 0.01 mm.

Research Results. The average values of the gaps between the pistons and chambers of the dough divider according to Fig. 3 are shown in Tables 1 and 2.

Table 1

Average values of the gap between suction chamber and main piston

Distance from front chamber edges, mm	Gap average value, mm (± 0.02)		
	Z_1	Z_2	Z_3
0	0.02	0.20	0.12
25	0.18	0.22	0.18
50	0.30	0.22	0.20
75	0.25	0.20	0.20
100	0.30	0.25	0.20
150	0.25	0.25	0.20
200	0.25	0.20	0.20

Table 2

Average values of the gap between division box and piston

Distance from front chamber edges, mm	Gap average value, mm (± 0.02)		
	Z_1	Z_2	Z_3
<i>Left chamber</i>			
5	0.50	0.35	0.30
25	0.50	0.45	0.35
50	0.55	0.50	0.35
75	0.50	0.35	0.30
<i>Right chamber</i>			
5	0.10	0.40	0.10
25	0.10	0.45	0.15
50	0.05	0.45	0.15
75	0.05	0.40	0.15

Tables 1 and 2 show that the side gap between the worn-out suction chamber and main piston reaches 300 μm in some areas. Given the increased wear of the output part of the lower plane of the chamber, the vertical clearance is at least 400-500 μm . Values of the lateral and vertical gaps between worn division boxes and pistons also far exceed the permissible value and reach 550 μm .

The average values of the gap between the drum and the suction chamber are shown in Table 3.

Table 3

Average values of the gap between drum and suction chamber

Sections	Clearance in mm (± 0.02) at points								
	1	2	3	4	5	6	7	8	9
A	0.06	0.15	0.15	0.13	0.10	0.20	0.18	0.21	0.07
B	<0.05	0.26	0.30	0.30	0.08	0.25	0.25	0.28	<0.05
C	<0.05	0.17	0.15	0.18	0.07	13	0.15	0.15	0.05
D	<0.05	0.09	0.10	0.08	<0.05	0.12	0.11	0.10	<0.05
E	0.05	0.07	0.08	0.08	0.05	0.05	0.06	0.08	<0.05
F	<0.05	0.16	0.14	0.15	0.09	0.15	0.15	0.13	<0.05
G	<0.05	<0.05	<0.05	<0.05	<0.05	<0.05	<0.05	<0.05	<0.05

As follows from Table 3, the gap between the drum and the suction chamber in 300 μm far exceeds the permissible value.

Tables 4–5 show the measurement schemes and average wear values of the part surfaces that determine the performance of the dough dividers.

Table 4

Results of micrometric measurements of main piston

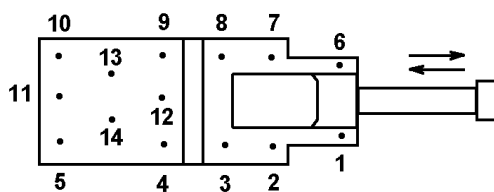
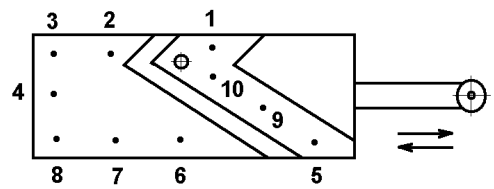
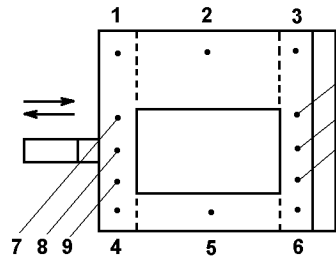
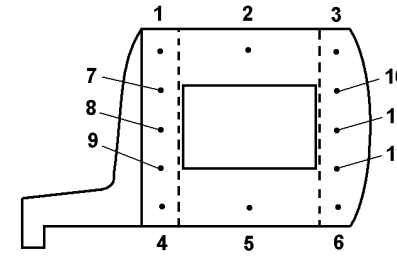
Sections	Average measurements, mm	Observations
1	2	3
Sectional piston height measurements, ± 0.01 mm		
Average measurements, mm		
1	99.95	In zones 1-2 on the bottom surface, wear is up to 0.2 mm deep, 20 mm long, and 5-6 mm wide On the total area of bottom and top surfaces of zones 3-14, there is tearing and furrows up to 0.1 mm in depth, some dents
2	99.93	
3	99.90	
4	99.86	
5	99.82	
6	99.95	
7	99.96	
8	99.92	
9	99.89	
10	99.87	
11	99.80	
12	99.82	
13	99.84	
14	99.80	
Sectional measurements of piston width, ± 0.05 mm		
Average measurements, mm		
1	189.80	There is tearing and furrows up to 0.1 mm in depth over the total area of the side surfaces
2	189.65	
3	189.60	
4	189.60	
5	189.80	
6	189.80	
7	189.70	
8	189.60	
9	189.80	
10	189.80	In this area, on the right side, there is longitudinal tearing up to 0.3 mm in depth

Table 5

Results of micrometric measurements of measuring pistons

Sections	Measurement results, mm (± 0.01 mm)	Observations	
1	2	3	
Average measurements, mm		Sectional measurement scheme of piston width	
PISTON No. 1 (left), sectional measurements of piston height			
1	99.88	On the bottom surface in zones 1-3, there is tearing up to 0.3 mm in depth	
2	99.88		
3	99.78		
4	99.80		
5	99.78		
6	99.69		
7	99.58		
8	99.57		
9	99.60		
10	99.42...60	On the top surface (half the area) in zones 10-12, there is fatigue wear, on the rest area, there is tearing up to 0.2 mm in depth	
11	99.40...50		
12	99.55		
PISTON No. 1 (left), sectional measurements of piston width			
1	82.33		
2	82.33		
3	82.27		
4	82.38		
5	82.36		
6	82.31		
7	81.92	In zones 7-9, there is uniform wear, the amount of wear on the left surface is greater than of the right one	
8	82.00		
9	82.15		
10	81.80...90	In zone 10, there is fatigue wear up to 3.5 cm ² in area	
11	82.00		
12	82.14		

PISTON No. 2 (right), sectional measurements of piston height		
1	99.78	On the bottom surface in areas 1-6, there is tearing and furrows
2	99.77	
3	99.68	
4	99.80	
5	99.83	
6	99.75	
7	99.50	
8	99.48	On the top surface in zones 10-12, there is fatigue wear up to 90% in area
9	99.47	
10	99.22...53	
11	99.22...49	
12	99.20...50	
PISTON No. 2 (right), sectional measurements of piston width		
1	82.29	
2	82.31	
3	82.18	
4	82.38	
5	82.41	
6	82.28	
7	81.66	
8	81.98	
9	82.22	
10	81.49...75	On both surfaces in zones 10-11, there is fatigue wear up to 50% in area
11	81.58...92	
12	82.10	

As follows from Table 4, the height of the main piston wear along the sections is uneven. It is minimal at the rear part of the piston (10–20 μm) and gradually increases to a maximum value up to 150 μm to its front face. The nature of the change in the size of the piston width is similar, in which the maximum value of wear of at least 200 μm is also located at its front face. Grooves of various depths (from 100 to 300 μm), furrows, some dents are visible on the total frictional area. Piston wear is caused by mechanical abrasion.

The inspection results of a measuring piston (Table 5) show that wear along the height and width is maximum in its front part (Table 3) and it can reach 800–900 microns. However, there is a feature caused by the presence of vertical and horizontal gates. The areas of friction surfaces opposite these gates are worn out more – by an average of 250–300 μm . Besides, in the fore piston lead-in, opposite the gates, on the top and side surfaces, there are sections of increased wear. This is clearly seen in Fig. 2, a.

The wear monitoring of the components of the suction chamber and division box shows that a long-term operation has also affected their size variation. As in the case with pistons, they are worn unevenly over sections along the total length of the working stroke. A characteristic feature of the suction chamber is increased wear (300–400 μm) of the bottom plane at the outlet part over all sections (Fig. 2, b). The width of the increased wear stripe of the suction chamber is 25–30 mm.

The measurement results of the radial deviation of the drum working made according to the scheme of Fig. 4 are shown in Table 6.

Table 6

Average values of radial deviation of drum working surface¹

Sections	Sectional measurement results					
	→			←		
	1	3	5	5	7	9
A	−0.03	−0.11	−0.06	−0.05	−0.13	−0.04
B	0	−0.28	−0.03	−0.03	−0.22	−0.02
C	0.01	−0.16	−0.04	−0.05	−0.11	−0.03
D	0	−0.05	−0.02	−0.03	−0.06	0.01
E	−0.02	−0.06	−0.02	−0.02	−0.04	−0.01
F	−0.01	−0.09	−0.05	−0.04	−0.10	0.01
G	0	−0.02	−0.01	−0.02	0	0
¹ Note. 1) → and ← are directions of the longitudinal movement of detecting head; 2) points G1 and G9 are basic						

Along with measuring the radial deviation of fixed surface points, it is possible, using the data from Table 3, to determine the boundaries of worn sections and the values of wear. The most worn sections of the drum working surface are in the sections opposite the division boxes in the upper and lower parts of the faceplate (Fig. 2c, 4)

As follows from Table 3, maximum wear on the most worn sections of the drum working surface reaches 280-300 μm.

To restore worn surfaces of dough divider components in the modern repair production, the most productive and economically viable technique is the electrospark machining [12].

Electrospark treatment is the process of transferring electrode material to a surface to be treated through the spark electric discharge. A feature of this method is a localization of worn areas, the absence of heating the components and the possibility of applying any conductive materials that provide high tribological properties of friction couples with minimal surface preparation.

Conclusion. Thus, the micrometric studies of dough divider parts show that they have appreciable distortions due to local wear of the working surfaces.

The investigation of gaps in the dough divider joints shows the following: the lateral gap between the suction chamber and the main piston is 6 times higher than the permissible one and reaches an average value of 300 μm; lateral and vertical gaps between the division box and the piston are 550 μm, which is more than 10 times the allowable gap; the gap between the drum and the suction chamber is 6 times the permissible gap and reaches an average value of 300 μm.

Wear of the working surfaces of the dough divider parts are local in character. The range of values for the main piston is 10-200 μm; for the measuring piston, it is 250-900 μm; for the suction chamber and division box, it is 300-400 μm; for the drum surfaces, it is 280-300 μm.

Based on the results obtained, it can be argued that the electrospark machining is the most productive and economically viable technique for restoring worn part surfaces of the dough dividers.

References

1. Khromeenkov, V.M. *Oborudovanie khlebopekarnogo proizvodstva*. [Bakery Equipment.] Moscow: Akademiya, 2000, 380 p. (in Russian).
2. Mashina testodelitel'naya «Voskhod-TD-4». *Rukovodstvo po ekspluatatsii V495.00.00.000RE* [Dough dividing machine “Voskhod-TD-4”. Operation Guide V495.00.00.000RE.] Borodino Trading House. Available at: <https://www.borodinsky.ru/images/files2/td-4.pdf> (accessed: 14.02.2019) (in Russian).
3. Apet, T.K., Pashuk, Z.N. *Khleb i bulochnye izdeliya (tekhnologiya prigotovleniya, retsepttsra, vypechka): spr. Posobie*. [Bread and bakery products (cooking technology, recipes, pastries.): Ref. book.] Minsk: Popurri, 1997, 320 p. (in Russian).
4. Testodelitel' Voskhod TD-2M (dvukhkarmanny). [Dough divider Voskhod TD-2M (twin-tub).] Petrocomplex+. Available at: <http://ptkomplex.ru/oborudovanie/xleb/3-testodel/30-td2> (accessed: 24.04.2019) (in Russian).

5. Pashchenko, L.P., Zharkova, I.M. Tekhnologiya khlebopekarnogo proizvodstva. [Baking technology.] Moscow: Kolos-S, 2008, 389 p. (in Russian).
6. Sidnev, Yu.V. Gal'vanicheskie pokrytiya. [Electroplating.] Moscow: Fenix, 2001, 256 p. (in Russian).
7. Golubev, I.G., Taratorkin, V.M. Tekhnologicheskie protsessy remontnogo proizvodstva. [Repair production processes.] 2nd ed. Moscow: Akademiya, 2017, 304 p. (in Russian).
8. Borovikov, V.P. STATISTICA. Iskustvo analiza dannykh na komp'yutere. [STATISTICA. The art of computer data analysis] St.Petersburg: Piter, 2003, 668 p. (in Russian).
9. Artemyev, Yu.N. Kachestvo remonta i nadezhnost' mashin v sel'skom khozyaystve. [Quality of repair and reliability of machinery in agriculture.] Moscow: Kolos, 1981, 239 p. (in Russian).
10. Chernoiyanov, V.I., Lyalyakin, V.P., Golubev, V.G. Organizatsiya i tekhnologiya vosstanovleniya detaley mashin. [Organization and technology of restoring machine parts.] Moscow: Rosinformagrotekh, 2016, 568 p. (in Russian).
11. Kuksenova, L.I., Gerasimov, S.A., Lapteva, V.G. Iznosostoykost' konstruktsionnykh materialov: ucheb. posobie. [Wear resistance of structural materials.] Moscow: Bauman University Publ. House, 2011, 237 p. (in Russian).
12. Burumkulov, F.Kh., et al. Elektroiskrovyie tekhnologii vosstanovleniya i uprochneniya detaley mashin i instrumentov (teoriya i praktika). [Electrospark technologies for restoration and hardening machine parts and tools (theory and practice).] Saransk: Krasnyy Oktyabr', 2003, 504 p. (in Russian).

Submitted 25.02.2019

Scheduled in the issue 05.04.2019

Authors:

Martynova, Elena G.

postgraduate of the Technical Service of Machines Department, Mechanics and Power Engineering Institute, Ogarev Mordovia State University (68, Bolshevistskaya St., Saransk, 430005, Republic of Mordovia, RF),
ORCID: <http://orcid.org/0000-0002-6870-0498>,
el.mart2012@yandex.ru

Velichko, Sergey A.,

professor of the Technical Service of Machines Department, Mechanics and Power Engineering Institute, Ogarev Mordovia State University (68, Bolshevistskaya St., Saransk, 430005, Republic of Mordovia, RF), Dr.Sci. (Eng.), associate professor,
ORCID: <https://orcid.org/0000-0001-6254-5733>,
Velichko2005@yandex.ru

Martynov, Alexey V.,

associate professor of the Technical Service of Machines Department, Mechanics and Power Engineering Institute, Ogarev Mordovia State University (68, Bolshevistskaya St., Saransk, 430005, Republic of Mordovia, RF), Cand.Sci. (Eng.), associate professor,
ORCID: <https://orcid.org/0000-0003-2869-2208>,
Martynov-230685@yandex.ru

MACHINE BUILDING AND MACHINE SCIENCE МАШИНОСТРОЕНИЕ И МАШИНОВЕДЕНИЕ



UDC 62-82

<https://doi.org/10.23947/1992-5980-2019-19-3-242-249>

Theoretical background of hydraulic drive control system analysis for testing piston hydraulic cylinders ***

A. T. Rybak¹, I. K. Tsybriy², S. V. Nosachev³, A. R. Zenin^{4**}

^{1, 2, 3, 4} Don State Technical University, Rostov-on-Don, Russian Federation

Теоретические основы расчета системы управления гидравлического привода стенда для испытаний поршневых гидравлических цилиндров *

А. Т. Рыбак¹, И. К. Цыбрий², С. В. Носачёв³, А. Р. Зенин^{4**}

^{1, 2, 3, 4} Донской государственный технический университет, г. Ростов-на-Дону, Российская Федерация

Introduction. The durability and performance of hydraulic machines is determined through life tests. At that, various braking devices (mechanical, electric, hydraulic, etc.) are used for strength loading of the hydraulic motor, as a result of which a significant amount of energy is lost. This can be avoided if the method of rotational motion with energy recovery is used during life tests. This approach is applicable for hydraulic pumps, motors, and hydraulic cylinders.

Materials and Methods. A test bench is presented, the design of which provides recreation of the conditions most appropriate for the field operation of hydraulic cylinders. In this case, energy recovery is possible. To solve the research problems, methods of mathematical modeling were used, the basic functional parameters of the proposed design were calculated. The determination of the pressure increment at various points in the hydraulic system is based on the theory of volumetric rigidity. When modeling the motion of the moving elements of the bench hydraulic system, the laws of rotor motion are used.

Research Results. In the structure of the test bench, the cylinders in question are located in the pressure main between the hydraulic pump and the hydraulic motor. This enables to significantly reduce the bench itself and to save a significant amount of energy due to its recovery. A basic hydraulic diagram of the test bench for piston hydraulic cylinders is presented, in which the operation of the moving elements of the system is shown. A mathematical modeling of the hydraulic system of the bench is performed. A kinematic diagram of the mechanism for transmitting motion between test cylinders is shown.

Discussion and Conclusions. The system of equations present-

Введение. Долговечность и работоспособность гидравлических машин определяется в результате ресурсных испытаний. При этом для силового нагружения гидравлического двигателя применяются различные тормозные устройства (механические, электрические, гидравлические и др.), в результате чего теряется значительное количество энергии. Этого можно избежать, если при ресурсных испытаниях использовать метод вращательного движения с рекуперацией энергии. Такой подход применим для гидравлических насосов, моторов, а также гидравлических цилиндров.

Материалы и методы. Представлен испытательный стенд, конструкция которого позволяет воссоздать условия, максимально соответствующие реальной эксплуатации гидравлических цилиндров. При этом возможна рекуперация энергии. Для решения задач исследования использованы методы математического моделирования, рассчитаны основные функциональные параметры предлагаемой конструкции. Определение приращения давления в различных точках гидравлической системы базируется на теории объемной жесткости. При моделировании движения подвижных элементов гидравлической системы стенда использованы законы движения ротора.

Результаты исследования. В структуре испытательного стенда рассматриваемые гидроцилиндры размещены в напорной магистрали между гидронасосом и гидромотором. Это позволяет существенно уменьшить сам стенд и сэкономить значительное количество энергии за счет ее рекуперации. Приведена принципиальная гидравлическая схема стенда для испытаний поршневых гидроцилиндров, в рамках которой показана работа подвижных элементов системы. Выполнено математическое моделирование гидравлической системы стенда. Показана кинематическая схема механизма передачи движения между испытуемыми цилиндрами.

Обсуждение и заключения. Представленная в статье система уравнений показывает, каким образом определяется



* The research is done within the frame of the independent R&D.

** E-mail: 2130373@mail.ru, irconst@mail.ru, nosachev-s@yandex.ru, azenin@donstu.ru

*** Работа выполнена в рамках инициативной НИР.

ed in the paper shows how the increment of pressure at the selected nodal points of the energy recovery system is determined (in particular, how the increment depends on time, reduced coefficient of volumetric rigidity, operating fluid consumption, and piston areas). The velocities of the hydraulic pistons are determined according to the kinematic scheme of the mechanical transmission of the bench. Thus it can be argued that, thanks to the solution presented in the paper, the life test results of hydraulic cylinders will adequately reflect their operation under rated duties.

Keywords: piston hydraulic cylinders, test bench, testing, energy recovery, math modeling, kinematic motion transmission scheme.

For citation: A.T. Rybak, et al. Theoretical background of hydraulic drive control system analysis for testing piston hydraulic cylinders. Vestnik of DSTU, 2019, vol. 19, no. 3, pp. 242–249. <https://doi.org/10.23947/1992-5980-2019-19-3-242-249>

приращение давления в выбранных узловых точках системы рекуперации энергии (в частности, как приращение зависит от времени, приведенного коэффициента объемной жесткости, расхода рабочей жидкости, площади поршней). Величины скоростей перемещения плунжеров гидравлических цилиндров определены согласно кинематической схеме механической передачи стенда. Итоги исследования позволяют утверждать, что, благодаря представленному в статье решению, результаты ресурсных испытаний гидравлических цилиндров будут адекватно отражать их работу при номинальном режиме эксплуатации.

Ключевые слова: поршневые гидравлические цилиндры, стенд, испытания, рекуперация энергии, математическое моделирование, кинематическая схема передачи движения.

Образец для цитирования: Теоретические основы расчета системы управления гидравлического привода стенда для испытаний поршневых гидравлических цилиндров / А. Т. Рыбак [и др.] // Вестник Дон. гос. техн. ун-та. — 2019. — Т. 19, № 3. — С. 242–249. <https://doi.org/10.23947/1992-5980-2019-19-3-242-249>

Introduction. One of the important stages of the machine-building production including the production of hydraulic machines is the end product qualification test [1].

The most significant (at the same time labor and energy consuming) tests are life time tests. They determine the durability and long-term intended operability. Life tests should be performed in the mode most closely approximate to the nominal conditions of hydraulic cylinders. In this case, various braking devices (mechanical, electrical, hydraulic and others) are used for power loading of the hydraulic motor, as a result of which a significant amount of energy is converted into heat. This is especially true for testing medium-duty and high-energy-rate hydraulic machines.

As a result of an active search for a solution to the indicated problem, a life time test for rotary hydraulic machines with energy recovery is developed [2–4]. This approach provides significant savings when testing hydraulic pumps and hydraulic motors. Test methods with energy recovery are also developed for hydraulic cylinders [5–10]. The schemes described in [9, 10] make it possible to produce a bench tester for hydraulic cylinders operating mode fully compatible with their field work.

Materials and Methods

Problem formulation. A stand design is proposed that provides recreating conditions most closely resembling the field work of hydraulic cylinders. At that, energy recovery is possible, which reduces significantly its costs, especially during resource tests. To solve the research problems, mathematical simulation techniques were used, the basic functional parameters of the proposed design were calculated.

Description of the test bench. The test bench for life time tests of piston hydraulic cylinders with energy recovery was developed on the basis of the previously proposed test method with energy recovery of rotary hydraulic volumetric machines [3, 4]. This solution implies that the hydraulic motor returns energy to the hydraulic pump shaft through the mechanical drive system. The tested hydraulic cylinders are located in the pressure line between the hydraulic pump and the hydraulic motor [5, 6]. Such tests can reduce drastically the stand itself and save a significant amount of energy due to its recovery.

The hydraulic circuit diagram of the test bench for piston hydraulic cylinders is shown in Fig. 1.

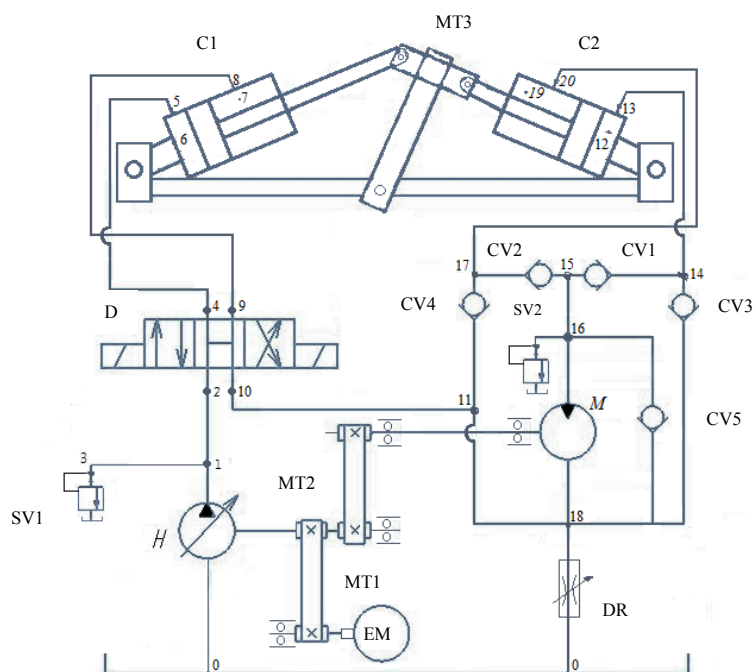


Fig. 1. Hydraulic circuit diagram of the stand for resource tests of piston hydraulic cylinders with energy recuperation

Fig. 1 shows that the tested hydraulic cylinders *C1* and *C2* interconnected by a mechanical transmission *MT3* are installed between a hydraulic pump and a hydraulic motor.

The stand operates as follows. The electric motor *EM* through the mechanical transmission *MT1* drives the shaft of the hydraulic pump *P*. The energy transported by the actuation fluid is transferred by it along the hydraulic line 1-2 to the input of the hydraulic distributor *D*, which directs it, for example, along the highway 4-5-6 to the piston cavity of the hydraulic cylinder *C1*.

The hydraulic cylinder *C1*, through the mechanical transmission *MT3*, transfers the energy received from the actuation fluid to the rod of the hydraulic-cylinder *C2*, which, in this case, acts as a pump and transfers the energy of the actuation fluid located in its piston cavity.

From the piston cavity of the hydraulic cylinder *C2*, the actuation fluid is fed through hydraulic line 12–13–14–15–16 to the input of the hydraulic motor *M*, which converts the energy obtained from the actuation fluid into the shaft rotation energy. The rotation of the shaft of the hydraulic motor *M* through a mechanical transmission *MT2* is transported to the shaft of the hydraulic pump *P*. *MT2* transmission is designed so that the speed transmitted to the shaft of the hydraulic pump *P* from the shaft of the hydraulic motor *M* is slightly higher than the frequency with which the primary energy source (electric motor *EM*) rotates the hydraulic pump shaft. This helps to slow down the rotation of the shaft of the hydraulic motor *M*. As a result, the inlet pressure rises, and the safety valve *SV2* opens. Pressure also increases in the cylinders *C1* and *C2*, which determines their operation in the corresponding mode.

When the hydraulic cylinder (*C1*) rod is extended at full travel, a position change command is sent to the distributor *D*, and the actuation fluid supplied to the input of the distributor *D* from the hydraulic pump *P* is sent along the hydraulic line 9–8–7 to the rod cavity of the hydraulic cylinder *C1*. This causes a reverse movement of its piston, but the energy recovery system operates as in the forward stroke of the piston.

Research Results

Mathematical modeling of the hydraulic system of the stand. We are developing a mathematical model of the proposed recuperative system for testing piston hydraulic cylinders. As a basis, we use the theory of volumetric rigidity [11–13] considering the given coefficients of volumetric rigidity of hydraulic elements. This approach more accurately simulates a system resembling field conditions of hydraulic cylinders [14–19]. Under modeling hydraulic drives, special attention should be given to determining the reduced volumetric rigidity coefficient of hydraulic lines. Its value for metal pipelines is calculated according to well-known dependencies, and for high pressure hoses (HPH), it is determined experimentally [20, 21].

In accordance with the theory of volumetric rigidity, the equation of pressure increment at any point of the hydraulic system can be determined from the equation:

$$dp = c_i \left(\sum Q_{\text{Bxi}} - \sum Q_{\text{Bvxi}} \right) dt ,$$

where $\sum Q_{\text{вх}i}$ and $\sum Q_{\text{вых}i}$ are total input and output flow rate of the actuation fluid during the time dt coming out of the considered (i -th) volume of the system; C_i is the reduced volumetric rigidity factor of the selected area of the hydraulic system.

Conventionally, we will divide the hydraulic system of the bench (see Fig. 1) by nodal points. We assume volume of the hydraulic tank with atmospheric pressure as point 0, and write the equations for determining pressure at the selected nodal points.

$$\begin{aligned} dp_1 &= C_1(Q_H - Q_{1-2} - Q_{1-3})dt, \\ dp_2 &= C_2(Q_{1-2} - Q_{2-4})dt, \\ dp_3 &= C_3(Q_{1-3} - Q_{\text{КП1}})dt, \\ dp_4 &= C_4(Q_{2-4} - Q_{4-5})dt, \\ dp_5 &= C_5(Q_{4-5} - Q_{5-6})dt, \\ dp_6 &= C_{\text{п1}}(Q_{5-6} - v_{\text{п1}}f_{\text{п}})dt, \\ dp_7 &= C_{\text{шт1}}(v_{\text{п1}}f_{\text{п.шт}} - Q_{7-8})dt, \\ dp_8 &= C_8(Q_{7-8} - Q_{8-9})dt, \\ dp_9 &= C_9(Q_{8-9} - Q_{9-10})dt, \\ dp_{10} &= C_{10}(Q_{9-10} - Q_{10-11})dt, \\ dp_{11} &= C_{11}(Q_{10-11} - Q_{11-18} - Q_{\text{ОК4}})dt, \\ dp_{17} &= C_{17}(Q_{\text{ОК4}} - Q_{17-20} - Q_{\text{ОК2}})dt, \\ dp_{20} &= C_{20}(Q_{17-20} - Q_{20-19})dt, \\ dp_{19} &= C_{\text{шт2}}(Q_{20-19} - v_{\text{п2}}f_{\text{п.шт}})dt, \\ dp_{12} &= C_{\text{п2}}(v_{\text{п2}}f_{\text{п}} - Q_{12-13})dt, \\ dp_{13} &= C_{13}(Q_{12-13} - Q_{13-14})dt, \\ dp_{14} &= C_{14}(Q_{13-14} + Q_{\text{ОК3}} - Q_{\text{ОК1}})dt, \\ dp_{15} &= C_{15}(Q_{\text{ОК1}} + Q_{\text{ОК2}} - Q_{15-16})dt, \\ dp_{16} &= C_{16}(Q_{15-16} + Q_{\text{ОК5}} - Q_{\text{КП2}} - Q_M)dt, \\ dp_{18} &= C_{18}(Q_{11-18} + Q_M - Q_{\text{ДР}} - Q_{\text{ОК3}} - Q_{\text{ОК5}})dt. \end{aligned}$$

Here, $dp_1 \dots dp_5$ are pressure increments at characteristic points of the pressure hydraulic line of cylinder $C1$ in the time dt ; $dp_7 \dots dp_{10}$ are pressure increments at characteristic points of the drain line of cylinder $C1$ in the time dt ; $dp_{11} \dots dp_{18}$ are pressure increments at the characteristic points of the hydraulic energy recovery system including the hydraulic cylinder $C2$ and hydraulic motor M , during the time dt ; dp_6 and dp_7 are pressure increments in the piston and rod cavities of the hydraulic cylinder $C1$ during the time dt ; dp_{12} and dp_{19} are pressure increments in the piston and rod cavities of the hydraulic cylinder $C2$ during the time dt ; dp_{20} is pressure increment at the outlet of the rod cavity of the cylinder $C2$ during the time dt ; $C_1 \dots C_5$, $C_8 \dots C_{11}$, $C_{13} \dots C_{18}$ and C_{20} are the reduced volumetric rigidity factors at the characteristic points of the bench hydraulic system; $C_{\text{п1}}$ and $C_{\text{п2}}$ are the volumetric rigidity factors of the piston cavities of the hydraulic cylinders $C1$ and $C2$ [11–13]; $C_{\text{шт1}}$ and $C_{\text{шт2}}$ are the reduced volumetric rigidity factors of rod cavities of hydraulic cylinders $C1$ and $C2$ [11–13]; Q_H is the hydraulic pump (P) capacity; Q_M is the flow rate of the actuation fluid through the hydraulic motor M ; $Q_{\text{ОК1}} \dots Q_{\text{ОК5}}$ are flow rates of the actuation fluid through the check valves $CV1 \dots CV5$; $Q_{\text{КП1}}$ and $Q_{\text{КП2}}$ are the flow rate of the actuation fluid through the safety valves $SV1$ and $SV2$; Q_{1-3} , Q_{1-2} , Q_{2-4} , Q_{4-5} , Q_{5-6} , Q_{7-8} , Q_{8-9} , Q_{9-10} , Q_{10-11} , Q_{11-18} , Q_{19-20} , Q_{13-14} are fluid flows in the corresponding sections of the bench hydraulic system; $v_{\text{п1}}$ and $v_{\text{п2}}$ are piston velocities of the hydraulic cylinders $C1$ and $C2$, respectively; $f_{\text{п}}$ are piston areas of the tested hydraulic cylinders $C1$ and $C2$; $f_{\text{п.шт}}$ are piston areas of the tested hydraulic cylinders $C1$ and $C2$ from the side of the rod cavities.

Flow rate values of the actuation fluid required to calculate the increment of pressure are determined from the formula:

$$Q_i = \mu f \sqrt{\frac{2}{\rho} |p_i - p_{i+1}|} \cdot \text{sign}(p_i - p_{i+1}).$$

Here, p_i and p_{i+1} are pressure values at the inlet and outlet of hydraulic resistances; f is a clear area of the corresponding resistance; μ is the drag coefficient; ρ is the fluid density.

For sections of the hydraulic lines (linear hydraulic resistances), the reduced flow coefficient is determined from the formula:

$$\mu = \mu_l = \frac{1}{\sqrt{\lambda_l \frac{l_l}{d_l}}},$$

where d_l and l_l are the inner diameter and length of the corresponding section of the pipeline; λ_l is the pipe friction number of the pipeline section determined with account for the flow regime of the actuation fluid and the properties of the pipeline.

The given volumetric rigidity factors of metal pipe wires are determined from the formula [11–13]:

$$C_l = \frac{4}{\pi d^2 l} \frac{E_{fl}}{1 + \frac{d E_{fl}}{8 E_l}},$$

where d and l are the diameter of the pipeline under study and its length; δ is the pipe wall thickness; E_{fl} and E_l are the elastic modulus values of the liquid and material of the pipeline wall.

The reduced volumetric rigidity factor of the HPH and pipelines made of elastic materials should be determined experimentally [20, 21].

The pump performance is determined by its volumetric efficiency:

$$Q_H = \frac{q_H \omega_H}{2\pi} \eta_0,$$

where q_H is the hydraulic pump displacement; ω_H is the rotational speed of the hydraulic pump shaft; η_0 is the momentary value of the pump volumetric efficiency.

$$\eta_0 = 1 - (1 - \eta_{0.nom}) \cdot \frac{p_H}{p_{nom}}.$$

Here, η_0 is the rated value of the pump volumetric efficiency (taken equal to the volumetric efficiency at the nominal pressure (PN) of the pump); p_{nom} is rated working pressure (RWP) of the hydraulic pump; p_H is the current pressure value at the pump outlet (pressure at point 1 of the hydraulic system).

Simulation of the movement of moving elements of the stand hydraulic system. Values of operating gaps of the check valves are determined from the equation of motion of their gates:

$$\frac{dv_{кл}}{dt} = \frac{1}{m_{кл}} \left[\frac{d_{кл}^2}{4} (p_{1кл} - p_{2кл}) - F_{пр} \right], \quad \frac{dh_{кл}}{dt} = v_{кл},$$

where $v_{кл}$ is the valve gate speed; $m_{кл}$ is the reduced valve gate mass; $h_{кл}$ is motion (size of the operating gap) of the valve gate; $d_{кл}$ is the valve bore diameter; $F_{пр}$ is the spring impact on the valve gate; t is time.

The law of rotor float of the hydraulic pump P and the hydraulic motor M is described by their motion equation:

$$\frac{d\omega_M}{dt} = \frac{1}{J_M} [w_M(p_{1M} - p_{2M}) - M_M],$$

$$\frac{d\omega_H}{dt} = \frac{1}{J_P} (M_{эд} i_{МП1} + M_M i_{МП2} - w_H(p_1 - p_{ат})).$$

Here, w_M , w_H are characteristic volumes of the motor M and pump P , respectively; ω_M and ω_H are angular rotational velocities of the shafts of the hydraulic motor M and pump P ; J_H , J_M are central moments of inertia of the rotors of the hydraulic pump and hydraulic motor; p_{1M} is the pressure at the inlet of the hydraulic motor M ; p_{2M} is the pressure at the outlet of the hydraulic motor M ; $p_{ат}$ is the pressure at the inlet of the pump P (pressure in the tank taken equal to the atmospheric pressure); p_1 is the pressure at the outlet of the hydraulic pump P ; $M_{эд}$ and M_M are torques created by the electric motor and hydraulic motor, respectively; $i_{МП1}$ and $i_{МП2}$ are gearing ratios of mechanical transmissions $MT2$ (from the shaft of the hydraulic motor to the shaft of the hydraulic pump H) and $MT1$ (from the shaft of the electric motor to the shaft of the hydraulic pump P), respectively.

The mechanical transmission $MT2$ provides the ratio of the shaft speeds of the hydraulic motor M and the hydraulic pump P described by the formula:

$$\omega_M = \omega_H i_{M\Pi 2}.$$

Simulation of the stand mechanical schematic. To determine the hydraulic piston velocities, we consider the kinematic scheme of the mechanical transmission of the MT3 bench (Fig. 2).

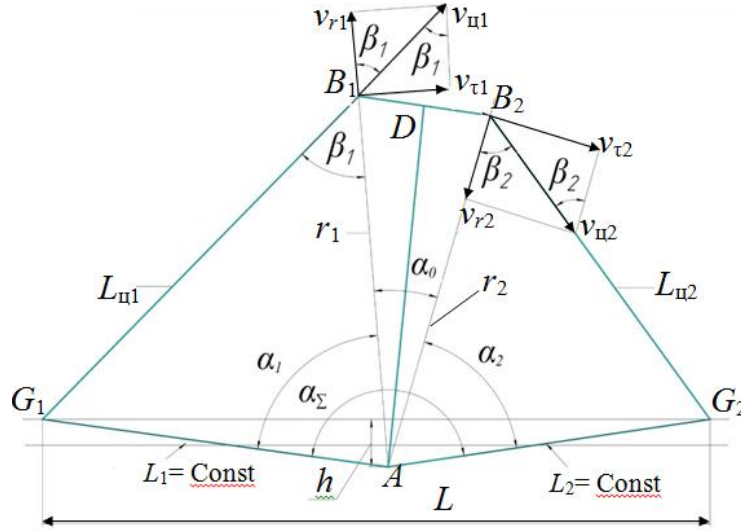


Fig. 2. Kinematic scheme of motion transmission mechanism between the tested cylinders

The transmission works as follows. Bodies of the hydraulic cylinders $C1$ (L_{u1}) and $C2$ (L_{u2}) are pivotally mounted at the points $G1$ and $G2$, respectively, and their pistons are pivotally connected at the points $B1$ and $B2$ to the rocker arm with a rotation axis at the point A .

Assume that the leading hydraulic cylinder (hydraulic engine) is the hydraulic cylinder L_{u1} , and the working cylinder (hydraulic pump) is the hydraulic cylinder L_{u2} . The hydraulic piston speed L_{u1} is set according to the flow rate Q_{5_6} of the actuation fluid entering its piston cavity. Then, its piston speed can be determined from the formula:

$$v_{u1} = \frac{Q_{5_6}}{f_{\Pi}}.$$

The hydraulic piston motion L_{u1} is transmitted through the pivot $B1$ to the rocker arm AD which rotates around the point A . Having decomposed the joint speed $B1$ into radial v_{r1} and tangential $v_{\tau1}$, we determine the value of the tangential component:

$$v_{\tau1} = v_{u1} \cdot \sin \beta_1.$$

Then the angular velocity ω_{AD} of rotation of the rocker arm AD can be determined from the expression:

$$\omega_{AD} = \frac{v_{\tau1}}{r_1},$$

where r_1 is the length of the radius connecting the point A of the rocker arm rotation with the pivot $B1$.

The motion of the piston of the hydraulic cylinder L_{u1} is transmitted through the rocker arm AD to the piston of the hydraulic cylinder L_{u2} connected to the rocker arm AD through the pivot $B2$. In this case, the tangential velocity of the pivot $B2$ is determined from the formula:

$$v_{\tau2} = r_2 \omega_{AD},$$

where r_2 is the length of the radius connecting the point A of the rocker arm rotation with the pivot $B2$.

Projecting the tangential velocity of the pivot $B2$ on the direction of piston motion of the hydraulic cylinder L_{u2} , we determine the speed of its movement:

$$v_{u2} = \frac{v_{\tau2}}{\sin \beta_2}.$$

The angles β_1 and β_2 are determined according to the law of cosines from the triangles AG_1B_1 and AG_2B_2 , respectively:

$$\cos \beta_1 = \frac{L_{u1}^2 + r_1^2 - L_1^2}{2L_{u1}r_1},$$

$$\cos \beta_2 = \frac{L_{u2}^2 + r_2^2 - L_2^2}{2L_{u2}r_2}.$$

Here, L_{u1} and L_{u2} are distances between axes of attachment of the respective hydraulic cylinders to the stand frame and to the rocker arm considering the degree of extension of their pistons; L_1 and L_2 are distances between the axis of rotation of the rocker arm and the attachment points of the pivots of the hydraulic cylinders bodies to the stand frame.

Discussion and Conclusions. The system of equations presented in the paper shows how the pressure increment at the selected nodal points of the energy recovery system is determined (in particular, how the increment depends on the time, the reduced volumetric rigidity factor, the flow rate of the actuation fluid, and the area of pistons). The motion velocities of the hydraulic pistons are determined according to the kinematic scheme of the stand mechanical transmission. The study findings show that, thanks to the solution presented in the paper, the results of the life tests of hydraulic cylinders will adequately reflect their operation under the rated duties.

References

1. Nikitin, O.F. Nadezhnost', diagnostika i ekspluatatsiya gidroprivoda mobil'nykh ob'ektov. [Reliability, diagnostics and operation of hydraulic drive of mobile objects.] Moscow: Bauman University Publ. House, 2007, 312 p. (in Russian).
2. Bashta, T.M. et al. Gidravlika, gidromashiny i gidroprivody. [Hydraulics, hydraulic machines and hydraulic drives.] Moscow: Mashinostroenie, 1982, 423 p. (in Russian).
3. Ustyantsev, M.V. Povyshenie effektivnosti privoda stenda ispytaniy gidromashin vrashchatel'nogo deystviya: avtoref. dis. ... kand. tekhn. nauk. [Improving the efficiency of the test bench drive of hydraulic machines of rotary action: Cand.Sci. (Eng.), diss., author's abstract.] Rostov-on-Don, 2012, 18 p. (in Russian).
4. Rybak, A.T. et al. Issledovanie rekuperativnoy gidromekhanicheskoy sistemy stenda ispytaniy ob'emnykh gidromashin. [Study on regenerative hydromechanical testing system of positive displacement hydraulic machines.] Vestnik of DSTU, 2011, vol. 11, no. 9 (60), pp. 1651–1661 (in Russian).
5. Chukarin, A.N., et al. Rekuperatsiya energii pri ispytanii gidrotsilindrov. [Recuperation of energy at the test of hydrocylinders.] Vestnik RGUPS, 2009, no. 4, pp. 12–16 (in Russian).
6. Chukarin, A.N., et al. Rekuperatsiya energii pri ispytanii porshnevykh gidrotsilindrov. [Energy recovery under testing piston hydraulic cylinders.] Innovatsionnye tekhnologii v mashinostroenii: sb. st. Mezhdunar. nauch.-prakt. konf. [Innovative technologies in mechanical engineering: proc. Int. Sci.-Pract. Conf.] Rostov-on-Don: DSTU Publ. Centre, 2009, pp. 64–67 (in Russian).
7. Rybak, A.T., Freint, S.A., Maznev, D.S. Modelirovanie i raschet stenda dlya ispytaniy plunzhernykh gidravlicheskikh tsilindrov. [Modeling and calculation of a bench for testing plunger hydraulic cylinders.] Sostoyanie i perspektivy razvitiya sel'skokhozyaystvennogo mashinostroeniya: tr. 10-y mezhhdunar. nauch.-prakt. konf. 1–3 marta 2017 g. [The state and prospects of development of agricultural engineering: Proc. 10th Int. Sci.-Pract. Conf., March 1–3, 2017] Rostov-on-Don: DSTU Publ. Centre, 2017, pp. 692–695 (in Russian).
8. Freint, S.A., Rybak, A.T. Matematicheskoe modelirovanie gidrosistemy stenda s uluchshennymi kharakteristikami. [Mathematical modeling of the hydraulic system bench with improved characteristics.] Sistemnyy analiz, upravlenie i obrabotka informatsii: tr. VII mezhhdunar. seminar 6–12 oktyabrya 2016 g. [System analysis, management and information processing: Proc. VII Int. Seminar, October 6–12, 2016] Rostov-on-Don: DSTU Publ. Centre, 2016, pp. 57–61 (in Russian).
9. Rybak, A.T., Freint, S.A., Pelipenko, A.Yu. Modelirovanie gidromekhanicheskoy sistemy ispytatel'nogo stenda s rekuperatsiey energii. [Modeling of the hydromechanical system of a test bench with energy recovery.] Mekhanika, oborudovanie, materialy i tekhnologii: mat-ly Mezhdunar. nauch.-prakt. konf. 29–30 marta 2018 g. [Mechanics, equipment, materials and technologies: Proc. Int. Sci.-Pract. Conf., March 29–30, 2018] Krasnodar: PrintTerra, 2018, pp. 163–169 (in Russian).
10. Rybak, A.T., et al. Modelirovanie i issledovanie dinamiki privoda stenda ispytaniy gidravlicheskikh mashin vozvratno-postupatel'nogo deystviya. [Modeling and studying the dynamics of the drive test bench of reciprocating hydraulic machines.] Dinamika tekhnicheskikh sistem «DTS-2018»: sb. tr. XIV mezhhdunar. nauch.-tekhn. konf. 12–14 sentyabrya 2018 g. [Dynamics of technical systems “DTS-2018”: Proc. XIV Int. Sci.-Pract. Conf., September 12–14, 2018] Rostov-on-Don: DSTU Publ. Centre, pp. 68–72 (in Russian).
11. Boguslavskiy, I.V., Rybak, A.T., Chernavskiy, V.A. Nauchno-metodologicheskie osnovy proektirovaniya privodov tekhnologicheskikh mashin. [Scientific and methodological foundations for the design of drives of technological machines.] Rostov-on-Don: Institute of Management and Innovations of Aircraft Industry, 2010, 276 p. (in Russian).
12. Rybak, A.T., Boguslavskiy, I.V. Sovershenstvovanie nauchno-metodologicheskikh osnov proektirovaniya sistem privodov tekhnologicheskikh mashin. [Improvement of the scientific-methodological design principles of the production machines drive systems.] Vestnik of DSTU, 2010, vol. 10, no. 2 (45), pp. 249–257 (in Russian).

13. Rybak, A.T., et al. Modeling and calculation of hydromechanical systems dynamics based on the volume rigidity theory. MATEC Web of Conferences, 2018, vol. 226, p. 6.
14. Temirkanov, A.R., et al. Teoreticheskie issledovaniya gidromekhanicheskogo privoda rabocheho organa mobil'noy tekhnologicheskoy mashiny. [Theoretical studies of hydromechanical drive of mobile technological machine member.] Vestnik of DSTU, 2015, vol. 15, no. 2 (81), pp. 56–64 (in Russian).
15. Rybak, A.T., Temirkanov, A.R., Lyakhnitskaya, O.V. Modelirovanie i issledovaniya sinkhronnogo gidromekhanicheskogo privoda mobil'noy tekhnologicheskoy mashiny. [Modeling and studies on synchronous hydro-mechanical drive of a mobile technological machine.] STIN, 2017, no. 9, pp. 15–20 (in Russian).
16. Rybak, A.T., Temirkanov, A.R., Lyakhnitskaya, O.V. Dinamika sinkhronnogo gidromekhanicheskogo privoda mobil'noy tekhnologicheskoy mashiny. [Synchronous hydromechanical drive of a mobile machine.] STIN, 2018, no. 3, pp. 4–7 (in Russian).
17. Rybak, A.T., Temirkanov, A.R., Lyakhnitskaya, O.V. Dynamics of Synchronous Hydromechanical Drive in Mobile Machine. Russian Engineering Research, 2018, no. 38 (9), pp. 702–704. DOI 10.3103/S1068798X18090253.
18. Rybak, A.T., Temirkanov, A.R., Lyakhnitskaya, O.V. Synchronous hydromechanical drive of a mobile machine. Russian Engineering Research, 2018, no. 38 (3), pp. 212–217.
19. Tsybry, I. K., Ignatenko, V.I. Analysis of the influence of positive feedback on the quality of the control system. Available at: https://www.researchgate.net/publication/320732047_Analysis_of_the_influence_of_positive_feedback_on_the_quality_of_the_control_system DOI:10.1051/mateconf/20201713202011 (accessed: 12.08.19).
20. Rybak, A.T., Lyakhnitskaya, O.V. K voprosu o vychislenii privedennogo koeffitsienta ob'emnoy zhestkosti gidrolinii. [On calculating the reduced coefficient of volumetric stiffness of hydraulic lines.] Mekhanika, oborudovanie, materialy i tekhnologii: tr. mezhdunar. nauch.-prakt. konf. [Mechanics, equipment, materials and technologies: Proc. Int. Sci.-Pract. Conf.] Krasnodar: Kuban State Tech. University Publ. House, 2018, pp. 169–175 (in Russian).
21. Rybak, A., Lyakhnitskaya, O. Modelling the reduced coefficient of volumetric rigidity in high-pressure rubber-cord shell hoses. Available at: https://www.researchgate.net/publication/320732124_Modelling_the_Reduced_Coefficient_of_Volumetric_Rigidity_in_High-Pressure_Rubber-Cord_Shell_Hoses (accessed: 12.08.19).

Submitted 25.02.2019

Scheduled in the issue 05.04.2019

Authors:

Rybak, Alexander T.,

professor of the Instrument Making and Biomedical Engineering Department, Don State Technical University (1, Gagarin Square, Rostov-on-Don, 344000, RF), Dr.Sci. (Eng.), professor,
ORCID: <https://orcid.org/0000-0001-9950-3377>
2130373@mail.ru

Tsybriy, Irina K.,

Head of the Instrument Making and Biomedical Engineering Department, Don State Technical University (1, Gagarin Square, Rostov-on-Don, 344000, RF), Cand.Sci. (Eng.), associate professor,
ORCID: <https://orcid.org/0000-0002-6281-1832>
irconst@mail.ru

Nosachev, Sergey V.,

senior lecturer of the Production Automation Department, Don State Technical University (1, Gagarin Square, Rostov-on-Don, 344000, RF), Cand.Sci. (Eng.),
ORCID: <http://orcid.org/0000-0003-0302-2937>
nosachev-s@yandex.ru

Zenin, Alexander R.,

postgraduate, Don State Technical University (1, Gagarin Square, Rostov-on-Don, 344000, RF),
ORCID: <https://orcid.org/0000-0003-0336-315X>
azenin@donstu.ru

MACHINE BUILDING AND MACHINE SCIENCE МАШИНОСТРОЕНИЕ И МАШИНОВЕДЕНИЕ



UDC 620.179

<https://doi.org/10.23947/1992-5980-2019-19-3-250-255>

Selection rationale for leakage monitoring in gas pipeline*

A. D. Lebed¹, S. P. Glushko^{2**}

^{1,2} Kuban State Technological University, Krasnodar, Russian Federation

Обоснование выбора способов контроля утечек на газопроводе***

А. Д. Лебедь¹, С. П. Глушко^{2**}

^{1,2} Кубанский государственный технологический университет, г. Краснодар, Российская Федерация

Introduction. Efficient leak detection methods and gas flow metering are analyzed. The work objective is to select an automatic system of methods providing the improvement of the quality of leakage monitoring and gas flow metering in gas pipelines.

Materials and Methods. The following techniques for detecting gas leakage in the pipeline are considered: according to the pressure profile, volume balance method, acoustic emission method, variable-pressure drop method on the forcing device, ultrasonic method.

Research Results. The analysis shows that all techniques for monitoring leakage and gas flow are dependent on the environmental parameters. Therefore, an important task is to achieve independence of the measurement results from changes in the environmental parameters. In most flow meters, changes in density, pressure and temperature affect drastically the measurement results. An additional error that arises in this case can reach large values.

Введение. Анализируются эффективные методы обнаружения утечек и учета расхода газа. Целью работы является выбор автоматической системы методов, позволяющей повысить качество контроля утечек и учета расхода газа на магистральных газопроводах.

Материалы и методы. Рассмотрены следующие методы обнаружения утечек газа в трубопроводе: по профилю давления, объемно-балансовый, метод акустической эмиссии, метод переменного перепада давления на вынуждающем устройстве, ультразвуковой метод.

Результаты исследования. Анализ показывает, что все методы контроля утечек и расхода газа зависят от параметров окружающей среды. Поэтому важной задачей является достижение независимости результатов измерений от изменения параметров среды. У большинства расходомеров изменение плотности, давления и температуры среды существенно сказывается на результатах измерения. Возникающая при этом дополнительная погрешность может достигать больших величин.

Keywords: main gas pipeline, control, leakage, control system, robot.

Ключевые слова: магистральный газопровод, контроль, утечки, система управления, робот.

For citation: A.D. Lebed, S.P. Glushko. Selection rationale for leakage monitoring in gas pipeline. Vestnik of DSTU, 2019, vol. 19, no. 3, pp. 250–255. <https://doi.org/10.23947/1992-5980-2019-19-3-250-255>

Образец для цитирования: Лебедь А. Д. Обоснование выбора способов контроля утечек на газопроводе / А. Д. Лебедь, С. П. Глушко // Вестник Дон. гос. техн. ун-та. — 2019. — Т. 19, № 3. — С. 250–255. <https://doi.org/10.23947/1992-5980-2019-19-3-250-255>

Introduction. Due to the high growth of the gas industry, the increase in the share of natural gas relative to other energy sources in the domestic Russian market and the increase in gas consumption in the world market, reducing gas losses and improving the safety of operation of gas pipelines is an urgent task [1]. Therefore, the most important problem is to maintain the working condition of the linear sections of the field and main gas pipelines (MGP). Underground gas pipelines operated under normal conditions can be maintained in working condition for several decades. The maintenance of the working condition of underground and aboveground MGP is facilitated through their condition monitoring and on-time scheduled maintenance.

Defects on the MG occur as a result of corrosion and, less commonly, due to mechanical damage. Detection of places of corrosion and damage is associated with time and material costs. Breaking a gas pipeline for direct visual inspection is economically unprofitable or impossible. Examination of only the outer surface of the pipe usually turns



* The research is done within the frame of the independent R&D.

**E-mail: anya-11-06@mail.ru, sputnik_s7@mail.ru

*** Работа выполнена в рамках инициативной НИР.

sour. Therefore, it is relevant to monitor the status of underground and aboveground field MGP without breaking. The solution to this problem is complicated by considerable technical difficulties; however, modern methods and means of measuring equipment enable to overcome them. These means vary in the following properties and parameters:

- physical phenomena underlying the work;
- principle of action;
- sensitivity;
- area of application;
- diagnosis locality or globality.

In gas leak detection systems in the pipelines, organoleptic and instrumental methods are used. The easiest method is odor fixation. For visual control methods, a foaming soap emulsion is used to record the occurrence of ice or a snow coat, the appearance of yellow grass in summer or brown snow in winter. Undoubtedly, instrumental methods are more advanced and accurate.

They are based on the use of automatic and manual gas analyzers. As automatic gas analyzers, gas sensors are widely applied: these are high-precision measuring devices used in continuous automatic monitoring of the amount of gases contained in air. Gas detectors are used in industrial, domestic and communal facilities. Gas sensors are available in the form of separate devices that can be placed autonomously and respond to changes in the concentration of certain gases. They instantly respond to an increase in the concentration of gases emanating from the gas transmission system. Modern models of sensors are equipped with liquid crystal displays on which measured values are displayed. Built-in memory provides recording the data and storing all measurement results. The display also shows information on the durability of the device and existing troubles. This feature allows changing worn-out components in proper time.

Gas control sensors are divided into two main types: household and industrial. Household alarms provide a number of responses to exceeding the set gas concentration. The main tasks of an industrial sensor are measuring and displaying gas content indices. Industrial devices are used to solve more significant problems and as part of automated systems together with a control panel that displays data from gas sensors. By the type of gas being monitored, methane and propane alarms are distinguished, as well as alarms designed to measure the concentration of carbon monoxide or carbon monoxide. Along with this, there are combined (multi-component) signaling devices. Gas sensors can be stationary, line-powered ones, located close to the electrical source, or portable, battery-driven sensors.

A gas contamination sensor is a multifunctional device; it has functions of audio and light warning. For example, in the CAK3-MK-1 (SAKZ-MK-1) system (Fig. 1), if the device responded to gas pollution, its indicator lights up and an audible alert is generated. Gas sensors have a relay output for connecting additional electrical devices: announcers, fans, mechanisms and devices of the fire and dispatcher panels.

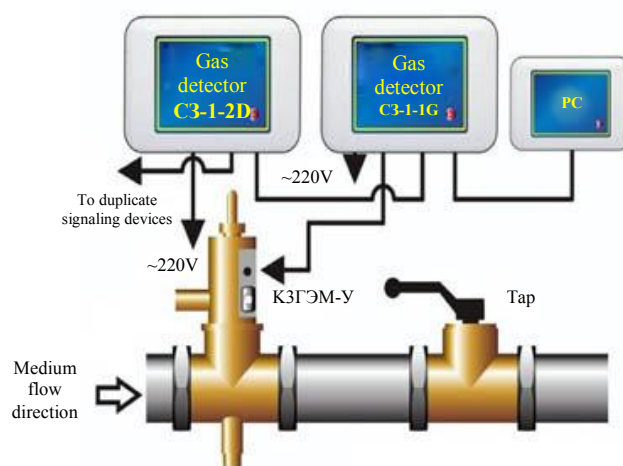


Fig. 1. Gas alarm system CAK3-MK-1 (SAKZ-MK-1)

Gas pollution sensors according to STO (company standard) Gazprom 5.37-2011 are used in nodes of measuring the flow rate and amount of flammable natural gas supplied from field treatment facilities, underground storage facilities, gas processing plants, to the main gas pipelines and then transported to consumers in the Russian Federation, to neighboring countries where it is utilized and consumed on in-home process needs. Gas sensors are disadvantageous to use throughout the main pipelines. Besides, in hard-to-reach locations of trunk pipelines, it is difficult to use organoleptic and instrumental methods for detecting gas leakage.

Materials and Methods. In addition to the above methods for detecting gas leakage in pipelines, the following techniques are used [2]:

- pressure profile analysis;
- volume-balance method;
- acoustic emission analysis;
- variable pressure drop analysis;
- mechanical method using velocity flowmeters;
- ultrasonic flow rate metering method.

According to the leakage detection method for pressure profile analysis, a simulation of the pressure distribution along the pipeline and a statistical analysis of this distribution are performed. In case of gas leakage, the flow rate in the controlled section becomes greater than the initial flow rate in this section, and the flow rate in the section after the leakage point becomes smaller than the initial flow rate. As a result, the pressure drop in the area to the leakage point increases, and after the leakage decreases, which leads to the appearance of a break in the pressure profile. The leak detection method through analyzing the pressure profile works only in the stationary mode since many factors cause similar changes. A significant drawback of this method is low accuracy and presence of false responses. To reduce false responses, deviations should be recorded at least at two adjacent points. For the same purposes, an averaged pressure distribution profile is used, which is a quasistationary profile. This profile is obtained through filtering pressure at points in the pipeline. The averaged pressure profile is not constant. It changes, but more slowly than the actual pressure, which leads to an increase in the detection time of leaks.

The volume-balance control technique rests on the fact that when a leak is formed, the inlet flow rate becomes greater than the outlet flow rate. In addition, this method considers the amount of gas in the pipe itself, which decreases when a leak occurs. To implement this technique, it is necessary to measure the flow rate at the boundaries of the controlled area using high-precision tools.

The control parameter in the volume-balance method is not the gas pressure, but its normalized flow rate. The control of the pipeline section is performed through determining the difference between the normalized volumes of gas entering and leaving the section between two local flowmeters. This method provides the diagnosis of both rapidly developing breaks in the pipe, and slowly developing leaks, as well as leaks in very large sections of the pipeline between the flowmeters. The minimum value of the diagnosed leak is determined, first of all, by the error in measuring the flow rate and, with current means of measuring the flow rate, is at the level of 0.5–1.0%. Accuracy of leakage monitoring depends on the precision of the flowmeters. It is impossible to detect a leak whose flow rate is less than the measurement error. In this case, it is not the absolute error that matters, but only a meter to meter error.

The volume-balance method does not determine the leakage coordinate – this is its major drawback. Besides, the volume-balance flow in the sections provides the determination of the point of leakage in the gas pipeline only to an accuracy of the estimation of this parameter to a specific section. This, in turn, leads to additional time and gas losses from the moment of leakage to the moment of its elimination.

The acoustic emission analysis method takes the lead in the industry of the automatic detection of gas leaks in pipelines [3]. This method is based on the registration and analysis of acoustic waves that occur during plastic deformation and microlysis of the pipeline material, as well as when gas flows through the open-end holes in the pipe. Piezo-electric transducers and high-speed pressure meters are used to receive acoustic emission signals.

The advantages of this method are as follows:

- high sensitivity to developing defects;
- short detection time;
- high accuracy of determining the leakage coordinates.

The disadvantage of this method is difficulty of the acoustic emission signal extraction against the background of noise and interference. To increase noise immunity and reduce the number of false alarms, adhoc techniques of processing the received signals are applied.

When developing a system for detecting gas leakage at gas pipelines and gas metering units at the production facilities, the following tasks should be addressed:

- obtaining independence of measurement results from changes in environmental parameters due to gas pressure control;
- improving the accuracy of monitoring leakage and gas flow.

Gas flow measurement is an important task in the gas industry since a gas metering system is infeasible without flow measurement tools. At the gas industry facilities, tachometers and counters are used to measure gas flow and its quantity. Recently, the state-of-the-art-type ultrasonic flowmeters are also actively introduced into the gas pipeline

control industry [4]. However, nowadays, a method of variable pressure drop on a constriction device (CD) is most widely used for measuring gas flow rate. The principle of method is to measure the pressure drop before and after the CD installed in the gas stream. Gas volumetric flow rate Q for special CD is determined from the formula:

$$Q = CE\varepsilon F_0 \sqrt{\frac{\Delta p}{\rho}},$$

where C is the discharge coefficient which is the ratio of the actual flow rate to the theoretical one; E is the input velocity coefficient; ε is the expansion coefficient considering an increase in the specific gas volume; F_0 is the area of CD, m^2 ; Δp is the drop created by the CD, Pa; ρ is the gas density, kg/m^3 .

Advantages of the variable pressure drop method are as follows:

1. Versatility. This method is used to measure the flow rate of almost any medium: liquid, gas, steam. For viscous liquids, CDs of special form are used.
2. Low initial cost. The cost of a flowmeter based on the method of variable differential pressure comprises the cost of the CD, impulse lines and differential pressure sensor.
3. A simple verification technique. For periodic calibration of flowmeters, it is necessary to measure the geometric dimensions of the CD and to check the differential pressure sensor.
4. Zero moving parts.
5. Possibility to measure flow under high pressure conditions. Pressure in the pipeline can reach 40 MPa.
6. Possibility to measure flow over a wide temperature range of the medium being measured – from minus 200 to plus 1000° C.
7. A wide range of sizes. The considered method is used on pipelines in the range of nominal diameters from 15 to 2000 mm.

Disadvantages of measuring gas flow by the method of variable pressure drop analysis on the CD are the following:

1. Narrow dynamic range. The standard dynamic range of the CD is approximately 1: 3. This limitation is associated, first of all, with a quadratic dependence between the flow rate and the pressure drop on the CD. The dynamic range can be increased by the use of high-precision differential pressure (DP) indicators.
2. High operation cost. CD-based flowmeters require periodic maintenance, which includes measuring the geometrical dimensions of the constriction device, cleaning the impulse lines, heating the impulse lines, and zero setting on the DP indicator.
3. Low accuracy of measurements. The measurement error is usually 3.0-3.5%.

The principle of operation of tachometric flowmeters is based on the dependence of the speed of the transducer, installed in the pipeline, on the gas flow. In the flowmeters of the “counter” type, the flow transducer shaft is connected to a counting mechanism through the gearbox, which provides measuring the amount of transmitted gas. The advantages of such devices are speed and a wide range of measurements.

The error of the counters is 0.5–1.5%. The application of tachometric transducers can reduce the error in converting the flow rate to the converter speed up to 0.3%. The major disadvantages of tachometric flowmeters are wear of supports and the presence of moving elements. The disadvantage in relation to flowmeters with CD is the need for calibration facilities.

The principle of operation of ultrasonic flowmeters is based on the phenomenon of displacement of sound vibrations by a moving medium. This method has the following disadvantages:

- dependence of the intrinsic ultrasonic velocity on the physicochemical properties of the medium being measured;
- flow velocity is averaged along the ultrasonic beam, and not over the cross section of the pipe.

Averaging the flow rate brings the developers to supply the design with additional sensors or reflectors, which makes the flow meter more complicated. This increases the chances of an error in case of the system sensors breakdown.

Advantages of this method are:

- zero pressure drop;
- high speed;
- zero moving elements.

Research Results. The analysis shows that the task of detecting and localization (accurate positioning) of gas leakage cannot be solved using one of the considered methods. Given the advantages and disadvantages of the methods discussed in this paper, it is proposed to solve the problem using three methods and stepwise:

- determine the section with gas leakage between stations using the volume-balance method;

- establish a local section of pipeline damage and gas leakage by the method of acoustic emission analysis;
- using ultrasonic flaw detection, determine the leakage coordinates within the specified local damage section.

To control horizontal and straight length sections of the gas pipeline and to accurately fix the leakage points using an ultrasound scanner, various robots can be applied [5–7], for example, video crawlers which are mobile and universal means of pipeline inspection. They are suitable for various applications due to the modular design and the ability to inspect the pipes with diameters from 150 to 900 mm from inside. Fig. 2 shows one of these robots, Rovver 600 video crawler. The remote control of the robot provides checking focus and lighting, as well as heading the motion in the area of obstructions or branches.



Fig. 2 Rovver 600 video crawler

Discussion and Conclusions. The authors propose to increase the reliability of detection and localization of gas leakage using a combined three-stage technique, which includes a sequential application of the volume-balance method, acoustic emission analysis, and ultrasonic flow rate metering. In certain situations, the use of task-specified robots is recommended. The authors hold that robots should be equipped with a 90-degree bend detection sensor mounted on the head link, as well as with speed and distance sensors for accurate positioning. This will reduce the time of diagnosing gas pipelines of various types and cut down the cost of monitoring their condition.

Analysis of information on accidents in the gas complex is of great importance, first of all, for evaluating risk factors and the reliability of the gas transmission system. The analysis results are required to validate design solutions of gas supply system facilities, and they are applied when planning measures to increase their reliability and safety under operation.

References

1. Edinye tekhnicheskie trebovaniya na oborudovanie uzlov izmereniya raskhoda i kolichestva prirodnogo gaza, primenyaemykh v OAO «Gazprom»: STO Gazprom 5.37-2011 [Uniform specifications of units for measuring the flow rate and amount of natural gas used in “Gazprom” OJSC: Gazprom industry standard 5.37-2011] Appr. and put into effect by order of Gazprom no. 500 dated 12/21/2010. Available at: <https://elima.ru/docs/index.php?id=6291> (accessed 23.12.2018) (in Russian).
2. Chupin, V.R., Guskov, E.V., Maizel, D.I. Metody obnaruzheniya utechek gaza iz magistral'nykh truboprovodov. [Methods to reveal gas leaking from trunk pipeline.] Proceedings of Universities. Investment. Construction. Real estate. 2012, no. 2 (3), pp. 123–127 (in Russian).
3. Tekhnicheskaya diagnostika. Akustiko-emissionnaya diagnostika. Obshchie trebovaniya: GOST R 52727-2007. [Technical diagnostics. Acoustic-emission diagnostics. General requirements: GOST R 52727-2007] Available at: <http://docs.cntd.ru/document/gost-r-52727-2007> (accessed 23.12.2018) (in Russian).
4. Raskhod i kolichestvo prirodnogo gaza. Metodika vypolneniya izmereniy s pomoshch'yu ul'trazvukovykh preobrazovateley raskhoda: STO Gazprom 5.2-2005. [Consumption and amount of natural gas. Measurement procedure using ultrasonic flow transducers: Gazprom industry standard 5.2-2005] Appr. and put into effect by order of Gazprom no. 271 dated 10.10.2005. Available at: https://ohranatruda.ru/ot_biblio/norma/248957/ (accessed 23.12.2018) (in Russian).
5. Poezzhaeva, E.V., Fedotov, A.G., Zaglyadov, P.V. Razrabotka robota dlya kontrolya truboprovodov. [Development of a pipeline control robot.] Young Scientist, 2015, no.16, pp. 218–222. URL <https://moluch.ru/archive/96/21567/> (accessed: 23.12.2018) (in Russian).
6. Chastikov, A.P., et al. Programmnyaya sistema testirovaniya i otladki upravlyayushchikh programm dlya robototekhnicheskogo kompleksa: Svidetel'stvo o gosudarstvennoy registratsii programmy dlya EVM. [Software system for testing and debugging control programs for robotic complex.] Certificate of software state registration no.2011611987, 2011] (in Russian).

7. Chastikov, A.P., Glushko, S.P., Totukhov, K.E. Komp'yuternaya simulyatsiya programmno upravleniya virtual'nym robotom. Issledovanie, razrabotka, ispytanie. [Computer simulation of virtual robot software control. Research, development, testing] Saarbrücken: LAP LAMBERT Academic Publishing, 2012, 136 p. (in Russian).

Submitted 25.02.2019

Scheduled in the issue 05.04.2019

Authors:

Lebed, Anna D.,

student of the Control Systems and Technological Complexes Department, Kuban State Technological University (2, Moskovskaya St., Krasnodar, 350072, RF),

ORCID: <https://orcid.org/0000-0003-4263-8806>

anya-11-06@mail.ru

Glushko, Sergey P.,

associate professor of the Control Systems and Technological Complexes Department, Kuban State Technological University (2, Moskovskaya St., Krasnodar, 350072, RF), Cand.Sci. (Eng.), associate professor,

ORCID: <https://orcid.org/0000-0002-7087-6572>

sputnik_s7@mail.ru

MACHINE BUILDING AND MACHINE SCIENCE МАШИНОСТРОЕНИЕ И МАШИНОВЕДЕНИЕ



UDC 631/635

<https://doi.org/10.23947/1992-5980-2019-19-3-256-261>

Comparison of graphic expression of dependences of transporter cut profile of threshing-separating unit on the second volume and spike fraction humidity***

A. G. Dyachenko¹, T. P. Savostina², S. B. Imad^{3**}

^{1,2} Don State Technical University, Rostov-on-Don, Russian Federation

³ University of Aleppo, Aleppo, Syrian Arab Republic

Сравнение графического выражения зависимостей профиля среза транспортирующего устройства молотильно-сепарирующего агрегата от секундного объема и влажности колосовой фракции*

А. Г. Дьяченко¹, Т. П. Савостина², С. Б. Имад^{3**}

^{1,2} Донской государственный технический университет, г. Ростов-на-Дону, Российская Федерация

³ Университет Алеппо, г. Алеппо, Сирийская Арабская Республика

Introduction. Threshing is a multifactorial process which is affected, in particular, by the feedrate of the crop, the specific weight of the threshed grain and return, separation rates, weediness and moisture of the crop. From this point of view, the issues of optimizing the profile of the transporter cut, which allows for threshing and separation with the least effort, are also relevant. It was also experimentally established that the threshing process is affected by the volume of grain material delivered per second (second feed) and the unit velocity.

Materials and Methods. The studies were conducted on a test bench equipped with a threshing-separating device in the form of a single-cavity hyperboloid. When performing the work, the width of the drum was divided into three zones, and the length – into five cells. Wheat grain, obtained through threshing and separation in each zone and cell, came to individual containers. Straw was collected separately. Then, the grain and straw were weighed. The resulting data was processed by statistical and mathematical methods.

Research Results. The lengths of each cell were calculated based on the ratio of the total separation and the amount of grain mass per unit length. The lengths of each cell were calculated depending on changes in humidity. Indicators of the ratio between mass humidity and cell length are presented in the form of a table.

By the given table values for different moisture levels of the grain mass, graphs were constructed, each of which was described by a mathematical model considering the drum length and width. An averaged cut profile is presented for the treated plant mass with humidity of 8%, 12%, 16%, 20%, and 24%.

Discussion and Conclusions. Analysis of the data in this paper

Введение. Обмолот представляет собой многофакторный процесс, на который влияют, в частности, скорость подачи растительной массы, удельный вес обмолоченного зерна и недомолота, показатели сепарации, засоренность и влажность растительной массы. С этой точки зрения актуальны и вопросы оптимизации профиля среза транспортирующего устройства, которая позволяет проводить обмолот и сепарацию с наименьшими усилиями. Опытным путем установлено также, что на процесс обмолота влияют объем подаваемого зернового материала за секунду (секундная подача) и скорость движения агрегата.

Материалы и методы. Исследования проводились на испытательном стенде, оснащённом молотильно-сепарирующим устройством в форме однополостного гипербоида. При выполнении представленной работы ширина барабана была разделена на три зоны, а длина — на пять ячеек. Зерно пшеницы, полученное при обмолоте и сепарации в каждой зоне и ячейке, поступало в отдельные контейнеры. Солома собиралась отдельно. Затем зерно и солома взвешивались. Полученные в итоге данные обрабатывались статистическими и математическими методами.

Результаты исследования. Рассчитаны длины каждой ячейки исходя из отношения суммарной сепарации и количества зерновой массы, приходящейся на единицу длины. Вычислены длины каждой ячейки в зависимости от изменения влажности. Показатели соотношения влажности массы и длин ячеек представлены в виде таблицы. По заданным табличным значениям для различных уровней влажности зерновой массы построены графики, каждый из которых описан математической моделью, учитывающей длину и ширину барабана. Представлен усредненный профиль среза для обрабатываемой растительной массы влажностью 8%, 12%, 16%, 20%, 24%.

Обсуждение и заключения. Анализ данных этой и более ранних работ позволил сравнить графическое выражение

*** The research is done within the frame of the independent R&D.

*Работа выполнена в рамках инициативной НИР.

** E-mail: Dyachenko_aleshka@bk.ru, kovtanya@yandex.ru, Imad12sb@gmail.com



and earlier ones provides the comparison of the graphic expression of the dependences of the transporter cut profile on the second volume and humidity of the grain mass entering it. It has been established that the cut profile curves are identical along the entire length of the drum. The confidence factor is close to 1, which indicates the accuracy of the model. The identity of the averaged cut profiles is obviously dependent on moisture of the plant mass and on the second feed.

Keywords: threshing and separating device, grain mass, spike fraction, plant mass input, transporter, cut profile, return, separation, weediness, humidity.

For citation: A.G. Dyachenko, et al. Comparison of graphic expression of dependences of transporter cut profile of threshing-separating unit on the second volume and spike fraction humidity. Vestnik of DSTU, 2019, vol. 19, no. 3, pp. 256–261. <https://doi.org/10.23947/1992-5980-2019-19-3-256-261>

зависимостей профиля среза транспортирующего устройства от секундного объема и влажности поступающего на него зернового вороха. Установлено, что кривые профиля среза идентичны по всей длине барабана. Коэффициент достоверности близок к 1, что говорит о точности модели. Очевидна идентичность усредненных профилей среза в зависимости от влажности растительной массы и от секундной подачи.

Ключевые слова: молотильно-сепарирующее устройство, зерновой ворох, колосовая фракция, подача растительной массы, транспортирующее устройство, профиль среза транспортирующего устройства, недомолот, сепарация, засоренность, влажность.

Образец для цитирования: Дьяченко, А. Г. Сравнение графического выражения зависимостей профиля среза транспортирующего устройства молотильно-сепарирующего агрегата от секундного объема и влажности колосовой фракции / А. Г. Дьяченко, Т. П. Савостина, С. Б. Имад // Вестник Дон. гос. техн. ун-та. — 2019. — Т. 19, № 3. — С. 256–261. <https://doi.org/10.23947/1992-5980-2019-19-3-256-261>

Introduction. Improving the quality indicators of grain is one of the important factors in the yield enhancement [1, 2]. In the process of grain harvesting, especially threshing, severe damage to grains occurs [3]. In a combine harvester, the grain is separated from straw impurities. At this stage, the grain gets damaged, its quality deteriorates, quantitative losses occur [4].

Negative impact of these factors can be reduced if the path of the mass in a uniform layer along the entire length of the drum during the threshing process will be increased. Previous studies show that the threshed grain passes in a denser layer in the middle of the drum [5], and separation increases in this zone. Closer to the edges of the drum, the mass is much less dense, and the volume of separated grain here is 2–3 times less than in the middle [6, 7]. From this point of view, the most promising is the design of the threshing-separating device of the tangential-axial type, which evenly distributes the threshed mass along the entire length of the drum.

Losses during threshing and separation depend on the quality indicators of grain and on the technical specifications of the drum [8, 9]. Optimization of the profile of the transporter cut which provides threshing and separation with the least effort is also relevant. The profile of the transporter cut is a part of the separator transition grate designed for uniform and continuous movement of the spike fraction along the width of the tangential axial threshing and separating unit (TSU) in the form of a rotation hyperboloid.

In the day, the dependence of the cut profile on the cutter speed, its height setting and the angle of the reaper cutting elements [10] was determined. In addition, it was experimentally established that the threshing process is also affected by the volume of supplied grain material per second (second feed) [8], as well as the speed of the unit [11].

The work objective is to develop a mathematical model of the threshing process with a uniform supply of the processed mass along the entire length of the threshing and separating drum.

Materials and Methods. The studies were performed on a test bench equipped with a threshing and separating unit in the form of a one-sheet hyperboloid (Fig. 1).

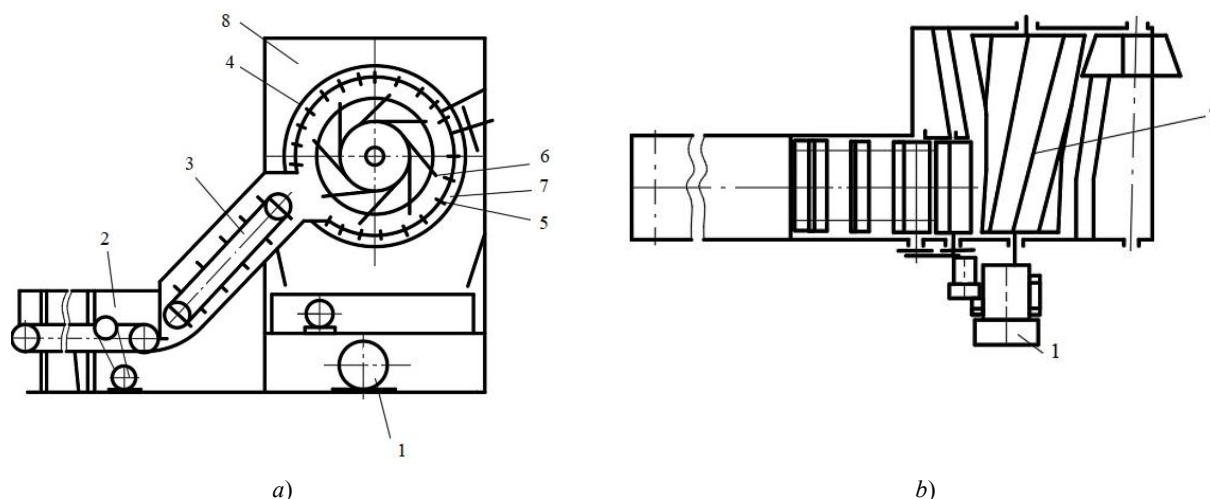


Fig. 1. Diagram of the stand equipped with threshing and separating unit: side view (a); top view (b)

The test bench consists of an electric motor (1). From it, rotation is transmitted to the drive drum (4) through a belt drive. A threshing and separating unit is installed on the drum. Its shape is a rotary one-sheet hyperboloid (7). The threshing and separating unit (7) consists of rear beaters (6) and a deck (5). The test bench is protected by a cover (8). An ear fraction enters the feeding section (2). This mass is fed through the conveyor belt (3) to the threshing and separating unit (7).

When studying, the width of the drum was divided into three zones, and the length – into five cells. Wheat grain obtained through threshing and separation in each zone and cell came to individual containers for collection. Straw was collected separately. Then the grain and straw were weighed.

The data obtained as a result of the study were processed by statistical and mathematical methods [10, 11].

Preliminary investigations [6, 7, 12] afford the following statement: as the threshed grain mass moves through the TSU, the total grain separation increases from the first zone to the third.

Within the framework of the presented paper, the cut profile was determined experimentally.

The objective of the study is to compare the dependence of the profile on:

- the volume of plant mass feeding per second;
- humidity of the plant mass.

The relationship between the cut profile and the second feed rate was established earlier [13, 14]; therefore, it is necessary to determine a similar dependence of the profile and the humidity index of the threshed mass. Table 1 shows the absolute values of cell separation depending on humidity [12].

Table 1

Absolute total cell separation values as a function of mass moisture

Grain moisture	$\sum S_1$	$\sum S_2$	$\sum S_3$	$\sum S_4$	$\sum S_5$	$\sum S$	Const
w = 8 %	10.8893	6.74	4.578	4.401	7.4922	34.1004	0.0341
w = 12 %	8.2186	5.291	3.603	3.264	5.3326	25.7084	0.02571
w = 16 %	6.7987	4.569	3.317	3.115	4.8956	22.6958	0.0227
w = 20 %	6.3305	4.172	3.154	2.916	4.4444	2.017	0.02102
w = 24 %	6.0782	3.906	3.029	2.786	4.2682	2.065	0.02007

Results and Discussion. To determine the cut profile, the following condition should be fulfilled: maintaining a constant (const) amount of the processed mass per unit length of the TSU. The const value is determined through the ratio of the total separation to the length of the drum $L = 1200$ mm. The determination technique was applied earlier when constructing cut profiles corresponding to various values of the second feed [14].

To calculate the length of each cell, it is necessary to determine the ratio of the total separation and the amount of grain mass per unit length:

$$\ell_i = \frac{\sum S_i}{const}, \quad (1)$$

where $\sum S_i$ is the absolute total separation value in the i-th cell; const is the volume of the processed mass per unit length of the TSU at a given moisture content of the plant mass.

Substituting the values from Table 1 to the formula (1) and calculating the length of each cell depending on the change in humidity, we obtain the results given in Table 2.

Table 2

The ratio of mass moisture and cell lengths

Grain moisture	ℓ_1 , mm	ℓ_2 , mm	ℓ_3 , mm	ℓ_4 , mm	ℓ_5 , mm	$\sum \ell$, mm
w = 8 %	319.331	197.7	134.3	129.1	219.71	1000
w = 12 %	319.685	205.8	140.1	127	207.43	1000
w = 16 %	299.558	201.3	146.2	137.3	215.71	1000
w = 20 %	301.209	198.5	150.1	138.7	211.47	1000
w = 24 %	302.925	194.7	151	138.8	212.72	1000

The total length of all cells $\sum \ell$ is equal to the width of the drum $B = 1000$ mm.

The length values ℓ_i are plotted on the abscissa and correspond to the i-th cells of the drum length (L).

Using the given tabular values for each of the moisture content of the grain mass, approximate functions $f(x)$ were obtained. Each graph shown in Fig. 2 is described by a mathematical model of the dependence of the drum length (L) on its width (B).

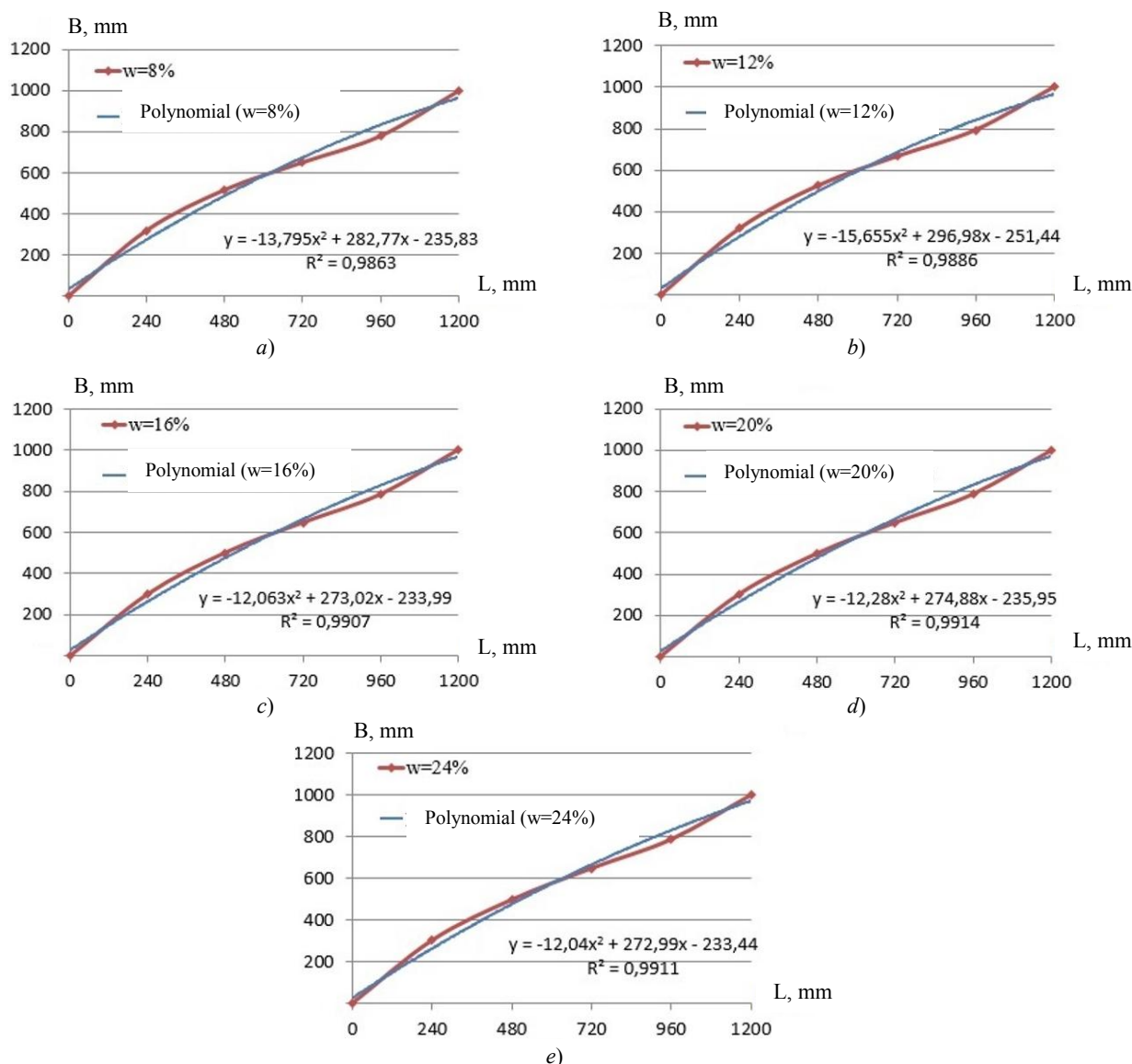


Fig. 2. Cut profiles depending on the moisture content of the grain mass: a) 8%; b) 12%; c) 16%; d) 20%; e) 24%

Fig. 2 shows the identity of the graphs. Consequently, it is possible to construct an averaged cut profile for a full moisture range of the processed grain mass. For this purpose, the length values of each cell are summed up and divided by the total number of humidity indices. By analogy with the previous graphs, an average cut profile is plotted (Fig. 3).

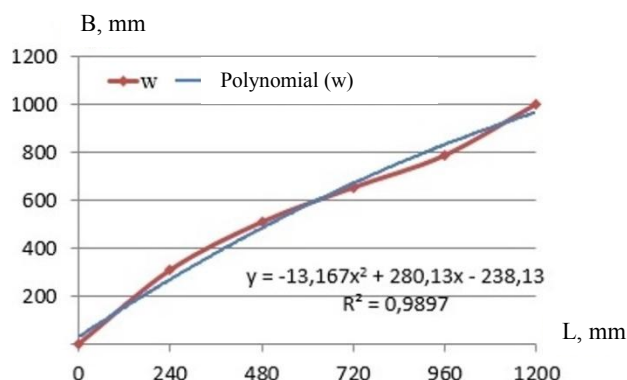


Fig. 3. Average cut profile for the treated plant mass with moisture of 8%, 12%, 16%, 20% and 24%

The data from Fig. 3 are compared to the earlier obtained averaged cut profile due to the second feed (Fig. 4).

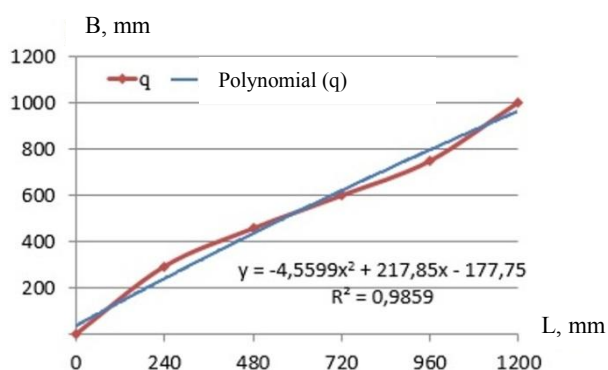


Fig. 4. Average cut profile for the treated plant mass depending on the second feed

Discussion and Conclusions

1. Fig. 2 shows that when the moisture content of the treated plant mass is changed, the curves of the cut profile are identical along the total length of the drum.
2. The confidence coefficient of the approximation R^2 shows the degree of compliance of the trend model with the initial data. The confidence coefficient is close to 1 which indicates the accuracy of the model.
3. The identity of the average cut profiles depends obviously on the moisture content of the plant mass (Fig. 3) and on the second feed (Fig. 4).

References

1. Krasnoshchekov, N.V. Innovative development of agricultural production in Russia. Moscow: Rosinformagrotekh, 2009, 388 p.
2. Maslov, G.G. Russian grain is not in high demand on the world market. Chief Agronomist, 2009, no. 11, p. 6.
3. Lipovsky, M.I. Rotary combine harvester quality improving. Agricultural machinery and technology, 2014, no. 2, p. 43.
4. Maslov, G.G., Palapin, A.V., Rinas, N.A. Grain crops complex harvesting perspectives: monograph. Krasnodar: Kuban State Agrarian University, 2014, 87 p.
5. Tarasenko, B.F., et al. Zernoubochnaya ochesyvayushchaya mashina : patent 2305395 Ros. Federatsiya: A01D 41/08 [Combine harvesting machine.] RF Patent no. 2305395, 2007 (in Russian).
6. Antypas, I.-R., Dyachenko, A.G., Savostina, T.P. Issledovanie protsessa obmolota tangentsial'no-aksial'nym separiruyushchim ustroystvom v zavisimosti ot raspredeleniya zernovoy massy po zonam. [Research of the threshing process with tangential-axial breaking unit in independence of grain mass zone division.] Science Review, 2016, no. 23, pp. 87–91 (in Russian).
7. Antypas, I.-R., Savostina, T.P. Vliyanie sekundnoy podachi na protsess obmolota tangentsial'no-aksial'nym molotil'no-separiruyushchim ustroystvom. [Impact of second feed for the threshing process of tangential-axial breaking unit.] Science Review, 2017, no. 3, pp. 47–51 (in Russian).

8. Antypas, I.-R., Savostina, T.P., Saed, B.I. Vliyanie parametrov molotil'no-separiruyushchego ustroystva na obmolot. [Effect of threshing-separating device parameters on threshing.] Vestnik of DSTU, 2017, vol. 17, no. 2 (89), pp. 108–115 (in Russian).
9. Antypas, I.-R., Savostina, T.P. Modelirovanie profilya sreza transportiruyushchego ustroystva. [Modeling a cut profile of a conveying device.] Sostoyanie i perspektivy razvitiya sel'skokhozyaystvennogo mashinostroeniya: sb. st. 11-y mezhdunar. nauch.-prakt. konf. v ramkakh 21-y mezhdunar. agroprom. vystavki «Interagromash-2018» [State and prospects of agricultural machinery development: Proc. 11th Int. Sci.-Pract. Conf. within framework of the 21st Int. Agroindustrial Exhibition “Interagromash-2018”] 2018, pp. 40–42 (in Russian).
10. Lapen, D.-R., et al. Combination cone penetration resistance/water content instrumentation to evaluate cone penetration-water content relationships in tillage research. Soil & Tillage Research, 2003, no. 58, pp. 193–206.
11. Salloum, W., Bahlawan, H. Design of Penetrometer Cone for Measuring Soil Penetration Resistance and Determine Soil Porosity. Research Journal of Aleppo University, 2009, no. 76, pp. 40–57.
12. Dyachenko, A.G., Savostina, T.P. Vliyanie vlazhnosti obmolachivaemogo materiala na protsess obmolota [Effect of threshed material moisture on threshing process] Innovatsionnye tekhnologii v nauke i obrazovanii (ITNO-2017): mat.-ly V Mezhdunar. nauch.-prakt. konf. [Innovative technologies in Science and Education (ITNO-2017): proc. V Int. Sci.-Pract. Conf.] Rostov-on-Don: DSTU-Print, 2017, pp. 88–91 (in Russian).
13. Savostina, T.P., Dyachenko, A.G. Profil' sreza transportiruyushchego ustroystva ot velichiny podachi khlebnoy massy. [Cut profile of conveying device on the value of bread mass supply.] Sostoyanie i perspektivy razvitiya sel'skokhozyaystvennogo mashinostroeniya: sb. st. 11-y mezhdunar. nauch.-prakt. konf. v ramkakh 21-y mezhdunar. agroprom. vystavki «Interagromash-2018» [State and prospects of agricultural machinery development: Proc. 11th Int. Sci.-Pract. Conf. within framework of the 21st Int. Agroindustrial Exhibition “Interagromash-2018”] Rostov-on-Don: DSTU-Print, 2018, pp. 44–46 (in Russian).
14. Savostina, T.P., Saed, B.I. Optimizatsiya profilya sreza transportiruyushchego ustroystva ot velichiny sekundnoy podachi. [Optimization of transporter cut profile on the second supply value.] Vestnik of DSTU, 2017, vol. 17, no. 4 (91), pp. 44–49 (in Russian).

Submitted 22/01.2019

Scheduled in the issue 12.04.2019

Authors:

Dyachenko, Alexey G.,

associate professor of the Machine Design Principles Department, Don State Technical University
(1, Gagarin Square, Rostov-on-Don, 344000, RF), Cand.Sci. (Eng.), associate professor ,
ORCID: <https://orcid.org/0000-0001-9934-4193>
alexey-a2@mail.ru

Savostina, Tatiana P.,

senior lecturer of the Machine Design Principles Department, Don State Technical University
(1, Gagarin Square, Rostov-on-Don, 344000, RF),
ORCID: <http://orcid.org/0000-0001-5550-7624>
kovtanya@yandex.ru

Saed Bakir Imad,

associate professor of Agricultural Engineering Department, Aleppo University(Syria, Aleppo, Aleppo University),
Dr..Sci. (Eng.),
ORCID: <https://orcid.org/0000-0003-3855-7691>
Imad12sb@gmail.com

MACHINE BUILDING AND MACHINE SCIENCE МАШИНОСТРОЕНИЕ И МАШИНОВЕДЕНИЕ



UDC 621.75.04

<https://doi.org/10.23947/1992-5980-2019-19-3-262-267>

Distinction between the concepts of mathematical and logical modeling*

E. N. Kolybenko^{1**}

¹Don State Technical University, Rostov-on-Don, Russian Federation

Разграничение понятий математического и логического моделирования***

Е. Н. Колыбенко^{1**}

¹Донской государственный технический университет, г. Ростов-на-Дону, Российская Федерация

Introduction. Technologies of mathematical and logical modeling of problem solving according to the existing practice of their distribution are divided into two areas: widespread mathematical modeling and infological modeling which is currently underdeveloped, especially for sophisticated systems. Fundamental differences between these technologies, in particular for the machining preproduction, are that logical modeling is informationally and logically related to organization systems, and mathematical modeling is associated with control processes in the organization systems. Logical modeling is used to operate with geometric objects in the technological schemes of their interaction through basing methods, geometric shaping in a static (ideal) setting of the corresponding schemes. Mathematical simulation is used to operate material objects in the control processes of their transformations through cutting methods, i.e. imperfectly, considering heterogeneous errors. Between the organization systems under study and management processes in them, there are information and logical links of their organic unity, which deny their separate consideration. In the information deterministic technology for solving problems of a high-level automation, the distinction between the concepts of “mathematical” and “logical” modeling is relevant; it has scientific novelty and practical significance.

Materials and Methods. To characterize the properties of the concepts of “mathematical modeling”, “logical modeling” and the knowledge functions resulting from the formulation of these concepts, fundamentally different methods and appropriate tools are used. The differentiation of the concepts under consideration is based on the differentiation of technologies (methods, appropriate tools, algorithms, operations) for solving applied problems of any knowledge domain.

Research Results. The ideas of “logical modeling” and “mathematical modeling” are conceptual general-theoretical notions with invariant properties required for solving practical problems of any application domain. In accordance with the distinction between these concepts, the problem solving technologies are divided into two types: system engineering technology – in the organization of information object systems, and

Введение. Технологии математического и логического моделирования решения задач по существующей практике их распространения распределяются на два направления: широко распространенное математическое моделирование и инфологическое логическое моделирование, которое в настоящий момент развито недостаточно, в особенности для сложноорганизованных систем. Принципиальные различия этих технологий, в частности для подготовки производства обработкой резанием, в том, что логическое моделирование информационно и логически связано с системами организации, а математическое — с процессами управления в системах организации. Логическое моделирование используется для оперирования геометрическими объектами в технологических схемах их взаимодействия методами базирования, геометрического формообразования в условиях статической, т. е. идеальной настройки соответствующих схем. Математическое моделирование используется для оперирования материальными объектами в процессах управления их преобразованиями методами обработки резанием, т. е. неидеально с учетом функционально различных погрешностей. Между рассматриваемыми системами организации и процессами управления в них существуют информационные и логические связи их органического единства, отрицающие их раздельное рассмотрение. Для информационной детерминированной технологии решения задач высокого уровня автоматизации разграничение понятий «математическое» и «логическое» моделирование актуально, обладает научной новизной и практической значимостью.

Материалы и методы. Для характеристики свойств понятий «математическое моделирование», «логическое моделирование» и функций знаний, следующих из формулирования этих понятий, используются принципиально различные методы и соответствующие инструментальные средства. В основу разграничения рассматриваемых понятий положено разграничение технологий (методы, соответствующие средства, алгоритмы, операции) решения прикладных задач какой-либо предметной области знаний. **Результаты исследования.** Понятия «логическое моделирование» и «математическое моделирование» являются концептуальными общетеоретическими понятиями, обладающими инвариантными свойствами, которые необходимы для решения задач практики какой-либо предметной области. В соответствии с разграничениями рассматриваемых понятий, технологии решения задач подразделяются на два типа: технология системной инженерии — в системах организации информационных объектов и технология

* The research is done within the frame of the independent R&D.

**E-mail: e.n.kolybenko@mail.ru

*** Работа выполнена в инициативном порядке.



system science – in the management processes of transformation of the corresponding material objects. These areas should exist in the information and logical link of their organic unity.

Discussion and Conclusions. The author distinguishes between the concepts of “logical modeling” and “mathematical modeling”, which is a key condition for a successful transition to the deterministic information technology of a high-level automation in solving practical problems of any knowledge domain, for example, of the production design machining.

Keywords: production design engineering, cutting, system analysis, information technology, decision modeling, system science.

For citation: E. N. Kolybenko. Distinction between the concepts of mathematical and logical modeling. Vestnik of DSTU, 2019, vol. 19, no. 3, pp. 262–267. <https://doi.org/10.23947/1992-5980-2019-19-3-262-267>

системотехники — в процессах управления преобразованиями соответствующих материальных объектов. Эти направления должны существовать в информационной и логической связи их органического единства.

Обсуждение и заключения. Автором разграничены понятия «логическое моделирование» и «математическое моделирование», что является важнейшим условием успешного перехода к детерминированной информационной технологии высокого уровня автоматизации в решении задач практики какой-либо предметной области знаний, например, технической подготовки производства резанием.

Ключевые слова: техническая подготовка производства, обработка резанием, системный анализ, информационная технология, моделирование решений, системная технология.

Образец для цитирования: Колыбенко, Е. Н. Разграничение понятий математического и логического моделирования / Е.Н. Колыбенко // Вестник Дон. гос. техн. ун-та. — 2019. — Т. 19, № 3. — С. 262–267. <https://doi.org/10.23947/1992-5980-2019-19-3-262-267>

Introduction. The main concepts of systems engineering as a creative technology for the integrated solution to engineering and organizational and management tasks are described in [1]. It is noted that the extremely high complexity and variety of large-scale highly automated systems significantly complicates the use of exclusively mathematical tools to determine them. The systems engineering concept was formed as part of the practice of successful development. However, this paper has come out with a change in the literal translation of the concept of “systems engineering” to the concept of “system science”. Further, the system science was developed as an independent field of knowledge. Functions of the system science include management of the transformation of material objects in the corresponding systems of the organization. After the introduction of the concept of “system science”, systems engineering in our country as a conceptual breakthrough competitive information technology for creating large complex powerful information systems was largely lost. The development went in the direction of designing control technological processes in organization systems through functionally different methods and means of the mathematical apparatus.

Functionally different aspects of the approach to system science in the cognition of the domain knowledge base for seven levels of the hierarchy of its basic objects of various types are described in [2] as an example of production design engineering (PDE) by cutting throughout its cycle.

Functions of systems engineering technology include the organization, on an invariant basis, of powerful deterministic systems for logical information modeling of the solution to a possible set of problems in models of basic knowledge objects and databases of their solutions with the issue of design documentation. Insight into the papers [3–13] marks that the direction of systems engineering technology is widely developed in terms of information and software for information processing systems on a computer, as well as in functionally different management. In the machining PDE, the development has gone towards translating traditional knowledge into an electronic form for computer perception. On the basis of such transformations of the knowledge form, ineffective dialog systems have been organized that do not have access to CAD systems for solving problems of low-level automation practice. System science is widely developed.

Deep properties of concepts are given in [14]: “... one of the human consciousness attributes is the ability to apply previously accumulated knowledge to solve emerging logical problems”; “... a concept can also be defined as a certain linguistic construction that has a certain meaning, that is, a figurative content”. Ib.: “The object under study is called an original, and the object investigated instead of the original one to study certain properties is called a model”. Ibid: “Modeling is a method (or process) of studying the properties of original objects through examining the corresponding properties of their models”.

If the properties of a real object are described in words, a mathematical formula, a drawing or a diagram, i.e., are formalized in a model, then such a model can be called an information one. Only knowledge of an informational nature is suitable for computer processing. A systematic analysis of knowledge on systems engineering technology is difficult to understand, but its results are informative and at the same time concise. Proceed from the need to embed formalized concepts in the structure of basic knowledge objects of various types of application domain, the content of con-

cepts should achieve maximum precision. The author's updated interpretation of the existing and new concepts is most important.

Materials and Methods. We introduce the updated concept of system principles. System principles are informational logical statements of the approach to solving the problems of analyzing technological systems, processes of functionally various purposes under the conditions of respectively static, dynamic setting, verified through the multiple practice of their application.

Next, we formulate system principles.

1. A necessary condition for a sequenced technological procedure of functionally various nature (engineering, physical, chemical, biological) of transformation of any object is the presence of a control system. The transformation management function is always specific, implemented in relation to the corresponding technological system. Consequently, a necessary condition for the existence of a transformation management system for an object is the existence of an appropriate technological system for its organization. We refer to the well-known and fair saying: “You can’t manage a poorly organized object well”.

At that, the concept of “organization” is further considered on the basis of compliance with the concept of “structure” in various aspects of its interpretation using the example of the machining PDE. The author has organized the solution to the PDE tasks on a possible set of workpieces, production facilities, machine tools, cutting tools, devices for installing cutting tools and production facilities; we use the notation $\{\dots\}$ — a set.

We introduce the updated concepts.

- A structure is a construction (organization) of an object determined by decomposition methods as part of structure elements and synthesis methods through superimposing relationships between structure elements of different levels and one level of structure, which are based on design quality parameters of the main elements of integration, structure disintegration.

- **The main elements of structure integration, disintegration** are the elements of knowledge that characterize functionally various elements of the object structures ($\{\text{details}\}$) of the stage of designing preproduction (DPP) and objects ($\{\text{primary blanks}\}$) of the stage of production design engineering (PDE), as well as links between structural elements.

- **The design quality of the main elements of integration, disintegration in the structure of objects ($\{\text{details}\}$) of the DPP stage and in the structure of objects ($\{\text{primary blanks}\}$) of the PDE stage** is a function that should be unconditionally executed for a set of design quality parameters that characterizes a possible set of various properties of objects in their distribution among various of the object structure elements and the relationships between the elements of the structure of objects.

- **The basic object of knowledge** is material that is defined on the basis of the concept of “structure” in the organic unity of its information and logical connections with the concepts of “content” and “form”, which deny their separate consideration.

- **The information “slave” (main) transformation object** is a primary material whose knowledge information display is possible only in a unified environment of one level of the structure of the technological scheme based on the interaction of structural elements of a “slave” object in a general case with the group of structural elements of a “master” object, and controlled transformation is realized only in the corresponding processes.

2. The conjugation of the “slave” and “master” objects of interaction through superimposing the links of its functional purpose from the side in a general case of a group of structure elements of the “master” object to the functional elements in the structure of a “slave” object allows us to determine the method for converting the “slave” object and the properties of the mating objects.

3. The information technology operations for solving the problems of the DPP and PDE stages are distributed into the main and auxiliary operations. We distribute the main operations in two directions — technological and designing ones. In main operations, we consider types of support for engineering systems for organizing work machines and work machine systems for cutting. In auxiliary operations, we consider types of support for engineering systems for controlling working machines for cutting. Auxiliary operations of the design direction should be assigned to the corresponding departments of the DPP stage. Types of support for engineering systems of organization and management are determined in the information and logical communication, consisting of organizational, methodological, logical, normative, informational, software, and technical.

4. The objects of transformation in the machining PDE are material objects $\{\text{details, assembly units of products}\}$ of the DPP stages and $\{\text{primary blanks, blanks}\}$ of the PDE stages. Geometric objects are ideal ones corresponding to the material objects of the DPP and PDE stages.

The structure of the objects of the DPP stage is considered in accordance with the composition of the work functions performed by each of the four groups of structure elements [15]. The work functions of the structural elements

in this paper are determined by combining the basing functions with other functions into their possible combinations. The composition of the functions includes basing, directing, torque transmission, division and fixation.

The structure of the objects {primary blanks blanks} of the PDE stage is considered in accordance with the composition of the work functions performed by two “slave” objects of interaction in the corresponding process flow-sheets. The composition of the functions includes basing, basing and geometric shaping of the structural element.

5. The knowledge of geometric objects is based on the distribution of the basic elements (integration, disintegration) of the structure of production objects (primary blanks, blanks), respectively, and their design quality parameters through the sequence of transformations by cutting into groups:

- linear and angular dimensions of elementary simple and superimposed (simple, complex) form elements;
- macrogeometric shape of form elements;
- microgeometric shape (height of microroughnesses) of form elements;
- positional relationships for the execution of the functions of the mutual arrangement between the centers of

the coordinate systems of functionally various groups of form elements in the structure of one object and various objects, as well as between the coordinate “geometric” axes of the “basic” and “superimposed” simple and complex form elements:

- functionally different relations for the execution of functions of relative position, for example (alignment, perpendicularity, parallelism) between the coordinate “geometric” axes of the form elements in their various groups of the structure of one object and between the coordinate “guide” axes of the process flowsheets of interaction of various objects.

6. We consider information models of organization systems on the basis of the following principles:

- timeless, in space, in a general combination of information and logically connected coordinate systems;
- ideally under the conditions of static adjustment of process flowsheets of interaction of information objects

without using any forces, but considering the time factor under the conditions of dynamic adjustment of transformation control processes of the corresponding real “slave” objects;

- taking into account functionally different errors in the design quality parameters of the main elements of integration, disintegration of the structure of real “slave” objects.

7. We consider the technology of information logical modeling of solving practical problems by methods and appropriate means on the basis of the following principles.

7.1. We operate with a functionally defined system of concepts, each of which has its own formalized designation. Problem solving is based on the distribution of the structure of information models for the basic objects of knowledge in two parts of information: invariant, typical object-oriented parametric. Information models of basic knowledge objects of a higher level are organized on the basis of typical object-oriented parametric parts.

7.2. In typical object-oriented parametric parts of information models of basic knowledge objects of all types, the tasks of unconditional maintenance of design quality for the basic elements (integration, disintegration) of the structure of “slave” transformation objects are solved. Problem solving is always specific within the record of information. It is performed in accordance with the integrated algorithm in the technique of mapping and converting the domain knowledge base in the hierarchy of the classification structure of its basic knowledge objects at seven levels of structure; in accordance with the graph of the structure of the basic object of knowledge of any type.

7.3. In the decision databases defined on the invariant parts of information models of the basic objects of knowledge, in the general case, within the framework of structure transformations, work functions and parameters of various properties, the problems on optimizing the material and labor resources are solved.

7.4. We use the means of a system analysis of knowledge: conceptual ideas, set theory, graph theory. Conceptual ideas are “reflection”, “transformation”, “structure”, “set”, etc. Graphic tools are formalized designations of concepts embedded in the structure of basic knowledge objects. Set theory is a branch of mathematics that includes the concept of a “logical operator” for expressing assertions through imposing connections between formalized concepts, etc. Graph theory is a branch of mathematics that studies, in particular, “structure graphs” used by “Venn diagrams” for imposing relations between functionally uniform objects of consideration.

8. Logical information modeling of the basic objects of knowledge of functionally various types of any subject area, which is based on the system analysis principles for establishing a continuous, flexible integral algorithm in technology (methods, appropriate tools, algorithms, operations) for mapping knowledge, reveals all “flaws” of the amorphous (outside the structure) mapping of knowledge. Here, the target properties of the concept of “logical modeling” and the knowledge functions following from its formulation are important.

9. We consider mathematical models of control processes on the basis of the following principles:

- in accordance with the algorithm in the technology for solving problems of the knowledge domain;

- considering the information and logical links of the integral organization systems and management processes, parameters of time and space;
- not ideal under the conditions of dynamic tuning of interaction between real objects of a technical, physical, chemical, biological nature using various forces.

Various errors of the design quality parameters of the main elements (integration, disintegration) of the structure of real “slave” objects determined by experimental measurements in the process of their transformation are subject to accounting with their subsequent regulatory ordering to the calculated maximum permissible accuracy deviations to use in the reference documentation in the form of recommended technical design conditions.

10. The mathematical modeling technology of solving practical problems is considered on the basis of the following principles:

- operating with a functionally defined system of parameters, each of which is indicated by its own symbol;
- using various techniques and appropriate means of the mathematical apparatus;
- problem solving is always specific within the limits of information recording; it is performed as a parameter transformation (parametric models).

Research Results. Under the control of the person’s goal-setting function [16], the concepts of “space - time”, “organization systems - control processes”, “logical modeling - mathematical modeling” are considered on an invariant basis with respect to any knowledge domains in their systemic information and logical connection. The identifier of their connection, which has the property of integrity, which denies separate consideration, is the concept of “Content of the transformation of “slave” objects” within certain engineering control elements [17].

The system engineering technology defined by the author for the machining PDE in the practice of contract works as an information technology for its domain knowledge base can be extended to pressure, welding, functionally various management, computer processing of information.

Discussion and Conclusions. The machining PDE stage is, of course, a large complex information product which includes both functionally various systems for organizing its information products and their management process. Multiple attempts to solve the problems of PDE automation throughout the whole cycle of its practice were unsuccessful due to the logically informal presentation of the source data and the presence of significant difficulties characteristic of large complex automated systems when implementing design solutions using only a mathematical apparatus. On the ground of the logical incompleteness of traditional descriptive knowledge, the transition to the technology of their mapping into knowledge of an informational nature to achieve a sufficient level of automation of solving practical problems is essentially difficult or impossible. To establish a continuous and flexible integrated algorithm in a deterministic technology for solving problems of a high level of automation, methods and tools of system engineering of information logical modeling are required.

References

1. Goode, Harry H., Machol, Robert E. Sistemotekhnika. Vvedenie v proektirovanie bol'shikh system. [System Engineering: An Introduction to the Design of Large-scale Systems.] K.N. Trofimov, S.E. Zhorno, I.V. Soloviev, trans. from English; G.I. Pivovarov, ed. Moscow: Sovetskoye Radio, 1962, 383 p. (in Russian).
2. Kolybenko, E.N., Mordovtsev, A.A. Funktsional'no razlichnye aspekty tekhnologii sistemnoy inzhenerii v poznanii bazy znaniy predmetnoy oblasti v primere tekhnologicheskoy podgotovki mekhanooabratyvyayushchego proizvodstva. [Functionally different aspects of system engineering technology in the cognition of the domain knowledge base in the example of the technological preparation of machining.] Sistemnyy analiz v proektirovanii i upravlenii: sb. nauch. trudov XXIII Mezhdunar. nauch.-prakt. konf. [System analysis in design and management: Proc. XXIII Int. Sci.-Pract. Conf.] St. Petersburg: Publ. House of Polytechnic University, 2019, vol. 3, pp. 281–293 (in Russian).
3. Kondakov, A.I., Vasilyev, A.S. Sistemnoe modelirovanie vzaimodeystviy v tekhnologicheskikh sredakh. [System modeling of interactions in technological environments.] Proceedings of Higher Educational Institutions. Machine Building, 1998, no. 4, pp. 92 (in Russian).
4. Vasiliev, A.S. Sovershenstvovanie metodologii tekhnicheskoy podgotovki proizvodstva detaley mashin. [The improvement of technical preparation of machine parts manufacturing.] HANDBOOK. An Engineering Journal, 2013, no. 10 (199), pp. 5–10 (in Russian).
5. Bezyazychny, V.F., Suslov, A.G. Osnovnye ponyatiya i polozheniya v tekhnologii mashinostroeniya. [Basic concepts and regulations in engineering techniques.] Science Intensive Technologies in Mechanical Engineering, 2018, no. 2(80), pp. 3–9 (in Russian).
6. Mitin, S.G., Bochkarev, P.Yu. Proektirovanie operatsiy so slozhnoy strukturoy v mnogonomenklaturnykh mekhanooabratyvyayushchikh sistemakh. [Designing operations with a complex structure in multiproduct machining systems.] Publ. House of Saratov State Tech. University, 2016, 108 p. (in Russian).

7. Volkova, V.N. Teoriya informatsionnykh sistem: ucheb. posobie. [Theory of Information Systems: study guide.] St.Petersburg: SPb Politechnic University Publ. House, 2012, 340 p. (in Russian).
8. Volkova, V.N., Kozlov, V.N., eds. Modelirovanie sistem: ucheb. posobie. [System modeling: textbook.] St.Petersburg: SPb Politechnic University Publ. House, 2012, 440 p. (in Russian).
9. Malikov, R.F. Osnovy razrabotki komp'yuternykh modeley slozhnykh sistem: ucheb. posobie. [Fundamentals of the development of computer models of complex systems: textbook.] Ufa: BSPU Publ. House, 2012, 256 p. (in Russian).
10. Devyatkov, V.V. Metodologiya i tekhnologiya imitatsionnykh issledovaniy slozhnykh sistem: sovremennoe sostoyanie i perspektivy razvitiya: vuzovskiy uchebnyk. [Methodology and technology of simulation studies of complex systems: current status and development prospects.] Moscow: INFRA, 2013, 448 p. (in Russian).
11. Chikurov, N.G. Modelirovanie sistem: ucheb. posobie. [System modeling: textbook.] Moscow: INFRA, 2013, 398 p. (in Russian).
12. Ghallab, Malik, Nau, Dana, Traverso, Paolo. Automated Planning and Acting. Publisher: Cambridge University Press (2016) DOI:10.1017/CBO9781139583923.
13. Emmanuel Caillaud, Bertrand Rose, Virginie Goepp. Research methodology for systems engineering: some recommendations. IFAC (International Federation of Automatic Control) 1567–1572 (2016) Hosting by Elsevier Ltd.
14. Ustenko, A.S. Osnovy matematicheskogo modelirovaniya i algoritimizatsii protsessov funktsionirovaniya slozhnykh sistem. [Fundamentals of mathematical modeling and algorithmization of the processes of complex systems.] Moscow: BINOM, 2000, 235 p. (in Russian).
15. Rakovich, A.G. Osnovy avtomatizatsii proektirovaniya tekhnologicheskikh prispособleniy. [Fundamentals of automation of designing machining attachments.] Minsk: Nauka i tekhnika, 1985, 285 p. (in Russian).
16. Smirnov, E.M. Analiz sistemy «sub"ekt — tekhnicheskoe sredstvo — ob"ekt». [Analysis of the “subject - technical means – object” system.] Russian Journal of Philosophical Sciences, 1983, no. 1, pp. 24–30 (in Russian).
17. Edinaya sistema tekhnologicheskoy dokumentatsii. Terminy i opredeleniya osnovnykh ponyatiy: GOST 3.1109–82. [GOST 3.1109-82. Unified system for technological documentation. Terms and definitions of main concepts.] Moscow: Standartinform, 2012, 98 p. (in Russian).

Submitted 22.01.2019

Scheduled in the issue 12.04.2019

Author:

Kolybenko, Evgeny N.,

Leading Research Scholar, Don State Technical University (1, Gagarin sq., Rostov-on-Don, 344000, RF)

Cand.Sci. (Eng.),

ORCID: <https://orcid.org/0000-0003-1851-3885>

e.n.kolybenko@mail.ru

INFORMATION TECHNOLOGY, COMPUTER SCIENCE, AND MANAGEMENT ИНФОРМАТИКА, ВЫЧИСЛИТЕЛЬНАЯ ТЕХНИКА И УПРАВЛЕНИЕ



UDC 519.87+004.421

<https://doi.org/10.23947/1992-5980-2019-19-3-268-280>

Modeling and numerical analysis of the effect of dissociation/recombination of water molecules on the transport of salt ions in diffusion layer*

N. O. Chubyr¹, A. V. Kovalenko², M. Kh. Urtenov³, A. I. Sukhinov⁴, V. A. Gudza^{5**}

¹ Kuban State Technological University, Krasnodar, Russian Federation

^{2,3,5} Kuban State University, Krasnodar, Russian Federation

⁴ Don State Technical University, Rostov-on-Don, Russian Federation

Моделирование и численный анализ влияния реакции диссоциации (рекомбинации) молекул воды на перенос ионов соли в диффузионном слое***

Н. О. Чубырь¹, А. В. Коваленко², М. Х. Уртенов³, А. И. Сухинов⁴, В. А. Гудза^{5**}

¹ Кубанский государственный технологический университет, Краснодар, Российская Федерация

^{2,3,5} Кубанский государственный университет, Краснодар, Российская Федерация

⁴ Донской государственный технический университет, Ростов-на-Дону, Российская Федерация

Introduction. The paper presents a theoretical study on binary salt ion transport considering the water dissociation/recombination reaction. The work objectives are as follows: to build a mathematical model; to develop an algorithm for the numerical solution to the boundary value problem corresponding to the mathematical model; to work out the similarity theory including the transition to a dimensionless form using characteristic quantities; to determine a physical meaning of trivial similarity criteria; to find nontrivial similarity criteria; to build and analyze the volt-ampere characteristic (VAC).

Materials and Methods. The theoretical study and numerical analysis of the transport of binary salt ions consider the dissociation/recombination reaction of water. In this case, the heat transfer equation and the mathematical model of electrodiffusion of four types of ions simultaneously (two salt ions, as well as H^+ and OH^- ions) in the diffusion layer of electromembrane systems with a perfectly selective membrane are used. For the first-order differential equations, a singularly perturbed boundary-value problem is set. In the equation for the electric field, the right side is independent of the intensity. In the numerical solution to the digitized system of equations by the Newton-Kantorovich method, this causes the stability of the method. In this regard, the boundary-value problem is reduced for numerical solution: a transition to a system of the second-order equations is provided, and the missing boundary

Введение. Статья посвящена теоретическому изучению переноса ионов бинарной соли с учетом реакции диссоциации (рекомбинации) воды. Цели исследования: построение математической модели; разработка алгоритма численного решения краевой задачи, соответствующей математической модели; развитие теории подобия, включая переход к безразмерному виду с использованием характерных величин; определение физического смысла тривиальных критериев подобия; нахождение нетривиальных критериев подобия; построение и анализ вольтамперной характеристики (ВАХ).

Материалы и методы. При теоретическом исследовании и численном анализе переноса ионов бинарной соли учитывается реакция диссоциации (рекомбинации) воды. При этом используются уравнение теплопроводности и математическая модель электродиффузии одновременно четырех видов ионов (двух ионов соли, а также ионов H^+ и OH^-) в диффузионном слое электромембранных систем с идеально селективной мембраной.

Для дифференциальных уравнений первого порядка ставится сингулярно возмущенная краевая задача. В уравнении для напряженности электрического поля правая часть не зависит от напряженности. При численном решении дискретизированной системы уравнений методом Ньютона — Канторовича это обуславливает проблемы устойчивости метода. В связи с этим краевая задача приводится к виду, удобному для численного решения: обеспечивается переход к системе уравнений второго порядка, рассчитыва-



* The research is done within the frame of the AR&D no. 14.577.21.0260 (federal target program “Research and development in priority areas for development of scientific and technological complex of Russia for 2014–2020”), as well as with the financial support of the RFFI in the framework of scientific project 19-08-00252 A “Theoretical and experimental study of the current-voltage characteristics of electromembrane systems”.

**E-mail: chubyr-natalja@mail.ru, savanna-05@mail.ru, urtenovmax@mail.ru, sukhinov@gmail.com, vitaliy.gudza@gmail.com

*** Работа выполнена в рамках ПНИЭР № 14.577.21.0260 (федеральная целевая программа «Исследования и разработки по приоритетным направлениям развития научно-технологического комплекса России на 2014–2020 годы»), а также при финансовой поддержке РФФИ в рамках научного проекта 19-08-00252 А «Теоретическое и экспериментальное исследование вольтамперных характеристик электромембранных систем».

conditions for the electric field strength are calculated.

Research Results. A new mathematical model, a numerical algorithm to solve a boundary value problem, and software are developed. A numerical analysis is carried out, and fundamental laws of the transport of salt ions are determined considering the dissociation/recombination reaction of water molecules, temperature effects, and Joule heating. The VAC is built and analyzed.

Discussion and Conclusions. The transport of binary salt ions through a diffusion layer near a cation exchange membrane is considered. A mathematical model of this process is proposed. It takes into account the temperature effects due to dissociation/recombination reactions of water molecules and Joule heating in a solution. The basic laws of the transport of salt ions are established considering the dissociation/recombination reaction of water molecules and temperature effects. The temperature effects of the dissociation/recombination reaction and the Joule heating in the electroneutrality region (ENR) are almost imperceptible (with the exception of the recombination region, RR). The Joule heating in the space-charge region (SCR) is by two orders of magnitude larger than the cooling effect of the water dissociation reaction. Upon recombination, approximately the same heat is released in the RR as during Joule heating in the expanded SCR. However, due to the small size of the RR, the effect of this heat is imperceptible. Therefore, we can assume that there is only one heat source at the interface in the SCR, which, due to its noticeable size, causes a significant increase in temperature in the entire diffusion layer. It follows that the emergence and development of gravitational convection is possible. General conclusions, following from the results obtained, open up the possibility of intensifying the process of transport of salt ions in the electrodialysis machines.

Keywords: membrane system, ion exchange membrane, space charge, extended space-charge region, dissociation-recombination reaction of water molecules.

For citation: N.O. Chubyr, et al. Modeling and numerical analysis of the effect of dissociation-recombination of water molecules on the transport of salt ions in diffusion layer. Vestnik of DSTU, 2019, vol. 19, no. 3, pp. 268–280. <https://doi.org/10.23947/1992-5980-2019-19-3-268-280>

Introduction. Intensive current mode involves using currents several times higher than the limited electrodiffusion. In this case, secondary (or conjugated) phenomena of concentration polarization occur in the membrane systems:

- spatial electric charge occupies a macroscopic region comparable to the thickness of the diffusion layer;
- the solution *pH* changes [1-3], which is explained by the water splitting;
- microconvective flows are formed, etc.

Considering impact of the dissociation (recombination) reaction of water molecules is essential to understanding the transport processes in the electromembrane systems, as some authors believe that the occurrence of new charge carriers H^+ and OH^- can cause a decrease or even disappearance of the space charge, which is the basis for other transfer mechanisms (e.g. electroconvection). The dissociation reaction of water molecules is endothermic, and the recombination reaction is exothermic. Centers of the reaction sites are separated in space. This causes an uneven temperature

ваются недостающие краевые условия для напряженности электрического поля.

Результаты исследования. Разработаны новая математическая модель, алгоритм численного решения краевой задачи, программное обеспечение. Проведен численный анализ и определены фундаментальные закономерности переноса ионов соли с учетом реакции диссоциации (рекомбинации) молекул воды, температурных эффектов и Джоулева разогрева. Построена и проанализирована ВАХ. **Обсуждение и заключение.** Рассмотрен перенос ионов бинарной соли через диффузионный слой у катионообменной мембраны. Предложена математическая модель названного процесса, которая учитывает температурные эффекты, обусловленные реакциями диссоциации (рекомбинации) молекул воды и Джоулевым нагревом в растворе. Установлены основные закономерности переноса ионов соли с учетом реакции диссоциации (рекомбинации) молекул воды и температурных эффектов. Температурные эффекты от реакции диссоциации (рекомбинации) и Джоулева разогрева в ОЭН практически незаметны (исключение — область рекомбинации, ОР). Джоулев нагрев в области пространственного заряда (ОПЗ) на два порядка больше охлаждающего эффекта реакции диссоциации воды. При рекомбинации в ОР выделяется примерно столько же тепла, сколько при Джоулевом нагреве в расширенной ОПЗ. Однако из-за малых размеров ОР влияние этого тепла незаметно. Значит, можно считать, что есть только один источник тепла на межфазной границе в ОПЗ, который благодаря своему заметному размеру обуславливает значительное повышение температуры во всем диффузионном слое. Отсюда следует, что возможно возникновение и развитие гравитационной конвекции. Общие выводы, следующие из полученных результатов, открывают возможность интенсификации процесса переноса ионов соли в электродиализных аппаратах.

Ключевые слова: мембранные системы, ионообменная мембрана, пространственный заряд, расширенная область пространственного заряда, диссоциация (рекомбинация) молекул воды.

Образец для цитирования: Моделирование и численный анализ влияния реакции диссоциации (рекомбинации) молекул воды на перенос ионов соли в диффузионном слое / Н. О. Чубырь [и др.] // Вестник Дон. гос. техн. ун-та. — 2019. — Т. 19, № 3. — С. 268–280. <https://doi.org/10.23947/1992-5980-2019-19-3-268-280>

distribution and, therefore, affects all the physical properties of water: dissociation coefficient, heat capacity, etc. In addition, an uneven temperature distribution can cause gravitational convection. Thus, the study of temperature effects associated with the reactions of dissociation and recombination of water molecules is an urgent task [4]. In this paper, we confine ourselves to considering the effect of the uneven temperature distribution on the dissociation coefficient of water molecules.

Materials and Methods

1. Mathematical model

1.1. Simultaneous equations

Consider a one-dimensional stationary transport process for single-charged salt ions in the Nernst diffusion layer. We take into account the dissociation (recombination) reactions of water and the temperature effects associated with the Joule heating of the solution. Such a case is described through a system of equations [5]:

$$j_1 = \frac{-F}{RT_0} D_1 C_1 \frac{d\varphi}{dx} - D_1 \frac{dC_1}{dx}, \quad (1)$$

$$j_2 = \frac{F}{RT_0} D_2 C_2 \frac{d\varphi}{dx} - D_2 \frac{dC_2}{dx}, \quad (2)$$

$$j_3 = \frac{-F}{RT_0} D_3 C_3 \frac{d\varphi}{dx} - D_3 \frac{dC_3}{dx}, \quad (3)$$

$$j_4 = \frac{F}{RT_0} D_4 C_4 \frac{d\varphi}{dx} - D_4 \frac{dC_4}{dx}, \quad (4)$$

$$\frac{d^2\varphi}{dx^2} = \frac{-F}{\varepsilon_r} (C_1 - C_2 + C_3 - C_4), \quad (5)$$

$$0 = \frac{-dj_i}{dx} + R_i, \quad i = 1, \dots, 4, \quad (6)$$

$$k \frac{d^2T}{dx^2} + E \cdot I + \beta(C_3 C_4 - k_w(T)) = 0. \quad (7)$$

Here, $R_1 = R_2 = 0, R_3 = R_4 = k_d C_{H_2O} - k_r C_3 C_4 = k_r(k_w - C_3 C_4)$, $k_w(T) = \dot{k}_w e^{b(T-T_0)}$, $i = 1, 2$ are salt ion indices; $i = 3$ and $i = 4$ are, respectively, the indices of hydrogen ions H^+ and hydroxyl OH^- ; $E = \frac{-d\varphi}{dx}$ is the electric field strength; C_i, j_i, D_i are, respectively, concentration, flux, diffusion coefficient of the i -th ion; $k_d(T)$ is the constant of water dissociation rate; k_r is the constant of the recombination rate of hydrogen ions H^+ and hydroxyl OH^- ; \dot{k}_w is the equilibrium constant; ε_r is the dielectric capacitivity; F is the Faraday number; I is the total current density; k is the coefficient of thermal conductivity; ρ_0 is the density of the solution; c_p is specific heat of the solution; $G = E \cdot I$ is the density of heat sources associated with the passage of electric current through the solution (Joule heating of the solution); $\beta = qk_r$, $Q = \beta \left(C_3 C_4 - \frac{k_d C_{H_2O}}{k_r} \right) = qk_r(C_3 C_4 - k_w(T))$ is the density of heat sources and sinks associated with the recombination and dissociation of water molecules.

The total current density I is equal to: $I = I_s + I_w$.

Here, I_s is partial current density by salt ions; I_w is partial current density by water ions.

From (6)–(8), it follows: $j_1 = \text{const}$, $j_2 = \text{const}$, $I_s = F \cdot (j_1 - j_2) = \text{const}$, $I_w = \text{const}$, but $j_3 \neq \text{const}$, $j_4 \neq \text{const}$, $\alpha^2 = \frac{k}{\rho_0 c_p}$ is thermal diffusivity of the solution.

1.2. Boundary conditions

Assume that $x = 0$ corresponds to the depth of the solution, where the electroneutrality condition $C_1 - C_2 + C_3 - C_4 = 0$ is fulfilled, and $x = \delta$ corresponds to the conventional “solution – membrane” interface. Thus, $\delta^{(u)}$ is the thickness of the Nernst diffusion layer.

In this paper, for definiteness, a cation-selective membrane (CSM) is considered, which for simplicity will be assumed to be ideally selective ($j_2^{(u)} = 0$).

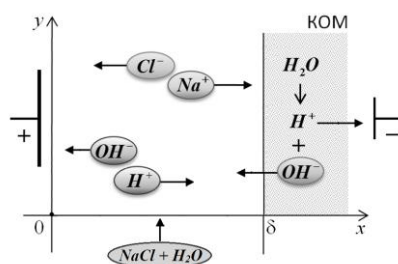


Fig. 1. Diagram of diffusion layer near cation-selective membrane

1) Boundary conditions in the depth of the solution ($x = 0$)

Assume, $C_1(0) = C_{10}$, $C_2(0) = C_{20}$, $C_3(0) = C_{30}$, $C_4(0) = \frac{\dot{k}_w}{C_{30}}$, while $C_{10} + C_{30} = C_{20}$, $T(\delta) = T_0$.

2) Boundary data at the “solution – membrane” interface ($x = \delta$)

Suppose that $C_1(\delta) = C_{1m}$, $C_3(\delta) = C_{3m}$. At this, the sum $C_{1m} + C_{3m}$ is comparable to the tabular value of the exchange capacity of the cation-selective membrane. The flux density $j_4(\delta) = j_{4m}$ of ions OH^- is determined by the catalytic reaction of dissociation of water molecules in a thin surface layer of a cation exchange membrane.

For temperature, the condition of flow balance is used at the point $x = \delta$ [1]:

$$-k \frac{dT(\delta)}{dx} = G(\delta)\delta + Q(\delta)\delta + q \frac{dj_4(\delta)}{dx}.$$

2. Transition to dimensionless form

2.1. Characteristic quantities and formulas for the transition to a dimensionless form

As a characteristic concentration of C_0 we take the concentration of salt cations C_{10} . Actual values of C_{10} are within the range of $10^{-5}M - 1M$. As a characteristic temperature, we take the room temperature $T_0 = 298K$. As a characteristic length, we consider the thickness of the diffusion layer δ , which is of the order of $10^{-4}m$. Denote $D_0 = \frac{2D_1D_2}{D_1+D_2}$

as the electrolyte ($NaCl$) diffusion coefficient $\varphi_0 = \frac{RT_0}{F}$ — as the thermal potential [5].

We pass to dimensionless quantities:

$$x^{(u)} = \frac{x}{\delta}, \varphi^{(u)} = \frac{\varphi}{\varphi_0}, E^{(u)} = \frac{-\delta}{\varphi_0} \frac{d\varphi}{dx}, I^{(u)} = \frac{I}{I_{np}}, D_i^{(u)} = \frac{D_i}{D_0}, I_s^{(u)} = \frac{I_s}{I_{np}}, I_w^{(u)} = \frac{I_w}{I_{np}}, C_i^{(u)} = \frac{C_i}{C_{10}}, j_i^{(u)} = \frac{j_i \delta}{D_i C_{10}} = \frac{j_i F}{D_i^{(u)} I_{np}}, i = 1, 2, 3, 4, T^{(u)} = \frac{T}{T_0}, I_{np} = \frac{D_0 C_{10} F}{\delta}.$$

Then, $k_w^{(u)}(T) = \frac{k_w(T)}{(C_{10})^2} = \gamma^{(u)} e^{b^{(u)}(T^{(u)}-1)}$, where $\gamma^{(u)} = \frac{k_w}{(C_{10})^2}$, $b^{(u)} = bT_0$.

Assume that $\varepsilon^{(u)} = \frac{RT_0 \varepsilon_r}{C_{10} F^2 \delta^2}$, $a^{(u)} = \frac{RT_0 \varepsilon_r}{F^2} \frac{k_r}{D_0}$.

2.2. Transition to dimensionless form in equations

Focusing on [6], we pass to the dimensionless form in the system of equations (1) - (6):

$$\frac{dC_1^{(u)}}{dx} = C_1^{(u)} E^{(u)} - j_1^{(u)}, \quad (9)$$

$$\frac{dC_2^{(u)}}{dx} = -C_2^{(u)} E^{(u)} - j_2^{(u)}, \quad (10)$$

$$\frac{dC_3^{(u)}}{dx} = C_3^{(u)} E^{(u)} - j_3^{(u)}, \quad (11)$$

$$\varepsilon^{(u)} D_3^{(u)} \frac{d}{dx} j_3^{(u)} = a^{(u)} \left(k_w^{(u)} e^{b^{(u)}(T^{(u)}-1)} - C_3^{(u)} C_4^{(u)} \right), \quad (12)$$

$$\frac{dC_4^{(u)}}{dx} = -C_4^{(u)} E^{(u)} - j_4^{(u)}, \quad (13)$$

$$\varepsilon^{(u)} D_4^{(u)} \frac{d}{dx} j_4^{(u)} = a^{(u)} \left(k_w^{(u)} e^{b^{(u)}(T^{(u)}-1)} - C_3^{(u)} C_4^{(u)} \right), \quad (14)$$

$$\varepsilon^{(u)} \frac{dE^{(u)}}{dx} = C_1^{(u)} - C_2^{(u)} + C_3^{(u)} - C_4^{(u)}. \quad (15)$$

We write the total current density in the form of $I_s^{(u)} + I_w^{(u)} = I^{(u)}$.

Here,

$$I_s^{(u)} = D_1^{(u)} j_1^{(u)} - D_2^{(u)} j_2^{(u)}, I_w^{(u)} = D_3^{(u)} j_3^{(u)} - D_4^{(u)} j_4^{(u)},$$

moreover, for a perfectly selective membrane $j_2^{(u)} = 0$ and, consequently,

$$I_s^{(u)} = D_1^{(u)} j_1^{(u)}.$$

Under the transition to a dimensionless form, the heat equation (7) takes the form:

$$k^{(u)} \frac{d^2 T^{(u)}}{(dx^{(u)})^2} + E^{(u)} \cdot I^{(u)} + \beta^{(u)} \left(C_3^{(u)} C_4^{(u)} - \gamma^{(u)} e^{b^{(u)}(T^{(u)}-1)} \right) = 0. \quad (16)$$

Here, $k^{(u)} = \frac{k}{D_0 C_{10} R}$ and $\beta^{(u)} = \frac{q K_r \delta^2 C_{10}}{D_0 R T_0}$.

2.3. Physical meaning and evaluation of the trivial similarity criteria

The parameters $\varepsilon^{(u)}$, $D_3^{(u)}$, $D_4^{(u)}$, $a^{(u)}$, $k^{(u)}$, $k_w^{(u)}$, $\beta^{(u)}$, $b^{(u)}$ are trivial similarity criteria. Let us determine their physical meaning and values at the characteristic input parameters of the problem.

1. $b^{(u)} \approx 15$.

2. The parameter $\gamma^{(u)}$ is the square of the ratio of the concentration H^+ or OH^- ions in a neutral solution ($pH = 7$) to the electrolyte concentration. Its values vary from 10^{-10} to 10^{-18} , and it can be considered a small parameter.

3. $\varepsilon^{(u)} = \frac{RT_0 \varepsilon_r}{C_{10} F^2 \delta^2} = 2 \left(\frac{l_d}{\delta} \right)^2$, where $l_d = \sqrt{\frac{RT \varepsilon_0}{2 C_{10} F^2}}$ is Debye length. Thus, the parameter $\varepsilon^{(u)}$ is the doubled

square of the Debye length ratio l_d to the diffusion layer width δ . The values of $\varepsilon^{(u)}$ vary from 10^{-11} to 10^{-7} , and this parameter can be considered small.

4. $a^{(u)} = \frac{RT_0 \varepsilon_r k_r}{F^2 D_0} = \frac{RT_0 \varepsilon_r}{2C_{10} F^2} \frac{2k_r C_{10}}{D_0} = \left(\frac{l_d}{l_r}\right)^2$. Here, $l_r = \sqrt{\frac{D_0}{2k_r C_{10}}}$. This value is proportional to the width of the recombination region (RR). Thus, the parameter $a^{(u)}$ is the square of the ratio of the Debye length to the width OP l_r . The parameter $a^{(u)} = 14$ and in the framework of this problem, it is a universal constant since it does not depend on the input parameters of the problem. So: $\frac{l_d}{l_r} = \sqrt{a^{(u)}} \approx 3.74$, i.e., the width of the OP is approximately 37 % of the width of the quasi-equilibrium region of the space charge (SCR, Debye length).

2.4. Nontrivial similarity criteria, physical meaning and evaluation of quantities

In the equation (16), the dimensionless coefficients $k^{(u)}$ and $\beta^{(u)}$ are trivial similarity criteria. Any relation between trivial criteria is called a nontrivial similarity criterion. Below, we express $k^{(u)}$ and $\beta^{(u)}$ through other known similarity criteria.

1) Consider $k^{(u)} = \frac{k}{D_0 C_{10} R} = \frac{\alpha^2 \rho_0 c_p}{D_0 C_{10} R} = \frac{\alpha^2}{D_0} \cdot \frac{\rho_0 c_p}{C_{10} R} = \frac{\rho_0 c_p}{C_{10} R}$. Here, $\frac{\alpha^2}{D_0}$ is the Lewis - Semenov number. We introduce the dimensionless number $\mu = \frac{C_{10} R}{\rho_0 c_p}$. Then, $k^{(u)} = \frac{1}{\mu}$. The number μ indicates the relative specific volumetric heat capacity, varies from indicates the relative specific volumetric heat capacity, it varies from 10^{-8} to 10^{-4} , and it can be considered as a small parameter.

2) Consider the parameter $\beta^{(u)} = \frac{q k_r \delta^2 C_{10}}{D_0 R T_0} = \frac{q \delta^2}{2 R T_0} \frac{2 k_r C_{10}}{D_0} = \frac{q}{2 R T_0} \frac{\delta^2}{\frac{D_0}{2 k_r C_{10}}} = Arn \frac{\delta^2}{2 l_r^2}$. Here, $Arn = \frac{q}{R T_0} = 22.8$ is the dimensionless quantity which is a thermal analogue of the Arrhenius criterion. It characterizes the sensitivity of the heat amount of a chemical reaction to temperature changes. As $\frac{1}{2} \left(\frac{\delta}{l_r}\right)^2 = \frac{1}{2} \left(\frac{l_d}{l_r}\right)^2 \left(\frac{\delta}{l_d}\right)^2 = \frac{a}{\varepsilon}$, and $\varepsilon = 2 \left(\frac{l_d}{\delta}\right)^2$, $a = 2 \left(\frac{l_d}{l_r}\right)^2$, then $\beta^{(u)} = Arn \cdot \frac{a}{\varepsilon}$. Thus, the heat equation (16) has the following dimensionless form:

$$\varepsilon Le \frac{d^2 T^{(u)}}{dx^2}.$$

3) The calculations show that

$$\gamma \mu = \frac{k_w}{C_{10}} \frac{R}{\rho_0 c_p} = \frac{k_w \varepsilon F^2 \delta^2}{R T_0 \varepsilon_r} \frac{R}{\rho_0 c_p} = \frac{k_w F^2 \delta^2}{\rho_0 c_p T_0 \varepsilon_r} \varepsilon.$$

Since $\varepsilon^{(u)} = 2 \left(\frac{l_d}{\delta}\right)^2$, then $N_a = \sqrt{\frac{k_w F^2 \delta^2}{\rho_0 c_p T_0 \varepsilon_r}} \approx 2,5 \cdot 10^{-3}$. Therefore, we obtain a nontrivial similarity criterion, which shows the relation

$$\gamma \mu = n_a^2 \varepsilon.$$

Likewise,

$$\varepsilon \mu = n_{a,1}.$$

Here,

$$n_{a,1} = \frac{R^2 T_0 \varepsilon_r}{\rho_0 c_p F^2 \delta^2} \approx 3,5 \cdot 10^{-14}, \quad (17)$$

$$\gamma = N_{a,2} \varepsilon^2, \quad (18)$$

$$N_{a,2} = \frac{F^4 \delta^4 k_w}{R^2 T_0^2 \varepsilon_r^2}.$$

Note that $n_a^2 = n_{a,1} N_{a,2}$.

2.5. Dimensionless form of a system of equations

Thus, a dimensionless system of equations describing the model has the form (index u is omitted for simplicity):

$$\begin{aligned} \frac{dC_1}{dx} &= C_1 E - j_1, \quad \frac{dC_2}{dx} = -C_2 E - j_2, \quad \frac{dC_3}{dx} = C_3 E - j_3, \\ \varepsilon D_3 \frac{d}{dx} j_3 &= a(\gamma e^{b(T-1)} - C_3 C_4), \quad \frac{dC_4}{dx} = -C_4 E - j_4, \\ \varepsilon D_4 \frac{d}{dx} j_4 &= a(\gamma e^{b(T-1)} - C_3 C_4), \quad \varepsilon \frac{dT}{dx} = C_1 - C_2 + C_3 - C_4, \\ \varepsilon Le \frac{d^2 T}{dx^2} &+ \varepsilon \mu EI + \mu a Arn (C_3 C_4 - \gamma e^{b(T-1)}) = 0. \end{aligned}$$

The system of equations contains three small parameters ε , μ and γ , connected by relations (17) and (18). The parameter ε enters the equations singularly, i.e., as a coefficient in the derivatives, and the parameter γ is regular, so the system of equations is simultaneously singularly and regularly perturbed.

2.6. Transition to dimensionless form under boundary conditions

The dimensionless boundary conditions have the form:

$$\begin{aligned} C_1|_{x=0} = 1, C_2|_{x=0} = 1 + C_{30}, C_3|_{x=0} = C_{30}, C_4|_{x=0} = C_{40} = \frac{\gamma}{C_{30}}, T(0) = 1, \\ C_1|_{x=1} = C_{1m}, C_3|_{x=1} = C_{3m}, j_4|_{x=1} = j_{4m}, \\ -k \frac{d}{dx} T(1) = \mu D_4 b_q \frac{d}{dx} j_4(1). \end{aligned}$$

Remark 1. Owing to continuity, the following is valid:

$$I_W = D_3 j_{3m} - D_4 j_{4m} = D_3 j_{30} - D_4 j_{40}.$$

3. Numerical solution algorithm

3.1. Transition to a boundary value problem for a system of second-order equations

Due to the small parameter ε in the equations (12), (14) and (15), the boundary-value problem (9) - (16) is singularly perturbed; therefore, the system is inconvenient for a numerical solution [7]. In addition, differential equations are of the first order, and a boundary-value problem is set for them. In the equation (15), for the electric field strength, the right-hand side is independent from E . This causes stability problems in the numerical solution to the discrete system of equations by the Newton – Kantorovich method [8]. Therefore, the boundary value problem (9) - (16) should be reduced to a form convenient for a numerical solution. To do this, we pass to the system of second-order equations:

$$\begin{aligned} \frac{d^2 C_1}{dx^2} = \frac{d}{dx} (C_1 E), \frac{d^2 C_2}{dx^2} = \frac{d}{dx} (C_2 E), \frac{d^2 C_3}{dx^2} = \frac{d}{dx} (C_3 E) - \frac{a(\gamma e^{b(T-1)} - C_3 C_4)}{\varepsilon D_3}, \\ \frac{d^2 C_4}{dx^2} = \frac{d}{dx} (C_4 E) - \frac{a(\gamma e^{b(T-1)} - C_3 C_4)}{\varepsilon D_4}, \varepsilon \frac{d^2 E}{dx^2} = E(C_1 + C_2) - j_1 + j_2 + \frac{dC_3}{dx} - \frac{dC_4}{dx}, \\ \varepsilon L e \frac{d^2 T}{dx^2} + \varepsilon \mu E I + \mu a A r n (C_3 C_4 - \gamma e^{b(T-1)}) = 0. \end{aligned} \quad (19)$$

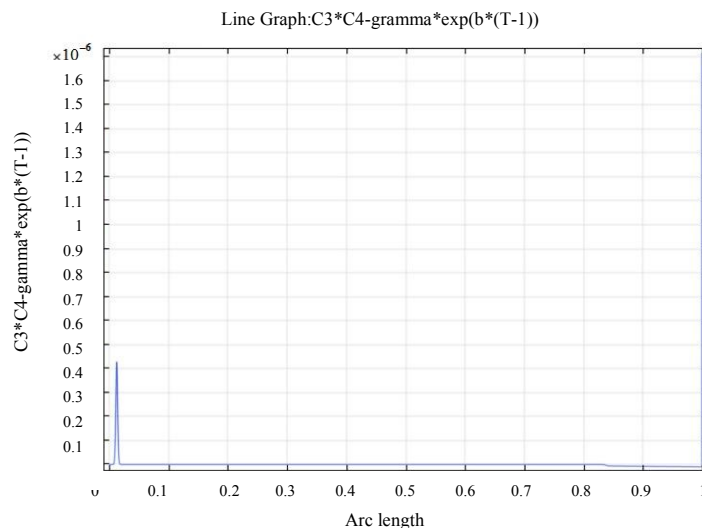
In connection with the transition to systems of the second-order equation, it is necessary to supplement the initial boundary conditions with the missing boundary conditions for the function E . From the boundary conditions, it follows that at the point $x = 0$, the electroneutrality condition $C_1 - C_2 + C_3 - C_4 \approx 0$ is satisfied. Due to the continuity, with some accuracy, in the vicinity of the point $x = 0$, $C_1 - C_2 + C_3 - C_4 \approx 0$ is fulfilled, therefore E_0 can be calculated from the electroneutrality condition. Adding the equations for C_i , $i = 1, \dots, 4$ and using the electroneutrality condition $C_{10} - C_{20} + C_{30} - C_{40} = 0$, we can obtain the relation $E|_{x=0} = \frac{I_s}{1+C_{20}} + \frac{d}{dx} (C_1(0) - C_2(0))$.

From the equation for E at $x = 1$, we have: $\varepsilon \frac{dE}{dx}|_{x=1} = (C_1 - C_2 + C_3 - C_4)|_{x=1}$.

Research Results

3.2. Numerical Results

To analyze the results of the numerical solution, along with the graphs of the desired functions C_i, E, j_3, j_4, T , we consider the graphs of the functions $\rho(x) = C_1 - C_2 + C_3 - C_4$, $p(x) = C_3 C_4 - \gamma e^{b(T-1)}$. The function $\rho(x)$ characterizes the distribution of charge density, and $p(x)$ is the deviation from the equilibrium of the dissociation (recombination) reaction.



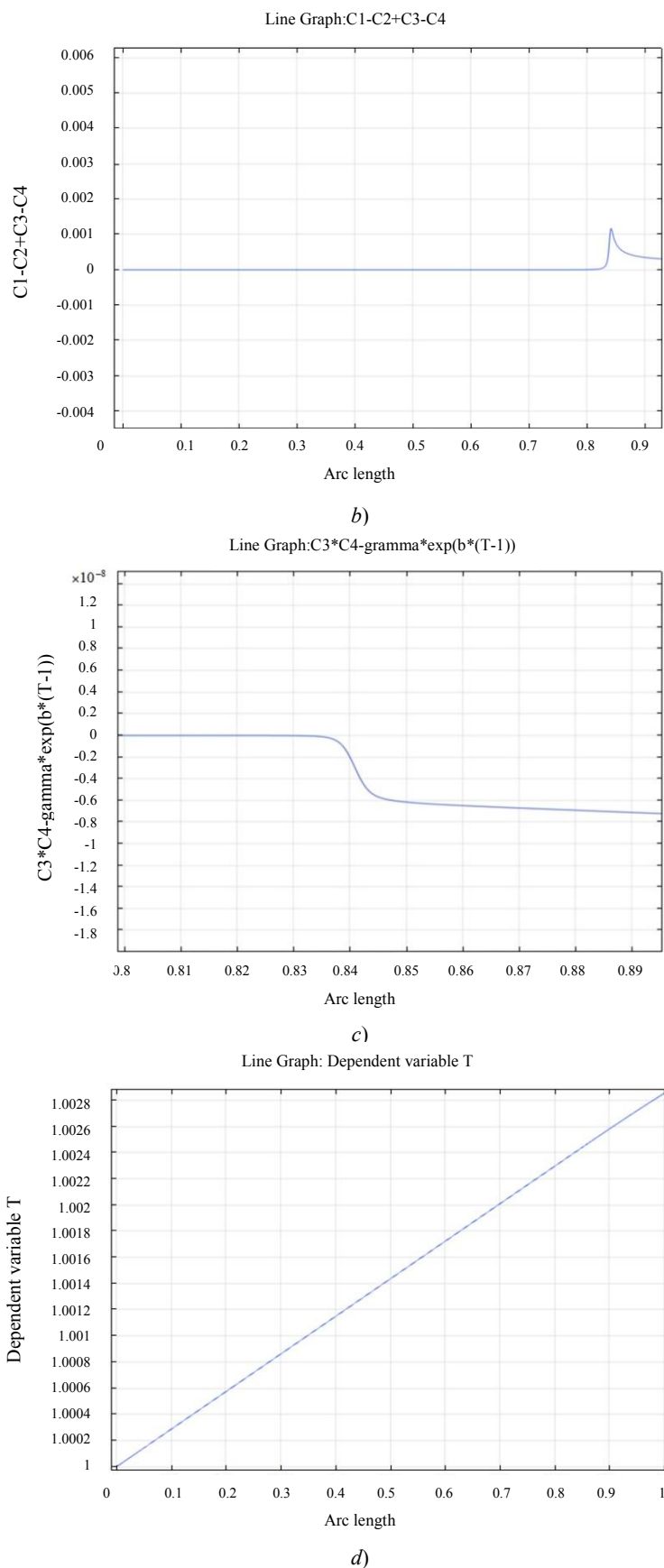


Fig. 2. Graph of function $\rho(x) = C_1 - C_2 + C_3 - C_4$ ([0; 0.93]) (a); graph of function $p(x) = C_3C_4 - \gamma e^{b(T-1)}$ (b); graph of function $p(x) = C_3C_4 - \gamma e^{b(T-1)}$ in SCR (c); temperature graph (d)

From Fig. 2(a), it follows that the diffusion layer is divided into three regions. The first is the region of electro-neutrality (ENR), where $\rho(x) = 0$. The second is the space charge region ($\rho(x) > 0$). The third is an intermediate layer

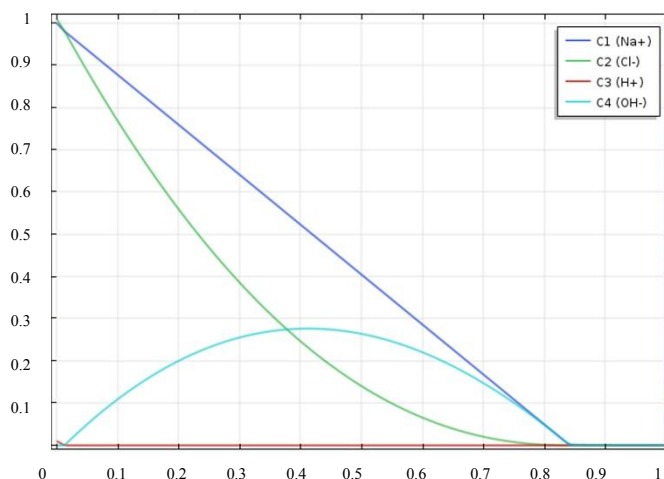
between them where the charge distribution density has a pronounced local maximum. The SCR itself is divided into two parts: extended and quasi-equilibrium (it is very small and adjacent to the interface). In the quasi-equilibrium part of the SCR, the charge density distribution obeys the exponential law (not shown in Fig. 2).

A general view of the graph of the function $p(x)$ (Fig. 2, b) shows that the deviation from equilibrium occurs:

- in the recombination region which is located inside the ENR;
- in the space charge region (Fig. 2, c).

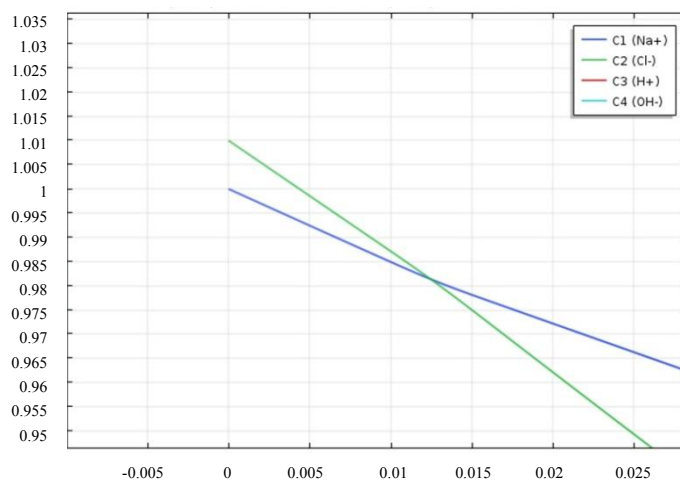
In the first case, $p(x) > 0$, .e., recombination prevails over the dissociation $C_3C_4 \gg \gamma e^{b(T-1)}$. In the second case, on the contrary, $p(x) < 0$, and dissociation prevails over recombination in the SCR, as well as in the intermediate layer. The temperature (Fig. 2, d) increases linearly by 0.0028 in a dimensionless form (or $0,0028 \cdot 298 = 0.83$ degrees). The increase depends on the total current density or potential jump in the diffusion layer and can be up to tens of degrees. Obviously, all terms of the equation (19) are small compared to the first one, that is, the second derivative is $\frac{d^2T}{dx^2} \approx 0$. From this, it follows that the temperature is linear and is determined by the boundary conditions.

Line Graph: Dependent variable C1 Line Graph: Dependent variable C2
 Line Graph: Dependent variable C3 Line Graph: Dependent variable C4



a)

Line Graph: Dependent variable C1 Line Graph: Dependent variable C2
 Line Graph: Dependent variable C3 Line Graph: Dependent variable C4



b)

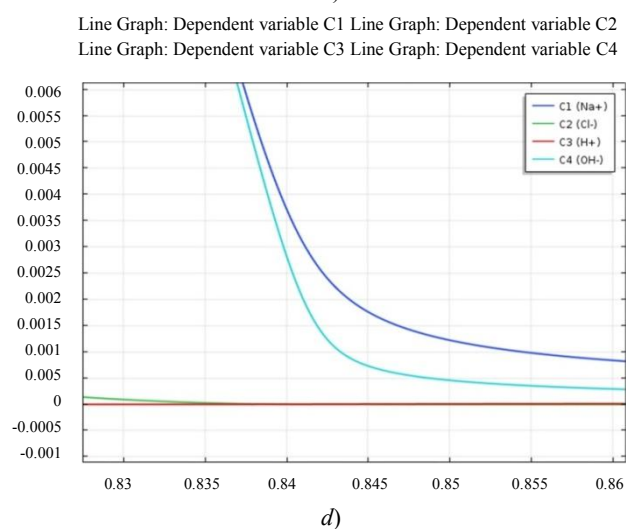
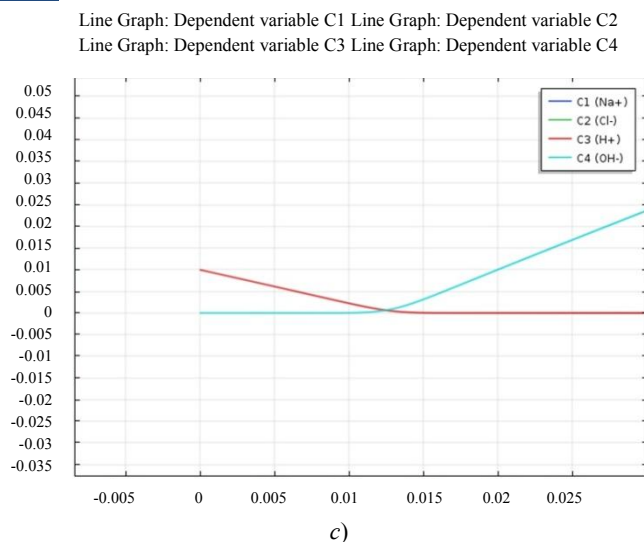
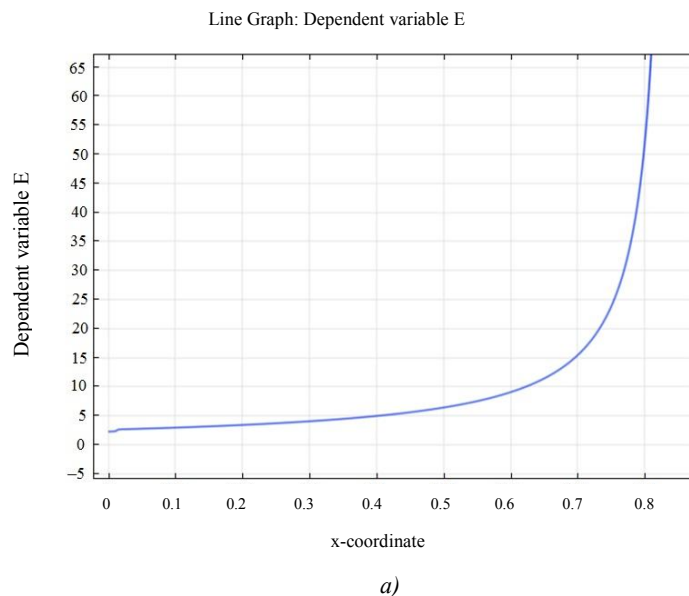
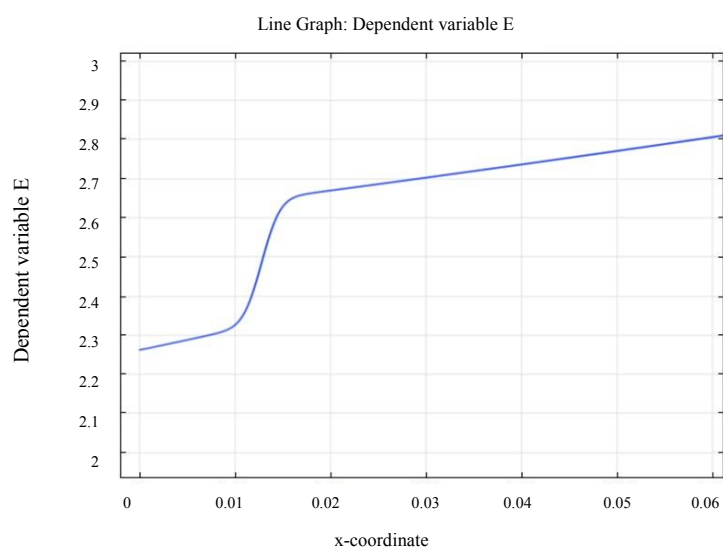


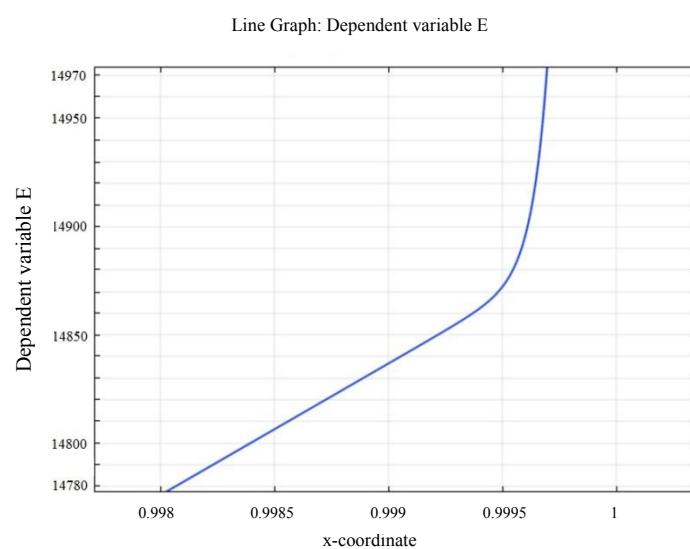
Fig. 3. General view of graphs of functions C_1 , C_2 , C_3 , C_4 (a); function graphs C_1 , C_2 near zero (b); function graphs C_3 , C_4 near zero (c); function graph C_1 , C_2 , C_3 , C_4 in space charge region (d)

As follows from Fig. 3 a, the sodium concentration decreases linearly in the ENR and becomes small in the SCR, but it is higher than the concentration of the remaining ions (Fig. 3 d). The center of the RR is the intersection point of the graphs of concentration of Na^+ и Cl^- and, respectively, of OH^- and H^+ . To the right of the center, the concentration of Cl^- decreases faster than the concentration of Na^+ . The deficit of negatively charged ions resulting from this is compensated by the rapid growth of hydroxyl ions, and the condition of electroneutrality is preserved (Fig. 3a).

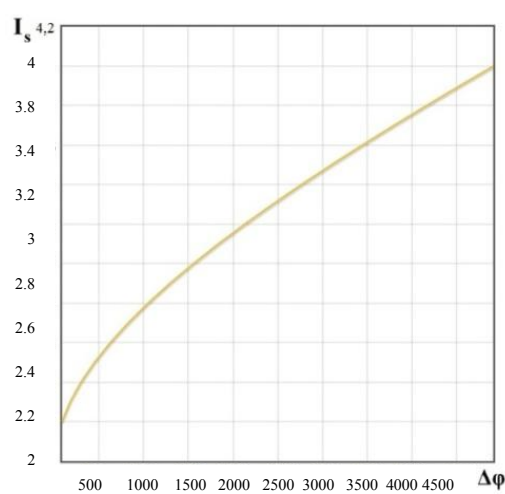




b)



c)



d)

Fig. 4. General view of graph of E function with exception of phase boundary (a); graph of E function near RR (b); graph of E function near phase boundary (c), volt-ampere characteristic (d)

From the data in Fig. 4, it follows that in ENR, the electric field strength increases rapidly tens of times (Fig. 4, *a*). A particularly high rate of the electric field strength is observed in the SCR upon reaching values of the order of $\frac{1}{\sqrt{\epsilon}}$. In the RR there is an internal boundary layer of E electric field strength (Fig. 4, *b*). This is due to the fact that charge carriers change: before RR, the charge is determined by Na^+ , Cl^- , H^+ ions, and after — by Na^+ , Cl^- , OH^- ions. The appearance of a “step” owes to the fact that the diffusion coefficient of hydrogen is approximately two times greater than the diffusion coefficient of hydroxyl. The VAC increases without limit with a growth of the potential jump in the over-extreme mode $I_s > 2$ (Fig. 4, *d*). This growth tends to be much slower than the experimentally observed one, which means that along with the dissociation (recombination) reaction of water, there is another mechanism of super-limit transfer. It is generally accepted that electroconvection is such a mechanism [9–11]. In this regard, a problem of evaluation and interaction of the dissociation (recombination) reaction and electroconvection occurs.

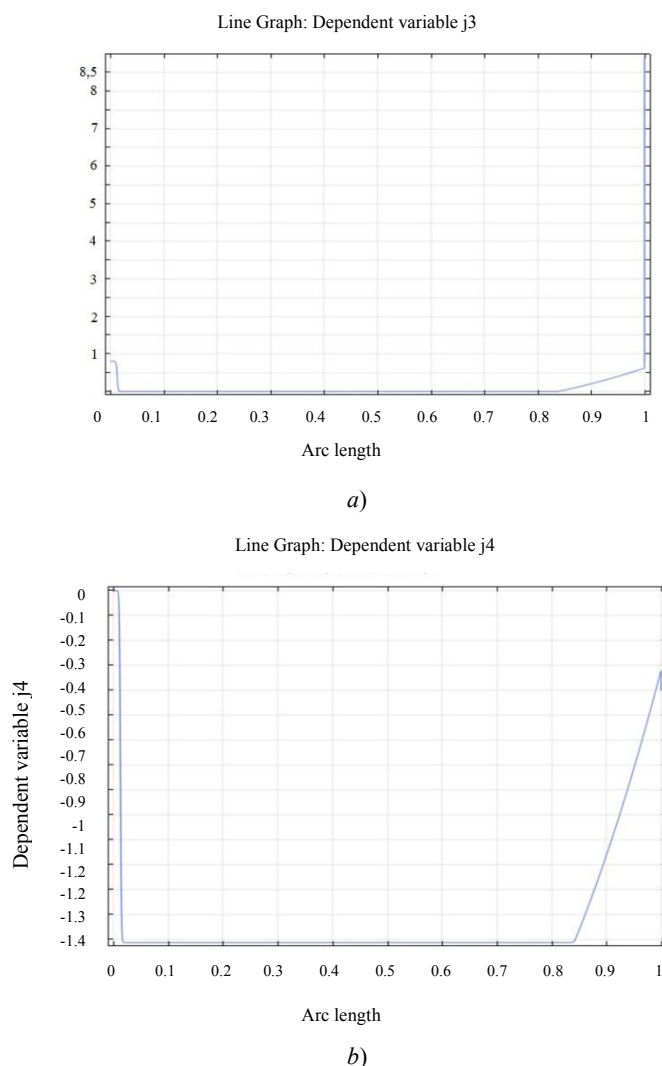


Fig. 5. Flux plot of hydrogen j_3 (*a*) and hydroxyl j_4 (*b*) ions

Fig. 5 shows that the flow of hydrogen ions is positive. It is constant to the left of the RR and is practically equal to zero to the right of the RR till the SCR. In the SCR, the flow of hydrogen ions increases linearly due to the intense dissociation of water. The flow of hydroxyl ions to the left of the RR is practically zero, and to the right, it is negative and constant until the SCR. In the SCR, the flow of hydroxyl ions, as well as the flow of hydrogen ions, increases linearly. In a quasi-equilibrium SCR, the hydroxyl ion flux changes sharply and satisfies the boundary condition $j_4(1) = j_4(m)$. The recombination region is an internal boundary layer for the flows of hydrogen and hydroxyl – they change sharply here.

Discussion and Conclusions. In this paper, the transport of binary salt ions through a diffusion layer near a cation exchange membrane is considered. A mathematical model of the process is proposed, which takes into account the temperature effects caused by the dissociation (recombination) of water molecules and the Joule heating in solution. This model consists of 9 ordinary differential equations with corresponding boundary conditions. An algorithm for the numerical solution to a boundary value problem is developed, and its computational investigation is presented. The

basic laws of the transfer of salt ions are defined considering the dissociation (recombination) reaction of water molecules and temperature effects.

It is shown that the VAC grows without limit with a growth of the potential jump in the over-extreme mode, and is much slower than in experiments. Therefore, along with the dissociation (recombination) reaction of water, there are other mechanisms of super-limit transfer (for example, electroconvection and gravitational convection). Thus, a challenge arises of assessing the interaction of dissociation (recombination) reactions, electroconvection, and gravitational convection.

Temperature effects from the dissociation (recombination) reaction and the Joule heating in the ENR are almost imperceptible (with the exception of RR). The Joule heating in the SCR is two orders of magnitude higher than the cooling effect of the water dissociation reaction. Upon the recombination, approximately the same heat is released in the RR as during the Joule heating in the expanded SCR. However, due to a small size of the RR, the effect of this heat is imperceptible. Thus, we can assume that there is only one source of heat at the interface in the SCR, which, due to its noticeable size, causes a significant increase in temperature throughout the diffusion layer. It follows that the emergence and development of gravitational convection is possible.

In the paper, a solution of sodium chloride is considered; however, the study is valid for a solution of any binary salt.

General conclusions following from the results obtained enable to intensify the process of salt ion transport in the electrodialysis machines.

References

1. Simons, R. Strong electric field effects on proton transfer between membrane-bound amines and water. *Nature*, Land, 1979, vol. 280, pp. 824–826.
2. Spravochnik khimika 21. Khimiya i khimicheskaya tekhnologiya. [Handbook of a chemist 21. Chemistry and chemical technology] / chem21.info. Available at: <https://chem21.info/info/14102/> (accessed 19.08.19) (in Russian).
3. Chubyr, N. O. About one particular solution of QECS tasks. Ion transport in organic and inorganic membranes. Tuapse: Kuban State University Publ. House, 2009, pp. 38–40.
4. Kovalenko, A.V., et al. Vliyanie reaktsii dissotsiatsii/rekombinatsii molekul vody na perenos 1:1 elektrolita v membrannykh sistemakh v diffuzionnom sloe. Chast' 1. Matematicheskaya model'. [The influence of reaction of dissociation-recombination of water molecules on electrolyte transportation 1:1 in membrane systems in the diffusion layer. Part 1. Mathematical model.] *Scientific Journal of KubSAU*, 2016, no. 7 (121). Available at: <http://ej.kubagro.ru/2016/07/pdf/122.pdf>. — IDA [article ID]: 1211607122. <http://dx.doi.org/10.21515/1990-4665-121-122> (in Russian).
5. Kovalenko, A.V., et al. Matematicheskoe modelirovanie vliyaniya osnovnykh temperaturnykh effektov na statsionarnyy perenos ionov soli v diffuzionnom sloe. [Mathematical modeling of influence of basic temperature effects on the stationary transport of salt ions in a diffusion layer.] *Ecological Bulletin of Research Centers of the Black Sea economic cooperation*, 2018, no. 3, pp. 78–86 (in Russian).
6. Kovalenko, A.V., et al. Vliyanie temperaturnykh effektov, svyazannykh s reaktsiyey dissotsiatsii/rekombinatsii molekul vody i Dzhouleevym nagrevom rastvora na statsionarnyy perenos ionov soli v diffuzionnom sloe. [Influence of temperature effects associated with the dissociation-recombination reaction of water molecules and Joule heating of the solution on the stationary transport of salt ions in the diffusion layer.] *Ecological Bulletin of Research Centers of the Black Sea economic cooperation*, 2018, no. 4, pp. 67–84 (in Russian).
7. Cole, J.D. *Metody vozmushcheniy v prikladnoy matematik.*, [Perturbation Methods in Applied Mathematics.] Moscow: Mir, 1972, pp. 274 (in Russian).
8. Urtenov, M.Kh., et al. Kraevaya zadacha dlya plotnosti toka v oblasti prostranstvennogo zaryada. [The boundary value problem for the current density in the space-charge region.] *Ecological Bulletin of Research Centers of the Black Sea economic cooperation*, 2010, no. 1, pp. 70–73 (in Russian).
9. Lavrentyev, A.V. et al. Chislennoe i asimptoticheskoe resheniya neodnomernoy sistemy uravneniy Nernsta — Planka — Puassona. [Numerical and asymptotic solutions of non-singular dimensional equation system by Nernst-Plank-Puasson.] *Izvestiya vuzov. Severo-Kavkazskiy region. Natural Sciences*, 2010, no. 5 (159), pp. 17–22 (in Russian).
10. Urtenov, M.Kh., et al. Matematicheskoe modelirovanie perenosa ionov soli i dissotsiatsii vody u granitsy ionoobmennaya membrana/rastvor v intensivnykh tokovykh rezhimakh. [Mathematical modeling of ion transport and water dissociation at the ion-exchange membrane/solution interface in intense current regimes.] *Membranes and Membrane Technologies*, 2018, vol. 8, no. 1, pp. 24–33 (in Russian).

11. Zabolotsky, V.I., Nikonenko, V.V. *Perenos ionov v membranakh. [Membrane ion transport.]* Moscow: Nauka, 1996, 392 p. (in Russian).

Submitted 22.01.2019

Scheduled in the issue 12.04.2019

Authors:

Chubyr, Natalia O.,

associate professor of the Applied Mathematics Department, Kuban State Technological University (2, Moskovskaya St., Krasnodar, 350072, RF), Cand.Sci. (Phys.-Math.),

ORCID: <https://orcid.org/0000-0003-3535-0361>

chubyr-natalja@mail.ru

Kovalenko, Anna V.,

associate professor of the Applied Mathematics Department, Kuban State University

(149, Stavropolskaya St., Krasnodar, 350040, RF), Cand.Sci. (Econ.), associate professor,

ORCID: <https://orcid.org/0000-0002-3991-3953>

savanna-05@mail.ru

Urtenov, Makhamet Kh.,

Head of the Applied Mathematics Department, Kuban State University (149, Stavropolskaya St., Krasnodar, 350040, RF), Drt.Sci. (Phys.-Math.), professor,

ORCID: <https://orcid.org/0000-0002-0252-6247>

urtenovmax@mail.ru

Sukhinov, Alexander I.,

Vice Rector for Research and Innovation, Don State Technical University (1, Gagarin Square, Rostov-on-Don, 344000, RF), Dr.Sci. (Phys.-Math.), professor,

ORCID: <https://orcid.org/0000-0002-5825-1523>

sukhinov@gmail.com

Gudza, Vitaly A.,

postgraduate of the Applied Mathematics Department, Kuban State University (149, Stavropolskaya St., Krasnodar, 350040, RF),

ORCID: <https://orcid.org/0000-0003-3199-3589>

vitaliy.gudza@gmail.com

INFORMATION TECHNOLOGY, COMPUTER SCIENCE, AND MANAGEMENT ИНФОРМАТИКА, ВЫЧИСЛИТЕЛЬНАЯ ТЕХНИКА И УПРАВЛЕНИЕ



UDC 004.94: 621.01

<https://doi.org/10.23947/1992-5980-2019-19-3-281-289>

The problem of mathematical finite element modeling of inhomogeneous deformable solids using scanning*

V. L. Duong^{1**}

¹ Irkutsk National Research Technical University, Irkutsk, Russian Federation

Проблема математического конечноэлементного моделирования неоднородных деформируемых твердых тел с применением сканирования***

В. Л. Зыонг^{1**}

¹ Иркутский национальный исследовательский технический университет, г. Иркутск, Российская Федерация

Introduction. In the mathematical finite element modeling, an average value of the mechanical characteristics of the deformable solid material is used. In aircraft, machine building, construction engineering, medicine and other fields, polymer composite materials and materials of natural origin are increasingly used. In the latter case, the actual change in the mechanical characteristics differs significantly from the averaged change; therefore, when using the averaged parameters to build and analyze finite element models, the results can be significantly distorted. This paper describes the creation of mathematical methods for studying changes in the mechanical characteristics of a material of inhomogeneous deformable solids. The results obtained in this way are used to construct finite element models and analyze their stress-strain state.

Materials and Methods. Naturally occurring materials and composites are considered as inhomogeneous deformable solids. To study the changes in the mechanical characteristics of the material, a method was developed based on the use of two components: the pixel characteristics of raster images scanned by a computer tomograph and the experimental data of field tests of standard samples.

Research Results. A complex of mathematical methods has been developed for modeling the interpretation of scanning raster images by a computer tomograph, which allows for the study of any complicated structures of real deformable solids. The results are used in the construction of finite element models of such bodies considering the heterogeneity of the mechanical characteristics of the material. The analysis of the stress-strain state of finite element models of test samples has

Введение. При математическом конечноэлементном моделировании используется усредненное значение механических характеристик материала деформируемых твердых тел. В авиа-, машиностроении, строительстве, медицине и других областях все шире применяются полимерные композитные материалы и материалы природного происхождения. В последнем случае реальное изменение механических характеристик значительно отличается от усредненного, следовательно, при использовании усредненных параметров для построения и анализа конечноэлементных моделей результаты могут существенно искажаться.

В данной статье описано создание математических методов исследования изменения механических характеристик материала неоднородных деформируемых твердых тел. Полученные таким образом результаты применены для построения конечноэлементных моделей и анализа их напряженно-деформированного состояния.

Материалы и методы. В качестве неоднородных деформируемых твердых тел рассмотрены материалы природного происхождения и композиты. Для исследования изменения механических характеристик материала разработан способ, основанный на использовании двух составляющих: пиксельной характеристики растровых изображений сканирования компьютерным томографом и экспериментальных данных натурных испытаний стандартных образцов.

Результаты исследования. Создан комплекс математических методов моделирования интерпретации растровых изображений сканирования компьютерным томографом, позволяющий проводить исследование любых сложных структур реальных деформируемых твердых тел. Результаты используются при построении конечноэлементных моделей таких тел с учетом неоднородности механических характеристик материала.

Анализ напряженно-деформированного состояния конечноэлементных моделей тестовых образцов доказал точность и сходимость численного решения метода конечных

* The research is done within the frame of the independent R&D.

** E-mail: bright1388@gmail.com

*** Работа выполнена в рамках инициативной НИР.



proved the accuracy and convergence of the numerical solution of the finite element method in modeling the property of heterogeneity of the mechanical characteristics of the material.

Discussion and Conclusions. The developed approach can be applied to any physical principles of scanning (X-ray, ultrasound, laser, etc.) and for any types of materials if the data obtained as a result of scanning is developed in the form of a digital (raster) image.

Keywords: finite element method, deformable solid, inhomogeneity, mechanical properties of material.

For citation: Duong, V.L. The problem of mathematical finite element modeling of inhomogeneous deformable solids using scanning. Vestnik of DSTU, 2019, vol. 19, no. 3, pp. 281–289. <https://doi.org/10.23947/1992-5980-2019-19-3-281-289>

элементов при моделировании свойства неоднородности механических характеристик материала.

Обсуждение и заключения. Разработанный подход может быть применен для любых физических принципов сканирования (рентгеновский, ультразвуковой, лазерный и др.) и для любых типов материалов, если информация, полученная в результате сканирования, сформирована в виде цифрового (растрового) изображения.

Ключевые слова: метод конечных элементов, деформируемое твердое тело, неоднородность, механические характеристики материала.

Образец для цитирования: Зьонг, В. Л. Проблема математического конечноэлементного моделирования неоднородных деформируемых твердых тел с применением сканирования // Вестник Дон. гос. техн. ун-та. — 2019. — Т. 19, № 3. — С. 281–289. <https://doi.org/10.23947/1992-5980-2019-19-3-281-289>

Introduction. In the finite element (FE) modeling, mechanical characteristics of the material of deformable solids (DS) are specified as an averaged value used for the whole model. For example, mechanical characteristics of steel are determined through tensile and compression tests of standard regular samples. This approach is acceptable for the design and engineering practice. However, in modern aircraft, engineering, construction, medicine and other fields, polymer composites and materials of natural origin are increasingly used. A real change in the mechanical characteristics of such materials differs drastically from an average value; therefore, when using average parameters to build and analyze finite element models, the results can be significantly distorted.

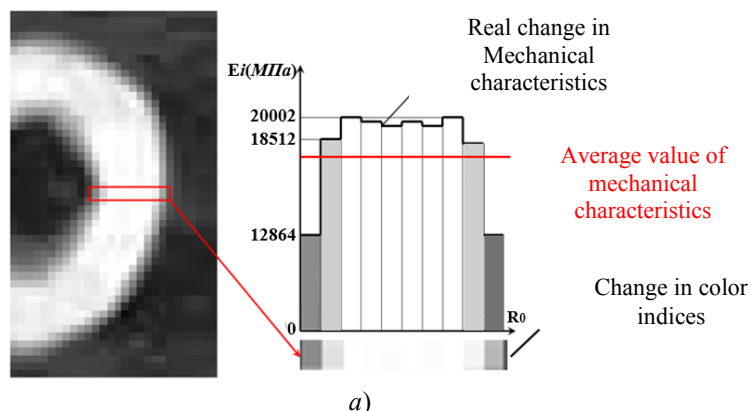
Research Results

1. The main mathematical dependence of modeling heterogeneity of real deformable solids. To solve the presented problem, a method for determining a real change in the mechanical characteristics of the material based on the use of:

- DS scan results;
- data of field tests of standard samples [1].

This method makes it possible to recognize any complex heterogeneous material structure and apply this data to increase accuracy and realism in mathematical finite element modeling of real DS.

Fig. 1a shows an example of a raster image of scanning a material of natural origin (human bone). Its section demonstrates a change in mechanical characteristics depending on the values of the color indices (pixels) [2]. Fig. 1b shows the scan result of the composite material in the form of a raster image of the cross section of a regular sample (the scanning was performed by V.G. Tolstikov). Real changes in the mechanical characteristics of the fibers and matrix (adhesive) in the structure are indicated. In addition, the scanning has shown the possibility to assess quality of the composite materials (fiber arrangement, adhesive layer thickness, internal defects, etc.).



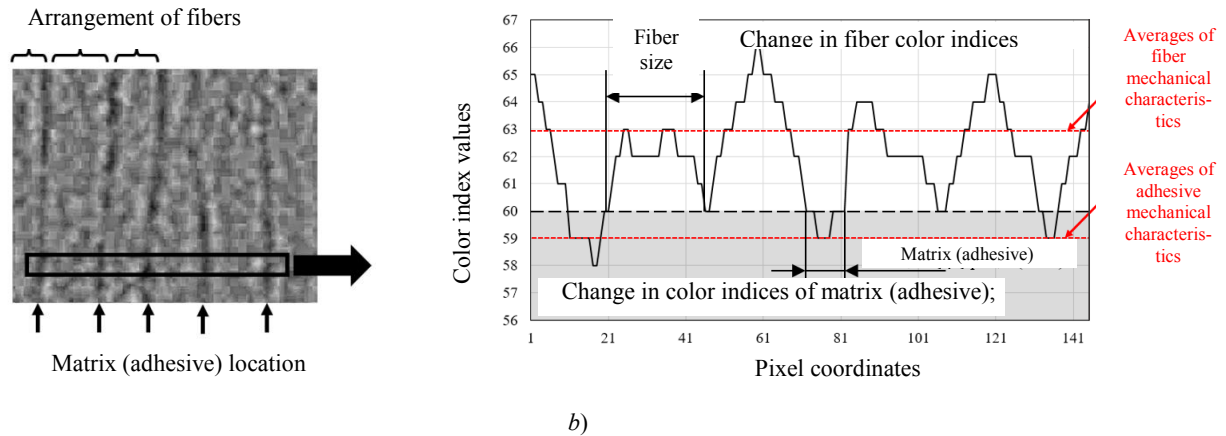


Fig. 1. Material of natural origin (a) and composite material (b) scan bitmap analysis

A general diagram of mathematical simulation and the algorithm of the proposed scanning technology are shown in Fig. 2 [2].

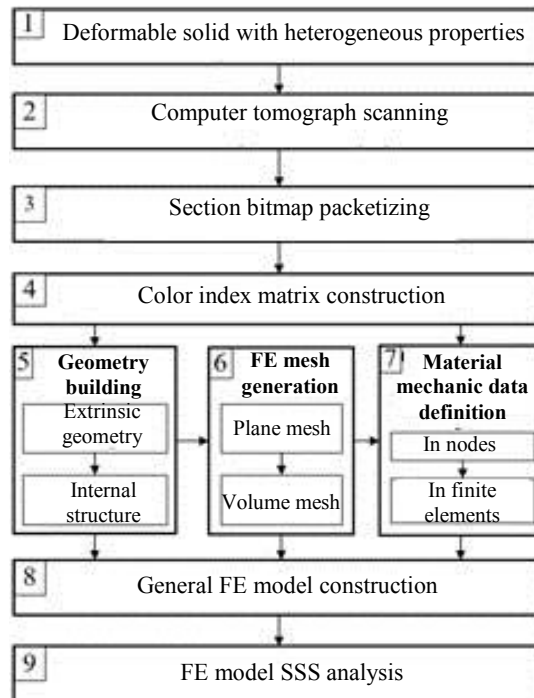


Fig. 2. Mathematical and finite element modeling of real deformable solids

The diagram reflects a full range of modules: from scanning DS to obtaining its FE model and analysis of the stress-strain state (SSS). If necessary, the cycle of operations is ensured within each block of the algorithm.

Scanning is performed using a computer tomograph (CT). When working with deformable objects, it provides image packetizing; each one is a raster image in a certain section [3, 4]. Standard raster image formats are jpeg, dicom, bmp, png, etc. Regardless of the format used, a raster image should be represented as a numerical matrix for further processing.

To determine the dependence of mechanical characteristics (for example, in the form of an elastic modulus) on the values of color indices, a special weight factor is applied [1], which establishes the relationship between the average value of the color indices n_{cp} and the experimental value E_{OII} . The average value of the elastic modulus (E_{OII}) obtained in the experiment on the tension (compression) of standard samples is used to interpret mechanical changes in the pixel characteristic.

Then the weight factor that determines the transition from the pixel color index to the elastic modulus is determined through an expression of the following form:

$$k_E = \frac{E_{OII}}{n_{cp}}. \quad (1)$$

Here, n_{cp} is an average value of color indices of a scanning bitmap packet:

$$n_{cp} = \frac{\sum_{i=1}^m \sum_{j=1}^n I(i, j)}{mn}. \quad (2)$$

However, for a large amount of CT SSS scan data with a high degree of the structure heterogeneity, it is required to use the mathematical expectation dependence when determining an average value of the color index. That is, n_{cp} is defined as an average value:

$$n_{cp} = E(n) = \sum_{i=1}^m n_i p_i(n_i), \quad (3)$$

where n_i is the color index value on the interval I ; $p_i(n_i)$ is the probability of occurrence of n_i (color index values) in the interval I .

Pixels, each of which has a corresponding color index, are assigned the values of the elastic modulus of the material E_i . For this, the weight factor k_E is used:

$$E_i = n_i k_E. \quad (4)$$

Here, E_i is the elastic modulus value corresponding to the value of the color index number n_i ; k_E is weight factor of the elastic modulus.

The dependence (4) for the FE model is implemented through solving the following tasks:

- determination of the dependence of mechanical characteristics on the values of color indices;
- determination of the mechanical characteristics of the material in the nodes and in the finite elements of the FE model.

A change in the elastic modulus is determined on the basis of a linear or non-linear dependence on the values of the color indices. For a material with a low degree of heterogeneity, the dependence can be constructed according to the linear law (4) using a single constant value of the weight factor of the elastic modulus.

However, such materials are rare in nature and engineering. Most often, several areas can be distinguished in the structure of a DS material, each of which has a different variation range of the elasticity modulus than the others.

It is proposed to apply a nonlinear law for such materials, which provides its own weight factor value in each region of the DS structure. In this case, the dependence of the change in the DS elastic modulus on the color indices is presented as a piecewise linear function (Fig. 3a).

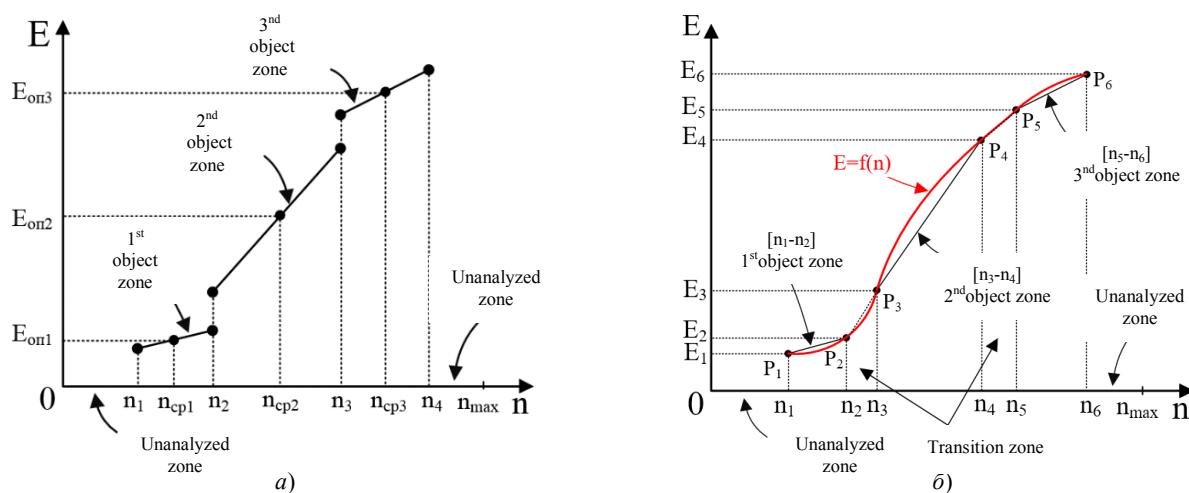


Fig. 3. Piecewise linear (a) and continuous (b) function of DS elasticity modulus variation from color index values

Using a piecewise linear function is difficult from the point of view of the computational algorithm efficiency, in particular, due to the following reasons:

- the larger the number of the DS structure regions, the greater the number of weight factors and the more complicated the calculation of the elastic modulus for nodes and finite elements;
- transition values of color indices between DS regions or objects involve not one value, but ranges of values of color indices in a bitmap (see Fig. 3b).

To solve this problem, a nonlinear dependence in the form of a spline, for example, a cubic one [5], can be constructed on the basis of a piecewise linear function. Such a nonlinear dependence of the DS elastic modulus on color indices is universal when combining several zones with different patterns of mechanical characteristics (see Fig. 3b).

Next, the interpretation of the scanning data is associated with the interpolation and transmission of color index values from pixels to the nodes of the FE mesh. In the most complex and general case, the FE nodes of the mesh lie between adjacent planes with a bitmap. They vary widely in shape and size. Besides, additional internal contours and other geometric features appear in them. In this case, a number of mathematical dependences are used for interpolation; they are determined with respect to a straight line inclined to the Z axis [6].

In [2], a more similar description of the mathematical dependence and the block diagram of the algorithm for determining the mechanical characteristics of the material in the nodes and finite elements of the DS FE model is presented (see Fig. 2, block 7).

To use the results of determining the heterogeneity of the material mechanical characteristics in the FE model, they are converted to a file with the *.pcl extension. Two functions of the Patran Command Language: “material.create” and “elementprops_create” [7, 8] are used for this.

2. Investigation of the accuracy and convergence of the analysis results of the FE models considering simulation of heterogeneity of mechanical characteristics. In the framework of this study, accuracy and convergence of the numerical solution by the finite element method (FEM) using the presented technique are determined. For this purpose, we used the SSS calculations of a human bone tissue (a fragment of the femur).

The selection of DS and its analysis are nonessential, but they are caused by important factors: heterogeneity of the bone material, individuality of its geometry, as well as high technology and quality of CT scanning in medicine. Bone tissue is well studied in practice, which makes it possible to reasonably consider the correctness of its mathematical simulation.

The first study uses parallelepiped specimens cut from a fragment of a human femur (Fig. 4a). The results of the study are shown in Fig. 4b as proof of accuracy and convergence of the FEM numerical solution with respect to the full-scale experiment data [9, 10].

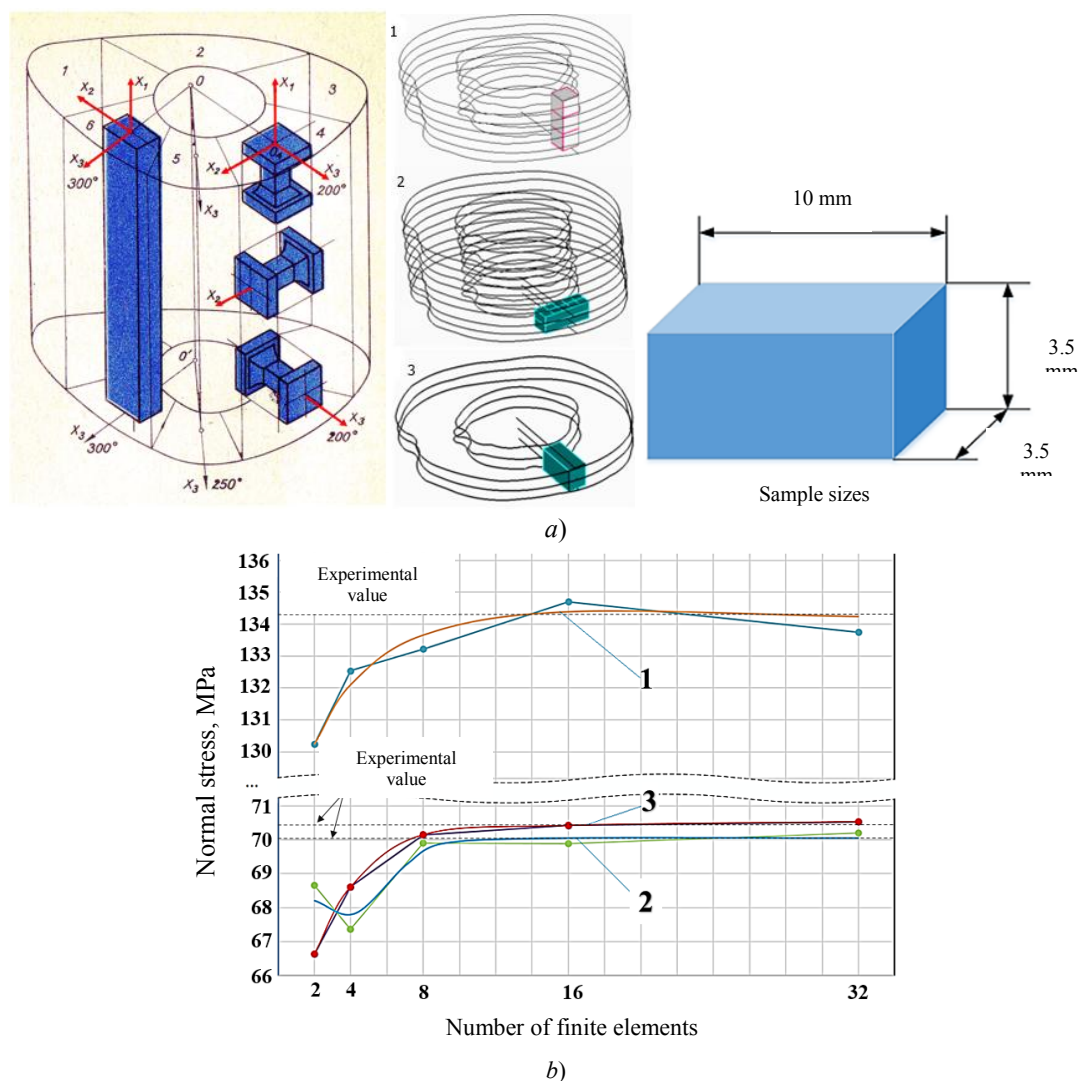


Fig. 4. Dimensions and orientation of real samples (a); graph of convergence of normal stress in the center of samples (b), longitudinally (1), circumferentially (2) and radially (3)

The results show that to achieve the desired accuracy of the FEM numerical solution, a FE mesh with a density of three or more finite elements per 1 mm is required [11]. It is also obvious that the heterogeneity property of the DS material mechanical characteristics can be reflected by a set of finite elements with their own elastic moduli and the isotropic structure of the material.

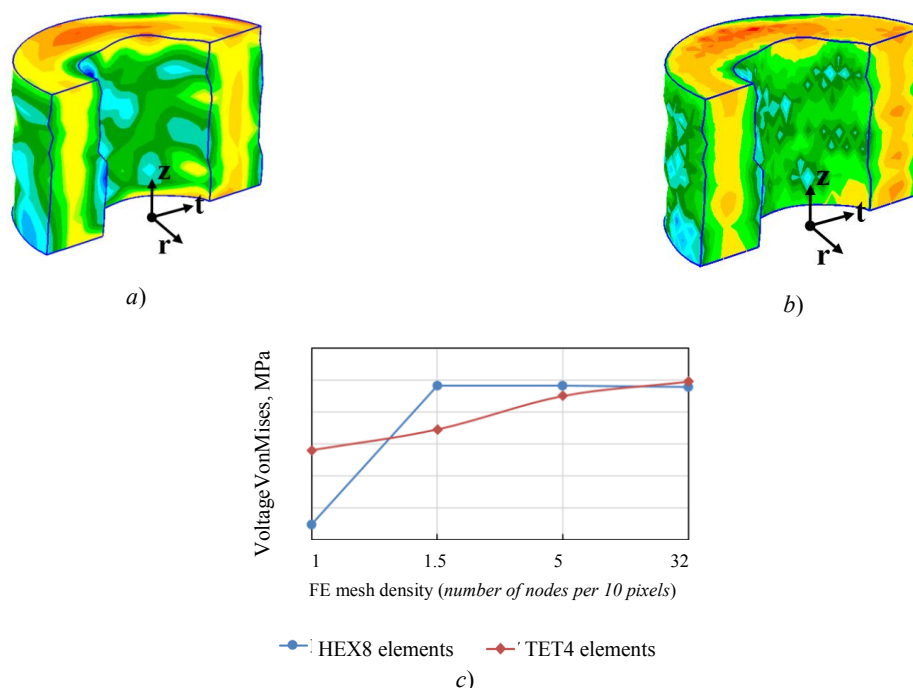
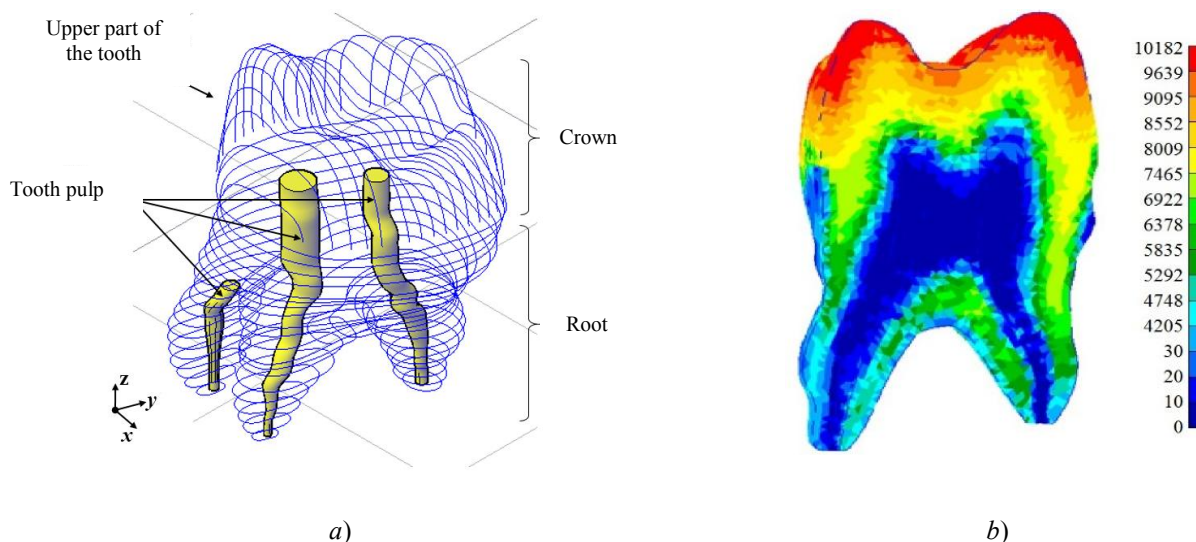


Fig. 5. SSS analysis result using HEX (a) and TET (b) type finite elements; graph of convergence results (c)

To study the applicability of two different types of solid FE (hexahedron and tetrahedron), an additional study was conducted using incompatible shape functions (see Fig. 5) [12]. The results show that hexahedron-type FE has the best indicators in terms of accuracy and convergence of results, as well as in the resource costs.

3. Modeling of real deformable solids. The technology presented is applied to real objects. For this purpose, the SSS of the FE of tooth setups with a defect and a sealant made of composite material was constructed and analyzed. One model presents a defect in the form of a carious region (cavity) in the upper part of the enamel. In the second version of the FE model, this area is filled with a sealant made of composite material. Both models are built considering heterogeneity of the material mechanical characteristics and an individual geometry.

A wireframe model of a human tooth, shown in Fig. 6a, is based on the scan results [13, 14]. A change in the material mechanical characteristics in the solid FE model (Fig. 6b) is simulated in a special program [13, 14]. Input data: results of scanning and field testing.



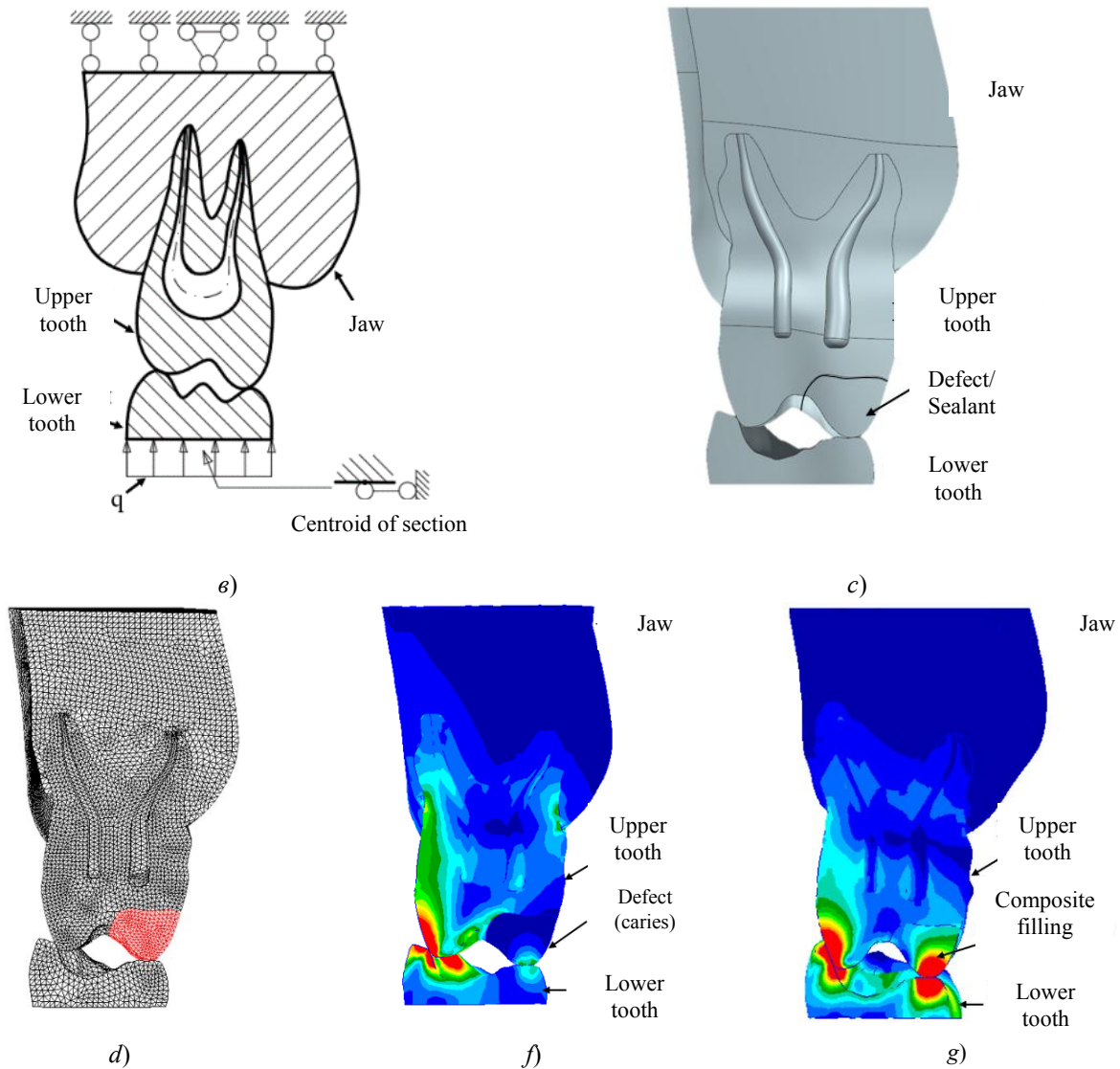


Fig. 6. Construction and analysis of FE models of a human tooth considering heterogeneity of material mechanical characteristics: a) wireframe model; b) change in elasticity tooth modulus in FE solid model; c) design scheme; d) solid geometric model; e) FE mesh generation; f) SSS analysis result of FE model of tooth with simulated defect; g) SSS analysis result of FE model of tooth with simulated composite fillings

The design scheme is presented in Fig. 6c. A defect and a composite filling are modeled on the upper tooth (see Fig. 6d and 6e).

The analysis result of the FE model with a defect (see Fig. 6f) shows that the carious part of the tooth does not absorb the load. That is, a healthy part of the tooth has an additional load, and the probability of decay increases. The analysis result of the second FE model, after filling the caries area with a sealant made of composite material (see Fig. 6g), shows that the tooth almost completely restores its functional capacities since the stress pattern is identical to the picture obtained for a healthy tooth [2].

Fig. 6g shows that stress maxima are observed at the contact points on the tops of the dental tubercles. A higher load is picked up by the area of enamel and dentin. The inner part of the tooth is less stressed. This result is compared to the calculation [2]. An average value of the mechanical characteristics of enamel and dentin is used. Heterogeneity of the structure of the tooth material is not taken into account. The comparison shows a more uniform stress distribution in the tooth body when modeling the distribution heterogeneity of its mechanical characteristics.

Discussion and Conclusions. The study results validate the accuracy and reliability of the presented method of FE modeling based on scanning real DS considering heterogeneity of the material mechanical characteristics.

The presented complex of mathematical methods for modeling the interpretation of CT scanning bitmaps allows the study of any complex structures of real DS. The results of such simulation are used to construct FE models

considering heterogeneity of the mechanical characteristics of the material.

The developed mathematical modeling technique can be applied for any physical scanning principles (X-ray, ultrasound, laser, etc.) and for any types of materials if the data received is a digital (raster) image.

References

1. Pykhalov, A.A., et al. Sposob opredeleniya znacheniy modulya uprugosti i ego raspredeleniya v konstruktivnykh elementakh, obladayushchikh neopredelennymi svoystvami prochnosti: patent № 2542918 Ros. Federatsiya: MPK G06T 1/00 A61B 6/00. [Method of determining values of elasticity modulus and its distribution in structural elements with indefinite strength properties.] RF Patent no. 2542818, 2015 (in Russian).
2. Pykhalov, A.A., Duong, V.L., Tolstikov, V.G. Postroenie i analiz konechno-elementnykh modeley neodnorodnykh deformiruemykh tverdykh tel na osnove skanirovaniya. [Construction and analysis of finite-element models of inhomogeneous deformable solids based on scanning.] PNRPU Mechanics Bulletin, 2018, no. 4, pp. 106–118 (in Russian).
3. Rentgenovskaya komp'yuternaya tomografiya. Rukovodstvo dlya vrachev. [X-ray computed tomography. Guide for doctors.] G.E. Trufankov, Rud, S.D., eds. St.Petersburg: Foliant, 2008, 1200 p. (in Russian).
4. Marusina, M.Ya., Kaznacheeva, A.O. Sovremennye vidy tomografii. [Modern types of tomography.] St.Petersburg: SPbGU ITMO, 2006, 132 p. (in Russian).
5. Golovanov, N.N. Geometricheskoe modelirovanie. [Geometric modelling.] Moscow: Izdatel'stvo fiziko-matematicheskoy literatury, 2002, 472 p. (in Russian).
6. Duong, V.L., Pykhalov, A.A., Tatarnikova, S.R. Interpolyatsiya geometrii i neodnorodnosti materiala deformiruemykh tel pri postroenii ikh ob'emnykh modeley metodom konechnykh elementov na osnove skanirovaniya komp'yuternym tomografom. [Interpolation of geometry and inhomogeneity of material of deformable solids when constructing their 3D models with the finite elements method based on the computer tomograph scanning.] Modern Technologies. System Analysis. Modeling. 2017, no. 3 (55), pp. 8–16, Irkutsk: IrGUPS (in Russian).
7. PATRAN 2013. PCL and Customization 2013. MSC Software Corporation. Santa Ana: MSC Software Corporation, 2013, 1010 p.
8. PATRAN 2013. PCL and Reference. MSC Software Corporation. Santa Ana: MSC Software Corporation, 2013, 2190 p.
9. Utenkin, A.A. Issledovanie mekhanicheskikh svoystv kompaktnogo veshchestva kosti kak anizotropnogo materiala: dis. ... kand. tekhn. nauk. [Investigation of the mechanical properties of compact bone matter as an anisotropic material: Cand.Sci. (Eng.) diss.] Riga, 1974, 199 p. (in Russian).
10. Knets, I.V., Pfafrod, G.O., Saulgozis, Yu.Zh. Deformirovanie i razrushenie tverdykh biologicheskikh tkaney. [Deformation and destruction of solid biological tissues.] Riga: Zinatne, 1980, 319 p. (in Russian).
11. Pykhalov, A.A., Pashkov, V.P., Duong, V.L. Issledovanie tochnosti chislennogo resheniya metodom konechnykh elementov analiza napryazhenno-deformirovannogo sostoyaniya obraztsov iz kostnoy tkani na osnove dannykh komp'yuternogo tomografa i naturnogo eksperimenta. [Studying accuracy finite element method-wise numerical solution of the stress-strain state analysis of samples made of inhomogeneous structure materials based on computerized tomography scanning and field experiment data.] Proceedings of Irkutsk State Technical University, 2017, vol. 21, no. 4, pp. 47–56 (in Russian).
12. Pykhalov, A.A. Kontaktnaya zadacha staticheskogo i dinamicheskogo analiza sbornykh rotorov turbomashin: dis. ... d-ra tekhn. nauk. [A contact problem of static and dynamic analysis of prefabricated rotors of turbomachines: Dr.Sci. (Eng.) diss.] Moscow, 2006, 428 p. (in Russian).
13. Pykhalov, A.A., Duong, V.L. Matematicheskoe modelirovanie dlya avtomatizatsii obrabotki rezul'tatov skanirovaniya deformiruemykh tverdykh tel slozhnoy geometricheskoy formy s neodnorodnymi mekhanicheskimi kharakteristikami dlya postroeniya ikh konechno-elementnykh modeley : sv-vo o gos. registratsii programm dlya EVM. [Mathematical modeling of automation of the processing of scanned data of deformable solids of complex geometric shape with heterogeneous mechanical characteristics to build their finite-element models: Certificate of state registration of com-

puter software no. 2017661241.] 2017 Available at: http://www1.fips.ru/registers-doc-view/fips_servlet?DB=EVM&DocNumber=2017661241&TypeFile=html (accessed 08.08.19) (in Russian).

14. Pykhalov, A.A., Duong, V.L. Matematicheskoe modelirovanie obrabotki rezul'tatov skanirovaniya deformiruemykh tverdykh tel dlya postroeniya geometrii ikh konechno-elementnykh modeley: sv-vo o gos. registratsii programm dlya EVM. [Mathematical modeling of processing the results of scanning deformable solids to build the geometry of their finite element models: Certificate of state registration of computer software no. 2018615239.] 2018. Available at: http://www1.fips.ru/registers-doc-view/fips_servlet?DB=EVM&DocNumber=2018615239&TypeFile=html (accessed 08.08.19) (in Russian).

Submitted 25.03.2019

Scheduled in the issue 17.06.2019

Author:

Duong Van Lam,

junior Researcher, Irkutsk National Research Technical University (83, Lermontov St., Irkutsk, 664074, RF),

ORCID: <https://orcid.org/0000-0001-5605-1323>

Bright1388@gmail.com

INFORMATION TECHNOLOGY, COMPUTER SCIENCE, AND MANAGEMENT ИНФОРМАТИКА, ВЫЧИСЛИТЕЛЬНАЯ ТЕХНИКА И УПРАВЛЕНИЕ



UDC 519.689

<https://doi.org/10.23947/1992-5980-2019-19-3-290-300>

Accelerated preprocessing in task of searching substrings in a string *

A. V. Mazurenko¹, N. V. Boldyrikhin^{2**}

¹ DDoS-GUARD LLC, Rostov-on-Don, Russian Federation

² Don State Technical University, Rostov-on-Don, Russian Federation

Ускоренный препроцессинг в задаче поиска подстрок в строке ***

A. В. Мазуренко¹, Н. В. Болдырихин^{2**}

¹ ООО «ДДОС-Гвард», г. Ростов-на-Дону, Российская Федерация

² Донской государственный технический университет, г. Ростов-на-Дону, Российская Федерация

Introduction. A rapid development of the systems such as Yandex, Google, etc., has predetermined the relevance of the task of searching substrings in a string, and approaches to its solution are actively investigated. This task is used to create database management systems that support associative search. Besides, it is applicable in solving information security issues and creating antivirus programs. Algorithms of searching substring in a string are used in signature-based discovery tasks.

Materials and Methods. The solution to the problem is based on the Aho-Corasick algorithm which is a typical technique of searching substrings in a string. At the same time, a new approach regarding preprocessing is employed.

Research Results. The possibility of constructing the transition function and suffix references through suffix arrays and special mappings, is shown. The relationship between the prefix tree and suffix arrays was investigated, which provided the development of a fundamentally new method of constructing the transition and error functions. The results obtained enable to substantially shorten the time intervals spent on the pre-election processing of a set of pattern strings when using an integer alphabet. The paper lists eight algorithms. The developed algorithms are evaluated. The results obtained are compared to the formerly known. Two theorems and eight lemmas are proved. Two examples illustrating features of the practical application of the developed preprocessing procedure are given.

Discussion and Conclusions. The preprocessing procedure proposed in this paper is based on the communication between the suffix array built on the ground of a set of pattern strings and the construction of transition and error functions at the

Введение. Бурное развитие таких систем, как Yandex, Google и пр., предопределило актуальность задачи поиска подстрок в строке. На сегодняшний день активно исследуются подходы к ее решению. Эта задача используется при создании систем управления базами данных, поддерживающих ассоциативный поиск. Кроме того, она применима при решении вопросов информационной безопасности, создании антивирусных программ. Алгоритмы поиска подстрок в строке используются в задачах обнаружения, основанного на сигнатурах.

Материалы и методы. Решение задачи базируется на алгоритме Ахо — Корасик, который представляет собой классический способ осуществления поиска подстрок в строке. Вместе с тем применен новый подход в части, касающейся предварительной обработки.

Результаты исследования. Показана возможность построения функции перехода и суффиксных ссылок при помощи суффиксных массивов и специальных отображений. Исследована взаимосвязь между префиксным деревом и суффиксными массивами. Это дало возможность разработать принципиально новый способ построения функций перехода и ошибок.

Полученные результаты позволяют существенно сократить время, затрачиваемое на предвыборную обработку множества строк образцов при использовании целочисленного алфавита.

В статье приведено восемь алгоритмов. Оценены разработанные алгоритмы. Полученные результаты сопоставлены с ранее известными. Доказаны две теоремы и восемь лемм. Приведены два примера, иллюстрирующие особенности практического применения разработанной процедуры препроцессинга.

Обсуждение и заключения. Предложенная в данной статье процедура препроцессинга основывается на связи между суффиксным массивом, созданным на основе множества строк образцов, и построением функций перехода и ошибок на начальных этапах работы алгоритма Ахо — Корасик. Такой подход отличен от традиционного и требует

* The research is done within the frame of the independent R&D.

** E-mail: mazurencoal@gmail.com, boldyrikhin@mail.ru

*** Работа выполнена в рамках инициативной НИР.



initial stages of the Aho-Corasick algorithm. This approach differs from the traditional one and requires the use of algorithms providing a suffix array in linear time. Thus, the algorithms that enable to significantly reduce the time for preprocessing of a set of pattern strings under the condition of using a certain type of alphabet in comparison to the known approach proposed in the Aho-Corasick algorithm are described. The research results presented in the paper can be used in anti-virus programs that apply searching for signatures of malicious data objects in the memory of a computer system. In addition, this approach to solving the problem on searching substrings in a string will significantly speed up the operation of database management systems using associative search.

Keywords: string searching, Aho-Corasick algorithm, prefix tree, suffix array, information search, error function, transition function

For citation: A.V. Mazurenko, N.V. Boldyrikhin. Accelerated preprocessing in task of searching substrings in a string. Vestnik of DSTU, 2019, vol. 19, no. 3, pp. 290–300. <https://doi.org/10.23947/1992-5980-2019-19-3-290-300>

использования алгоритмов, позволяющих построить суффиксный массив за линейное время. Таким образом, описаны алгоритмы, позволяющие существенно сократить время на предварительную обработку множества строк образцов при условии использования определенного типа алфавита по сравнению с известным подходом, предложенным А. Ахо и М. Корасик.

Результаты исследований, приведенные в статье, могут быть применены в антивирусных программах, использующих поиск сигнатур вредоносных информационных объектов в памяти вычислительной системы. Кроме того, данный подход к решению задачи поиска подстроки в строке позволяет значительно ускорить работу систем управления баз данных, применяющих ассоциативный поиск.

Ключевые слова: поиск подстроки, алгоритм Ахо — Корасик, префиксное дерево, суффиксный массив, поиск информации, функция ошибок, функция перехода.

Образец для цитирования: Мазуренко, А.В. Ускоренный препроцессинг в задаче поиска подстрок в строке / А. В. Мазуренко Н. В. Болдырихин // Вестник Дон. гос. техн. ун-та. — 2019. — Т. 19, № 3. — С. 290–300. <https://doi.org/10.23947/1992-5980-2019-19-3-290-300>

Introduction. Nowadays, awareness of the cybersecurity of distributed information systems and individual computing facilities is growing essentially [1]. A range of such tasks is wide enough [1–10]. Of special interest is the creation of powerful antivirus software (SW). One of the most important tasks solved through such SW is searching substrings in a string [1, 5, 6, 10–13].

Materials and Methods. The task of substring searching is to find all the lines in the text T with a total length m matching any pattern from a given set of patterns P . Suppose that the sum of the lengths of all elements P consisting of characters of the alphabet I is n . A solution to this problem was proposed by A. Aho and M. Corasick [6, 10]. In their algorithm, the pre-election processing time is $O(n|I|)$, and the search time is $O(m|I| + k)$. Here, k is a number of matches found in the text with lines belonging to a set of samples.

Currently, the task of finding a substring in a string is being intensely investigated for two reasons:

- search engines are rapidly developing [11];
- the detection process in antivirus software products is based on signatures [1].

In this regard, algorithms have been created that have to be selected due to specific needs of the user. The latest results obtained under solving the problem of searching a set of substrings are described in [13].

The results presented in this paper are based on the relationship between the suffix array created from a set of pattern strings and the construction of transition and error functions at the initial stages of the Aho - Corasick algorithm. This approach differs from the traditional one and requires using algorithms to construct a suffix array in linear time. So, the paper describes the algorithms by which the pre-election processing time is reduced to $O(n)$.

Given the alphabet I , a set of patterns $P = \{P_1, P_2, \dots, P_k\}$ where $P_i \in I^*$, $i = \overline{1, k}$. Let us denote by $n = \sum_{i=1}^k |P_i|$. Assume that the alphabet I is a limited range of integers. The boundary may depend on the length of the string in question $s \in I^*$ or may involve an interval $[0, c]$ where c is a positive integer: $c \geq |s|$. Let $\varepsilon \in I$ be an empty string.

Let *goto* be a transition function and a *failure* — an error function. These modifications are concerned with the methods for constructing the mentioned functions used in the Aho – Corasick algorithm [6, 10].

Suppose $SuffArr(s)$ is a certain algorithm for constructing a suffix array for a string $s \in I^*$ in linear time. A description of such algorithms can be found, for example, in [12–15].

Suppose $x, y \in I^*$. Then, $lcp(x, y)$ is the largest common prefix of the strings x and y .

Consider the string $s \in I^*$, $s = s[s[0]s[1]...s[n-1]]$. Let $s[s[i]s[i+1]...s[j]]$ be a substring s including characters from i to j where $i \leq j$, $i, j = \overline{0, n-1}$. Let us denote p_s by the suffix array corresponding to the string s . Suppose

$$p_s = p_s[p_s[0]p_s[1]...p_s[n-1]],$$

that is $s[s[p_s[0]]...s[n-1]] < s[s[p_s[1]]...s[n-1]] < ... < s[s[p_s[n-1]]...s[n-1]]$.

To construct a suffix array, the algorithm described in [15] will be used.

Suppose $\alpha_i \notin I$, $\alpha_i \neq \alpha_j$, $1 \leq i < j \leq k+1$, $\alpha_1 < \alpha_2 < ... < \alpha_{k+1}$. Let $\forall b \in I \alpha_i < b$, where $1 \leq i \leq k+1$. Granting $P \neq \emptyset$, $alpha = \{\alpha_1, \alpha_2, ..., \alpha_k, \alpha_{k+1}\}$.

Suffix Array Processing Algorithm p_s

Here, $s \in I^*$: $s = \alpha_1 P_1 \alpha_2 P_2 ... \alpha_k P_k \alpha_{k+1}$, $P_i \in I^*$, $1 \leq i \leq k$.

Adaptation($s, p_s, alpha$)

```

1. new_array  $\leftarrow \varepsilon$ 
2. for ( $i \leftarrow |alpha|; i < |s|; i++$ ) {
3.  $j \leftarrow 0$ 
4. while ( $s[s[p_s[i]]...s[|s|-1]][j] \notin alpha$ ) {
5. new_array[i][j]  $\leftarrow s[s[p_s[i]]...s[|s|-1]][j]$ 
6.  $j \leftarrow j + 1$ 
7. }
8. }
9. ordered_list[0]  $\leftarrow$  new_array[0]
10. for ( $i \leftarrow 1; i < |s| - |alpha|; i++$ ) {
11.  $j \leftarrow 0$ 
12. if ( $new\_array[i] \neq new\_array[i-1]$ ) {
13. ordered_list[i]  $\leftarrow$  new_array[i]
14.  $j \leftarrow j + 1$ 
15. }
16. }
17. return ordered_list

```

Lemma 1. Let $P = \{P_1, P_2, ..., P_k\}$, $s = \alpha_1 P_1 \alpha_2 P_2 ... \alpha_k P_k \alpha_{k+1}$. Then the *Adaptation* algorithm builds an array of lexicographically ordered suffixes of the patterns belonging to P over the time $O(|s| - |alpha|)$.

Proof. In the loop of 2–8, the construction of the *new_array* is performed, whose i -th element is a prefix of the corresponding suffix s which includes all the characters of this suffix starting with the zero position to its first element belonging to the set *alpha*. In this case, using the suffix array p_s , all suffixes s are looped over according to their lexicographic order. Thus, the *new_array* consists of all suffixes of the patterns belonging to P according to their lexicographic sequencing, and the recurrence of some suffixes is possible.

Note that all strings starting with characters belonging to the *alpha* array, that is, the first $|alpha|$ suffixes, are excluded from consideration. Then, in the loop of 10–16, using the *new_array*, the *ordered_list* array is constructed through eliminating repetition strings. To do this, due to the lexicographic sequence of the strings, it is sufficient to check whether the string in question coincides with the previous one.

The loop of 2–8 is executed over the time $O(|s| - |alpha|)$ since all strings starting with characters belonging to the *alpha* array are excluded from consideration. In the loop 10–16, $|s| - |alpha|$ of string matches occur. Thus, we obtain an asymptotic estimate of $O(|s| - |alpha|)$ algorithm running time. The lemma is proved.

Partitioning algorithm according to lexicographic sequencing

Here, s is an array of lexicographically ordered strings.

```

DandC(s)
1. sub[0] ← 0
2. j ← 0
3. for (i ← 0; i < |s| - 1; i++) {
4. if (s[i] ≠ s[i+1]) {
5. sub[j] ← i + 1
6. j ← j + 1
7. }
8. sub[j] ← |s|
9. return sub
    
```

Lemma 2. The *DandC* algorithm based on an array of lexicographically ordered strings s constructs a *sub* array consisting of positive integers that show the indices corresponding to the first strings among the strings with the first characters equal over the time $O(|s|)$.

Proof. The boundary corresponding to the first character begins with 0, which corresponds to the assignment performed in step 1. In the loop of 3–7, the first characters of the i -th and $(i + 1)$ -th strings are sequentially compared where $i = 0, |s| - 2$. If the characters are not equal, then the beginning of the boundary corresponding to the next character is written to the *sub* array. Otherwise, the loop execution continues. The right boundary of the last character corresponds to the number of strings in the s array (step 8).

The comparison in step 4 occurs over the time $O(1)$, as the recording in step 5 and the increment in step 6 do. Thus, the loop of 3–7 is performed over the time $O(|s|)$. The lemma is proved.

First link algorithm

Here, *tree* is a tree, $lex_words \in I^*$, *link_num* is the number of some character in *lex_words* string, v is a serial number of a new node that joins the node with the serial number *node_number*.

```

BuildFirstLink(tree&, lex_words&, v&, link_num, node_number)
1. new tree.node[v]
2. tree.node[v].state ← lex_words[lex_words[0]..lex_words[link]]
3. new tree.node[node_number].link ← tree.node[v]
4. tree.node[node_number].link.symbol ← lex_words[link_num]
5. v ← v + 1
    
```

Lemma 3. The *BuildFirstLink* algorithm constructs a new node with the sequence number v and an arc leading from *node_number* to a new node v , in the *tree* over the time $O(1)$.

Substring link algorithm

Here, *tree* is a tree, $lex_words \in I^*$, v is a serial number of a new node that joins the node with the serial number *start*.

```

BuildSubstringLink(tree&, lex_words&, v&, start)
1. for (k ← start; k < |lex_words|; k++) {
2. new tree.node[v]
3. tree.node[v].state ← lex_words[lex_words[0]..lex_words[k]]
4. new tree.node[v-1].link ← tree.node[v]
5. tree.node[v-1].link.symbol ← lex_words[k]
6. v ← v + 1
7. }
    
```

Lemma 4. The *BuildSubstringLink* algorithm constructs new nodes in *tree* matching all prefixes of the string *lex_words* starting with the prefix $lex_words[lex_words[0]..lex_words[start]]$ over the time $O(|lex_words| - start)$.

Last link algorithm

Here, *tree* is a tree, $lex_words \in I^*$, *v* is a serial number of a new arc, *I* is an alphabet.

BuildLastLink(*tree*, *lex_words*, *v*, *I*)

1. $new\ tree.node[0].link[v] \leftarrow tree.node[0]$
2. $symbols \leftarrow \emptyset$
3. **for** ($i \leftarrow 0; i < |lex_words|; i++$) {
4. $symbols[i] \leftarrow lex_words[i][0]$
5. $j \leftarrow 0$
6. **for** ($i \leftarrow 0; i < |I|; i++$) {
7. **if** ($I[i] \notin symbols$) {
8. $tree.node[0].link[v].symbol[j] \leftarrow I[i]$
9. $j \leftarrow j + 1$
10. }
11. }

Lemma 5. The *BuildLastLink* algorithm builds a loop at the root node. Its marking corresponds to a set of symbols by which it is impossible to go to other nodes of the *tree* from the root node over the time $O(|lex_words| + |I|)$.

Transition Algorithm

Here, *lex_words* is an array of lexicographically ordered strings.

CreateLink(*lex_words*)

1. $str \leftarrow \emptyset$
2. $sub \leftarrow DandC(lex_words)$
3. $v \leftarrow 1$
4. $tree \leftarrow \emptyset$
5. $tree.node[0].state \leftarrow \epsilon$
6. **for** ($i \leftarrow 0; i < |sub| - 1; i++$) {
7. *BuildFirstLink*(*tree*, $lex_words[sub[i]]$, *v*, 0, 0)
8. *BuildSubstringLink*(*tree*, $lex_words[sub[i]]$, *v*, 1)
9. **for** ($j \leftarrow sub[i] + 1; j < sub[i + 1]; j++$) {
10. $temp \leftarrow |lcp(lex_words[j - 1], lex_words[j])| + 1$
11. $z \leftarrow tree.getStateNumber(lcp(lex_words[j - 1], lex_words[j]))$
12. *BuildFirstLink*(*tree*, $lex_words[j]$, *v*, *temp*, *z*)
13. *BuildSubstringLink*(*tree*, $lex_words[j]$, *v*, *temp*)
14. }
15. }
16. *BuildLastLink*(*tree*, *lex_words*, *v*, *lex_words*)
17. **return** *tree*

Lemma 6. The *CreateLink* algorithm builds a prefix *tree* with a loop at the root node over the time $O\left(\sum_{i=0}^{|lex_words|-1} |lex_words[i]|\right)$.

Proof. In step 2, the *DandC* algorithm is executed (see Lemma 2), after which, in step 5, the root node with the serial number 0 of the *tree* is created. Its state is taken equal to a blank string ε . Consider the loop of 6–15 at the i -th step.

In step 7, using the *BuildFirstLink* algorithm, a node is created whose state corresponds to the first character of the string $lex_words[sub[i]]$. Given the construction of the *sub* array, it can be argued that such a character has not occurred before among the first characters of the previous strings. Then, in step 8, the implementation of the *BuildSubstringLink* algorithm sequentially creates nodes whose state matches all prefixes of the string $lex_words[sub[i]]$ excluding the prefix built in the previous string.

In the loop of 9–14, using *BuildFirstLink* and *BuildSubstringLink* algorithms, we perform the same actions with strings lying in an integer space $[sub[i]+1, sub[i+1]-1]$. Since each such string has a common non-zero prefix with the previous string, the algorithm immediately switches to the state corresponding to the largest common prefix, starting with which, it is required to build new nodes. In step 16, using the *BuildLastLink* algorithm, a loop at the root node is created.

Steps 12 and 13 are performed over the time

$$\begin{aligned} O(1) + O(|lex_words[j]| - |lcp(lex_words[j-1], lex_words[j])| - 1) = \\ = O(|lex_words[j]| - |lcp(lex_words[j-1], lex_words[j])|). \end{aligned}$$

Thus, it follows from Lemmas 2, 3, and 4 that the loop of 9-14 is executed over the time

$$O\left(\sum_{j=sub[i]+1}^{sub[i+1]-1} |lex_words[j]| - |lcp(lex_words[j-1], lex_words[j])|\right).$$

The loop of 6–14 is executed over the time

$$\begin{aligned} O\left(\sum_{i=0}^{|sub|-2} |lex_words[sub[i]]|\right) + \\ + O\left(\sum_{i=0}^{|sub|-2} \sum_{j=sub[i]+1}^{sub[i+1]-1} |lex_words[j]| - |lcp(lex_words[j-1], lex_words[j])|\right) = \\ = O\left(\sum_{i=0}^{|sub|-1} |lex_words[sub[i]]| - |lex_words|\right). \end{aligned}$$

It follows from Lemma 5, that step 16 is performed over the time $O(|lex_words| + \sum_{i=0}^{|lex_words|-1} |lex_words[i]|)$. Thus, we obtain an asymptotic estimate of the running time of the algorithm

$$\begin{aligned} O(|lex_words|) + O\left(\sum_{i=0}^{|sub|-1} |lex_words[sub[i]]| - |lex_words|\right) + \\ + O\left(|lex_words| + \sum_{i=0}^{|lex_words|-1} |lex_words[i]|\right) = O\left(\sum_{i=0}^{|lex_words|-1} |lex_words[i]|\right). \end{aligned}$$

The lemma is proved.

The goto function algorithm

Here, P is a set of pattern strings.

ConstructGoto(P)

1. $s \leftarrow \alpha_1 P_1 \alpha_2 P_2 \dots \alpha_k P_k \alpha_{k+1}$
2. $p_s \leftarrow \text{SuffArr}(s)$
3. $\alpha \leftarrow \{\alpha_1, \alpha_2, \dots, \alpha_k, \alpha_{k+1}\}$
4. $\text{ordered_list} \leftarrow \text{Adaptation}(s, p_s, \alpha)$
5. $j \leftarrow 0$
6. $lex_words \leftarrow \emptyset$
7. $P_length \leftarrow \{|P_1|, |P_2|, \dots, |P_k|\}$
8. for ($i \leftarrow 0; i < |\text{ordered_list}|; i++$)

9. if $((|ordered_list[i]| \in P_length) \text{ and } (ordered_list[i] \in P))$
10. $lex_words[j++] \leftarrow ordered_list[i]$
11. $goto \leftarrow CreateLink(lex_words)$
12. return goto

We should remind that $n = \sum_{i=1}^k |P_i|$ for a set of patterns $P = \{P_1, P_2, \dots, P_k\}$.

Theorem 1. The *ConstructGoto* algorithm develops the *goto* function over the time $O(n)$.

Proof. In step 2, a suffix array p_s for the string s is constructed. In step 4, using the *Adaptation* algorithm, all suffixes of the strings belonging to a set of patterns P are written to the *ordered_list* array. In this case, recurrences are not excluded. In the loop of 8–10, an array *lex_words* containing suffixes belonging to P and arranged in lexicographic sequence without recurrences is constructed. In step 11, a prefix tree is built with a loop at the root node based on the strings contained in the *lex_words* array. The data structure returned by the *CreateLink* algorithm defines exactly the *goto* function.

Step 2 is completed over the time $O(n+k+1)$ [12]. From Lemma 1, it follows that step 4 is completed over the time $O(n+k+1-k-1) = O(n)$. In the loop of 8–10, only strings whose length is equal to the length of any pattern are considered.

Thus, no more than $O(n)$ checks are needed to find patterns of P . From Lemma 6, it follows that step 11 is completed over the time $O\left(\sum_{i=0}^{|lex_words|-1} |lex_words[i]|\right) = O(n)$. Since $k \leq n$, we obtain an asymptotic estimate of the running time of the $O(n) + O(n+k+1) = O(n)$ algorithm. The theorem is proved.

Research Results

Example 1.

Suppose $P = \{one, on, once, cell, lull, eye, near\}$. Then

$$s = \alpha_1 one \alpha_2 on \alpha_3 once \alpha_4 cell \alpha_5 lull \alpha_6 eye \alpha_7 near \alpha_8. \quad (1)$$

Table 1 shows the result of the *goto* function algorithm on the entry of the string s (1).

Table 1

Prefix tree structure			
node number	node state	link branched states from node	symbols on link branches from node
0	ϵ	1. c; 2. e; 3. l; 4. n; 5. o	1. c; 2. e; 3. l; 4. n; 5. o
1	c	1. ce	1. e
2	ce	1. cel	1. l
3	cel	1. cell	1. l
4	cell	–	–
5	e	1. ey	1. y
6	ey	1. eye	1. e
7	eye	–	–
8	l	1. lu	1. u
9	lu	1. lul	1. l
10	lul	1. lull	1. l
11	lull	–	–
12	n	1. ne	1. e
13	ne	1. nea	1. a
14	nea	1. near	1. r
15	near	–	–
16	o	1. on	1. n
17	on	1. onc; 2. one	1. c; 2. e
18	onc	1. once	1. e
19	once	–	–
20	one	–	–

Suppose $\tilde{s} = \alpha_{k+1}\tilde{P}_k\alpha_k \dots \alpha_2\tilde{P}_1\alpha_1\tilde{P}_0\alpha_0$ is mirroring of the string s .

Failure function algorithm

Here, P is a set of pattern strings.

$FalseSuff(P)$

```

1.  $\tilde{s} \leftarrow \alpha_{k+1}\tilde{P}_k\alpha_k \dots \alpha_2\tilde{P}_1\alpha_1\tilde{P}_0\alpha_0$ 
2.  $p_{\tilde{s}} \leftarrow SuffArr(\tilde{s})$ 
3.  $alpha \leftarrow \{\alpha_1, \alpha_2, \dots, \alpha_k, \alpha_{k+1}\}$ 
4.  $ordered\_list \leftarrow Adaptation(\tilde{s}, p_{\tilde{s}}, alpha)$ 
5.  $link \leftarrow \emptyset$ 
6. for ( $i \leftarrow 0; i < |\tilde{s}|; i++$ )
7.  $inLink[i] \leftarrow \varepsilon$ 
8.  $sub \leftarrow DandC(ordered\_list)$ 
9.  $str \leftarrow \emptyset$ 
10. for ( $i \leftarrow 0; i < |sub| - 1; i++$ )
11. for ( $j \leftarrow sub[i]; j < sub[i+1] - 1; j++$ )
12.  $str[j] \leftarrow |lcp(ordered\_list[j], ordered\_list[j+1])|$ 
13. for ( $i \leftarrow 0; i < |sub| - 1; i++$ )
14. for ( $k \leftarrow sub[i+1] - 1; k > sub[i]; k--$ ) {
15. for ( $j \leftarrow sub[i]; j < k; j++$ )
16.  $min\_element \leftarrow \min(str[k-1], str[k-2], \dots, str[j])$ 
17. if ( $min\_element = |ordered\_list[j]|$ )
18.  $min\_temp[j - sub[i]] \leftarrow min\_element$ 
19. }
20.  $max\_element \leftarrow \max(min\_temp[0], min\_temp[1], \dots, min\_temp[w])$ 
21. найти  $max\_index$ :  $min\_temp[max\_index] = max\_element$ 
22.  $inLink[k] \leftarrow ordered\_list[max\_index + sub[i]]$ 
23. }
24. for ( $i \leftarrow 0; i < |inLink|; i++$ ) {
25.  $link[i][0] \leftarrow ordered\_list[i]^-$ ; //string mirroring
26.  $link[i][1] \leftarrow inLink[i]^-$ ; // string mirroring
27. }
28. return link

```

Remark. In string 20, $w \leq sub[i+1] - sub[i] - 1$.

Theorem 2. The *FalseSuff* algorithm constructs the *failure* function over the time $O(n)$. Proof. In step 1, we construct an array of characters that contains mirror images of strings belonging to a set of patterns P and some unique characters. In step 2, we construct a suffix array $p_{\tilde{s}}$ for the string \tilde{s} . In step 4, using the *Adaptation* algorithm, all suffixes of the strings belonging to a set of patterns \tilde{P} (a set of patterns consisting of mirrored strings P) are written to the *ordered_list* array, and recurrences are not excluded.

In step 8, the *DandC* algorithm is executed (see Lemma 2), after which, in the loop of 10–12, we find the length of the largest common prefix between the strings that match the first character. We write the result to the *str* array. Note that this value is zero for the strings for which this condition is not satisfied. In the loop of 13–23, a special mapping is constructed between the strings for which the first character matches. We describe this mapping. Indicate some string

$$s \in ordered_list[ordered_list[sub[i]], \dots, ordered_list[sub[i+1]-1]].$$

Consider a set of strings belonging to $ordered_list[ordered_list[sub[i]], \dots, ordered_list[sub[i+1]-1]]$. Their length is equal to the length of the largest common prefix with s excluding s itself. From this set, we find the string s' that has an overall length, and assign it to s . Obviously, the constructed mapping is a bijection under the condition of $s' \neq \varepsilon$. The result is written to the *inLink* array. In the loop of 24–27, using the *inLink* array, we explicitly indicate the constructed mapping while mirroring each of the strings. Thus, we assign the s' node to the \tilde{s} node of the prefix tree constructed on the basis of the array of patterns P . Its state is equal to the largest proper suffix \tilde{s} that occurs among the many states of the considered prefix tree. But according to the definition of the *failure* function, this is the desired result.

Suppose $n = \sum_{i=1}^k |P_i|$. Step 2 is completed over the time $O(n+k+1)$ [12]. From Lemma 1, it follows that step 4 is performed over the time $O(n+k+1-k-1) = O(n)$. The loop of 6–7 is executed over the time $O(|\tilde{s}|) = O(n)$. From Lemma 2, it follows that step 8 is performed over the time $O(n)$. The loop of 10–12 is executed over the time $O\left(\sum_{i=0}^{|sub|-2} \sum_{j=sub[i]+1}^{sub[i+1]-1} \gamma_j\right) = O(k)$, $\forall j \gamma_j = 1$. The loop of 14–23 is completed over the time

$$O\left(\sum_{k=sub[i]+1}^{sub[i+1]-1} \sum_{j=sub[i]}^{k-1} \gamma_j\right) = O\left(\sum_{j=0}^{sub[i+1]-sub[i]-2} \gamma_j\right) = O(sub[i+1]-sub[i]-1), \forall j \gamma_j = 1.$$

Then the loop of 13–23 is executed over the time

$$O\left(\sum_{i=0}^{|sub|-2} (sub[i+1]-sub[i]-1)\right) = O(sub[|sub|-1]) = O(k).$$

Since $|inLink| < n$, then the loop of 24–27 is executed over the time $O(|inLink|) = O(n)$. Thus, considering that $k \leq n$, we obtain an asymptotic estimate of the running time of the $O(n) + O(n+k+1) + O(k) = O(n)$ algorithm. The theorem is proved.

Example 2.

Suppose, as in example 1, $P = \{one, on, once, cell, lull, eye, near\}$. Then

$$\tilde{s} = \alpha_8 r a e n \alpha_7 e y e \alpha_6 l l u l \alpha_5 l l e c \alpha_4 e c n o \alpha_3 n o \alpha_2 e n o \alpha_1. \quad (2)$$

Table 2 shows the result of the *failure* function algorithm on the entry of the string \tilde{s} (2).

Table 2

False links between nodes

<i>inLink</i> array	<i>link</i> array	<i>inLink</i> array	<i>link</i> array
0. ε	0. $0. nea; 1. \varepsilon$	10. l	10. $0. cel; 1. l$
1. ε	1. $0. c; 1. \varepsilon$	11. l	11. $0. cell; 1. l$
2. c	2. $0. onc; 1. c$	12. l	12. $0. lull; 1. l$
3. ε	3. $0. e; 1. \varepsilon$	13. l	13. $0. lul; 1. l$
4. e	4. $0. ce; 1. e$	14. ε	14. $0. n; 1. \varepsilon$
5. ec	5. $0. once; 1. ce$	15. n	15. $0. on; 1. n$
6. e	6. $0. ne; 1. e$	16. ε	16. $0. o; 1. \varepsilon$
7. en	7. $0. one; 1. ne$	17. ε	17. $0. near; 1. \varepsilon$
8. e	8. $0. eye; 1. e$	18. ε	18. $0. lu; 1. \varepsilon$
9. ε	9. $0. l; 1. \varepsilon$	19. ε	19. $0. ey; 1. \varepsilon$

For all nodes for which Fig. 1 does not show false links, we believe that a false link leads to a root node.

8. Mazurenko, A.V., Stukopin, V.A. Geometricheskaya realizatsiya metoda provedeniya elektronnykh vyborov, osnovannogo na porogovom razdelenii sekreta. [Geometric realization of electronic elections based on threshold secret sharing.] Vestnik of DSTU, 2018, vol. 18, no. 2, pp. 246–255 (in Russian).
9. Cherkesova, L.V., et al. Algoritmicheskaya otsenka slozhnosti sistemy kodirovaniya i zashchity informatsii, osnovannoy na porogovom razdelenii sekreta, na primere sistemy elektronnoy golosovaniya. [Complexity calculation of coding and information security system based on threshold secret sharing scheme used for electronic voting.] Vestnik of DSTU, 2017, vol. 17, no. 3, pp. 145–155 (in Russian).
10. Antonov, E.S. Kak nayti million. Sravnenie algoritmov poiska mnozhestva podstrokov. [How to find a million. Substring set searching algorithms comparison.] RSDN Magazine, 2011, no. 1, pp. 60–67 (in Russian).
11. Tarakeswar, M.K., Kavitha, M.D. Search Engines: A Study. Journal of Computer Applications, 2011, vol. 4, no. 1, pp. 29–33.
12. Karkkainen, J., Sanders, P., Burkhardt, S. Linear work suffix array construction. Journal of the ACM, 2006, vol. 53, no. 6, pp. 918–936.
13. Baklanovsky, M.V. Khanov, A.R. Povedencheskaya identifikatsiya program. [Identification of programs based on the behavior.] Modeling and Analysis of Information Systems, 2014, vol. 21, no. 6, pp. 120–130 (in Russian).
14. Becher, V., et al. Efficient repeat finding in sets of strings via suffix arrays. Discrete Mathematics and Theoretical Computer Science, 2013, vol. 15, no. 2, pp. 59–70.
15. Shrestha, A.M.S., Frith, M.C., Horton, P. A bioinformatician's guide to the forefront of suffix array construction algorithms. Briefings in Bioinformatics, 2014, vol. 15, no. 2, pp. 138–154.

Submitted 22.01.2019

Scheduled in the issue 12.04.2019

Authors:

Mazurenko, Alexander V.

mathematician-programmer, DDoS-GUARD LLC (62/2, Budenovsky Pr., Rostov-on-Don, 344002, RF)

ORCID: <http://orcid.org/0000-0001-9541-3374>

mazurencoal@gmail.com

Boldyrikhin, Nikolay V.

associate professor of the Cybersecurity of IT Systems Department, Don State Technical University (1, Gagarin Square, Rostov-on-Don, 344000, RF), Cand.Sci. (Eng.)

ORCID: <http://orcid.org/0000-0002-9896-9543>,

boldyrikhin@mail.ru